Medical School, University of Crete

IMBB, FORTH

Διδακτορική διατριβή:

Η ομοιόσταση του πυρήνα στη γήρανση και το νευροεκφυλισμό: μηχανισμοί νουκλεοφαγίας και επιδιορθώσεις του DNA

PhD Thesis:

Nuclear homeostasis in aging and age-related neurodegeneration: Nucleophagy and DNA damage repair mechanisms

Margarita Elena Papandreou

Biologist, MRes

Supervisor: Professor Nektarios Tavernarakis, Neurogenetics & Aging Lab

Heraklion Crete, 2021

PhD Committee

Supervisor: Professor Nektarios Tavernarakis

Co-supervisors: Professor George Garinis

Professor Achilleas Gravanis

Viva Committee

Chamilos George	**Professor**
	Department of Medicine, University of Crete
Garinis George	**Professor**
	Department of Biology, University of Crete
Gravanis Achilleas	**Professor**
	Department of Medicine, University of Crete
Kollias George	**Professor**
	Department of Medicine, University of Athens
Mavrothalassitis George	**Professor**
	Department of Medicine, University of Crete
Talianidis Iannis	**Research Director, IMBB, FORTH**
Tavernarakis Nektarios	**Professor**
	Department of Medicine, University of Crete

Acknowledgements

I would first like to thank my supervisor, professor Nektarios Tavernarakis, for guiding me through this journey with his targeted succinct ideas while at the same time allowing me to literally experiment and develop my inquisitive and imaginative nature. I would also like to thank the other two members of my Committee, professor Achilleas Gravanis and George Garinis for consulting me in my work. I would also like to thank the other lab members and Mrs. Aggela Pasparaki for performing the confocal microscopy experiments. Last but not least, I would especially like to thank Dr. Mary Markaki, for her everyday support, advice and protective nature and my parents who gave me the freedom of mind, choice and error to develop the tools of self-discipline, hard work, experimentation and imagination to successfully complete my PhD.

Work in the authors' laboratory is funded by grants from the European Research Council (ERC), the European Commission Framework Programmes, and the Greek Ministry of Education. Margarita-Elena Papandreou was supported by the European Commission Marie Curie Initial Training Network (ITN) CODAGE.

CONTENTS

ΠΕΡΙΛΗΨΗ (Ι)

Η Ομοιόσταση του πυρήνα στη γήρανση και το νευροεκφυλισμό: Μηχανισμοί νουκλεοφαγίας και επιδιόρθωσης του DNA.

Η αυτοφαγία είναι ένας φυσιολογικός ευκαρυωτικός μηχανισμός που διατηρεί την κυτταρική ομοιόσταση. Είναι το κύριο κυτταρικό καταβολικό μονοπάτι, το οποίο διασπά μακρομόρια όπως πρωτεΐνες, λιπίδια και οργανίδια, μέσω του κύριου αποικοδομητικού οργανιδίου, του λυσοσώματος. Παρόλο που αρχικά θεωρήθηκε ως οδός μαζικής αποδόμησης, τα πρόσφατα στοιχεία υπογραμμίζουν τον ιδιαίτερα επιλεκτικό χαρακτήρα του. Αυτός ο αυστηρά ελεγχόμενος, μηχανισμός λαμβάνει χώρα υπό φυσιολογικές συνθήκες αλλά μπορεί να προκληθεί και από διάφορες μορφές κυτταρικού στρες, όπως η στέρηση θρεπτικών ουσιών, το οξειδωτικό στρες και η βλάβη του DNA. Μπορεί να διαιρεθεί σε τρεις μηχανισμούς, την μακροαυτοφαγία, που αναφέρεται ως αυτοφαγία, την μικροαυτοφαγία και την αυτοφαγία με πρωτεΐνες-συνοδούς.

Ο πυρήνας είναι το μεγαλύτερο οργανίδιο του κυττάρου, ωστόσο, οι μηχανισμός στους οποίους βασίζεται η ομοιόστασή του, δηλαδή η ανακύκλωσή του μέσω αυτοφαγίας ή άλλων καταβολικών μονοπατιών δεν είναι γνωστοί. Ο πυρήνας αποτελείται από μια μεγάλη ποικιλία μακρομορίων, τα οποία μπορούν να είναι αποκλειστικά πυρηνικά ή να εναλάσσονται διαρκώς μεταξύ του πυρήνα (νουκλεοπλάσματος) και του κυτταροπλάσματος μέσω της φωσφολιπιδικής

διπλοστιβάδας του. Η εσωτερική πυρηνική μεμβράνη αποτελείται κυρίως από τις λαμίνες, τις πρωτεΐνες SUN, την εμερίνη και την HP1 που αλληλεπιδρά με την χρωματίνη και επηρεάζει τον εντοπισμό της και συνεπώς την γονιδιακή έκφραση. Οι πρωτεΐνες SUN αλληλεπιδρούν με τις νεσπρίνες (SYNEs), οι οποίες είναι πρωτεΐνες εξωτερικής πυρηνικής μεμβράνης που συνδέουν τον πυρήνα με τον κυτταροσκελετό. Οι πρωτεΐνες SUN μαζί με τις νεσπρίνες σχηματίζουν το σύμπλοκο LINC (συνδετήρας του συμπλέγματος πυρηνοσκελετού-κυτταροσκελετού). Οι νεσπρίνες ρυθμίζουν την πυρηνική μεταφορά, το σχήμα του πυρήνα, καθώς και την μεταφορά συστατικών και μακρομορίων μέσα και έξω από τον πυρήνα.

Η νουκλεοφαγία περιγράφηκε αρχικά στον σακχαρομύκητα, με δύο μορφές, την τμηματική μικροπυρηνοφαγία (PMN) και την όψιμη πυρηνοφαγία (LN). Έτσι, οι ζυμομύκητες εκτελούν μικροπυρηνοφαγία καθώς και μακροπυρηνοφαγία σε φυσιολογικές συνθήκες ή μετά από πείνα. Στα θηλαστικά από την άλλη, το πυρηνικό LC3 αλληλεπιδρά με την λαμίνη Β μέσω της ειδικής και συγκεκριμένης LIR αλληλουχίας του, την οποία μεταφέρει μαζί με ετεροχρωματίνη στο κυτταρόπλασμα για λυσοσωμική αποδόμηση. Σε αντίθεση με τη ζύμη, η πείνα ή η αναστολή mTOR (mechanistic Target Of Rapamycin) δεν προκαλεί αυτήν την απόκριση με τη λαμίνη, τονίζοντας την ειδικότητα των διαφορετικών μεθόδων νουκλεοφαγίας σε διαφορετικά είδη. Η γενετική

αναστολή αυτού του τύπου νουκλεοφαγίας οδηγεί σε πρόωρη γήρανση, αν και ο ακριβής μηχανισμός δεν έχει ακόμη διευκρινιστεί.Επιπρόσθετα, το DNA έχει αποδειχθεί ότι προκαλεί αυτοάνοσες διαταραχές όταν δεν αποδομείται από το λυσοσωμάτιο. Η ανεπάρκεια σε Dnase2a, το ένζυμο που είναι υπεύθυνο για την αποδόμηση του DNA, προκαλεί συσσώρευση DNA εκτός πυρήνα κάτι το οποίο προκαλεί σοβαρή φλεγμονώδη απόκριση μέσω της οδού STING. Η ανεπάρκεια της Dnase2a αποκαλύπτει τη λυσοσωμική κάθαρση του κατεστραμμένου πυρηνικού DNA μέσω αυτοφαγίας. Η συμβολή της δυσλειτουργικής επιλεκτικής αυτοφαγίας στον νευροεκφυλισμό είναι γνωστή, όταν συσσωματώματα πρωτεϊνών και οργανιδίων είναι άμεσο αποτέλεσμα της ελαττωματικής αυτοφαγίας. Οι ασθένειες πολυγλουταμίνης (PolyQ) προκαλούνται από την επέκταση των επαναλήψεων CAG στα γονίδια που κωδικοποιούν τις πρωτεΐνες PolyQ. Η ατροφία του ‘Dentatorubral-pallidoluysian’ που προκαλεί αταξία, άνοια και επιληψία, προκαλείται από μεταλλάξεις ατροφίνης και καταδεικνύει έναν ιδιόμορφο παθολογικό τρόπο πυρηνοφαγίας.

Οι μεταβολές στην πυρηνική μορφολογία αποτελούν σημαντικό χαρακτηριστικό της γήρανσης, των συνδρόμων και άλλων παθολογιών που σχετίζονται με την γήρανση. Η μοριακή βάση και η φυσιολογική σημασία αυτών των αλλαγών παραμένουν ασαφείς. Εδώ, δείχνουμε ότι η πυρηνοφαγία, η αυτοφαγική αποδό-

μηση του πυρηνικού υλικού, είναι ένας σημαντικός καθοριστικός παράγοντας για το μέγεθος του πυρηνίσκου. Διαπιστώνουμε ότι η πρωτεΐνη αγκύρωσης πυρηνικού φακέλου του νηματώδη *Caenorhabditis elegans*, ANC-1 και οι ορθόλογές της στα θηλαστικά, νεσπρίνη 1 και 2, είναι βασικοί ρυθμιστές της νουκλεοφαγίας. Η εξασθένηση της νουκλεοφαγίας μειώνει την αντίσταση στο στρες και τη μακροζωία, η οποία προκαλείται από ασθενή σηματοδότηση ινσουλίνης και του προσομοιάζοντος στην ινσουλίνη αυξητικού παράγοντα (insulin/IGF1). Είναι αξιοσημείωτο ότι η πυρηνοφαγία απαιτείται για τη διατήρηση του μικρού πυρηνίσκου, που είναι ένδειξη μακροζωίας. Πράγματι, η αφθονία των κυριότερων συστατικών του πυρηνίσκου, όπως η φιμπριλαρίνη και τα νουκλεολικά προϊόντα, 18S rRNA και 45S rRNA, ρυθμίζεται από την πυρηνική αυτοφαγία. Έτσι, η ανακύκλωση της πυρηνικής μεμβράνης και άλλων πυρηνικών συστατικών μέσω της νουκλεοφαγίας είναι ένας εξελικτικά συντηρημένος μηχανισμός διασφάλισης μακροζωίας που προωθεί τη νεανικότητα και καθυστερεί τη γήρανση υπό συνθήκες στρες, διατηρώντας την πυρηνική αρχιτεκτονική και αποτρέποντας την πυρηνική επέκταση.

Γενικότερα, το μέγεθος του πυρηνίσκου είναι βιοδείκτης για τη διάρκεια ζωής του οργανισμού ανεξάρτητα από τον τύπο των κυττάρων. Στον C. elegans, τα daf-2, eat-2, ife-2 και glp-1 μεταλλαγμένα ζώα, που ζουν περισσότερο από τα αγρίου τύπου στελέχη αποτελούνται από κύτταρα με μικρότερους πυρηνίσκους σε σύγκριση με τα φυσιολογικά. Έτσι, αυτά τα μονοπάτια σηματοδότησης

επεκτείνουν τη διάρκεια ζωής τουλάχιστον μερικώς μέσω του ελέγχου του μεγέθους του πυρηνίσκου και της ριβοσωμικής βιογένεσης. Ομοίως, σε σύνδρομα πρόωρης γήρανσης όπως το σύνδρομο Hutchison-Gilford progeria, τα κύτταρα εμφανίζουν μεγαλύτερους πυρηνίσκους, υποδηλώνοντας αυξημένους ρυθμούς βιογένεσης ριβοσώματος και πρωτεϊνικής μετάφρασης.

Εν κατακλείδι, αποκαλύπτουμε έναν νέο μηχανισμό με τον οποίο πρωτείνες της πυρηνικής μεμβράνης, οι νεσπρίνες, ανακυκλώνονται επιλεκτικά μέσω της αυτοφαγίας, ειδικά σε συνθήκες θερμιδικού περιορισμού in vivo. Παραδόξως, πρόκειται για μία αμφίδρομη αλληλεπίδραση, καθώς οι νεσπρίνες φαίνεται να προάγουν τον σχηματισμό αυτοφαγοσωμάτων, που θα μπορούσε ενδεχομένως να δρα ως αρνητική ανατροφοδότηση. Επιπλέον, διαπιστώνουμε ότι η αυτοφαγία που επάγεται από πείνα, μέσω των νεσπρινώνκαθορίζει το μέγεθος του πυρηνίσκου μέσω ενός νέου και εξελικτικά διατηρημένου κυτταρικού μηχανισμού με το να ελέγχει τα επιπέδα της φιμπριλαρίνης, της βασικής πρωτεΐνης του πυρηνίσκου. Επισημαίνουμε το γεγονός ότι η φιμπριλαρίνη είναι υπόστρωμα της αυτοφαγίας που επάγεται από πείνα. Υπό θερμιδικό περιορισμό, που προκαλεί παράταση στη διάρκεια ζωής, η αυτοφαγία και οι νεσπρίνες δρουν στο ίδιο μοριακό μονοπάτι για τη ρύθμιση της

ριβοσωμικής βιογένεσης. Αυτός ο διακριτός μηχανισμός πυρηνοφαγίας θα μπορούσε να λειτουργήσει ως ρεοστάτης για τη φυσιολογική γήρανση.

I. Nucleophagy & Aging

1. Introduction

1.1 General autophagy

Autophagy from the Greek words “auto,” self, and “phagy,” eating, is a physiological eukaryotic mechanism which maintains cellular homeostasis. It is the main cellular catabolic pathway, which breaks down macromolecules such as proteins, lipids, and organelles, through the main degradative compartment, the lysosome. Although it was initially considered to be a bulk degradation pathway, recent evidence underlines its highly selective nature. This tightly controlled stepwise mechanism takes place at basal levels under physiological conditions but can be induced by several cellular stresses, such as nutrient deprivation, oxidative stress and DNA damage. It can be subdivided into three mechanisms, macroautophagy, thereby referred to as autophagy, microautophagy and chaperone-mediated autophagy (Figure 1) [1].

Autophagy consists of the formation of a double membranous vesicle, the autophagosome, which encircles the cargo to be degraded. Specificity and selectivity is accomplished through recruitment of selective autophagy receptors or adaptors. Yeast Atg19 and mammalian p62/SQSTM1(sequestosome 1) are examples of receptors which mediate the interaction between core autophagic components and substrates

through different domains discussed below [2].

Briefly, initiation of autophagy involves Atg1/Unc-51-like, autophagy activating kinase (ULK1), ATG13 and FIP200 which trigger phagophore formation followed by vesicle nucleation through class-III phosphatidylinositol-3-kinase (PI3K) complex which comprises of VPS34, VPS15 and Beclin-1 [3].

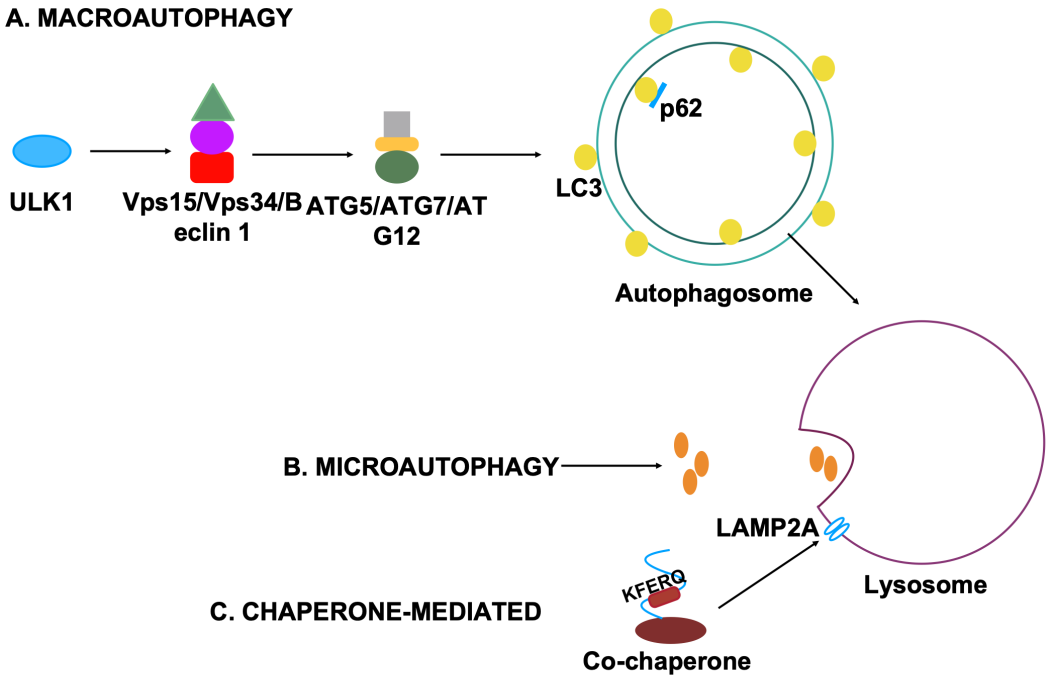

Figure 1. Schematic diagram of autophagic pathways

Autophagy receptors interact with ubiquitin- like proteins (UBLs), small globular proteins, such as the yeast Atg8 or mammalian LC3 (microtubule-associated proteins

1A/1B light chain 3), required for autophagosomal biogenesis and recruited to the autophagosomal membranes through phosphatidyl-ethanolamine (PE) conjugation, which causes the conversion of LC3-I to the membrane bound form, LC3-II. The Atg5/Atg12 complex aids the maturation of the autophagosome. An Atg8-interacting motif (AIM)/ LC3-interacting region (LIR) is found in selective autophagy receptors and targeted by Atg8/LC3. The general core motif, which includes W/F/Y-X-X-L/I/V, contains negatively charged residues upstream of the motif and allows for a higher affinity interaction as well as additional post-translational modifications, such as phosphorylation[4] Autophagic receptor proteins contain domains such as the UBA motif, which recognizes ubiquitinated proteins for degradation. K27-linked mono-ubiquitination and K63 poly-ubiquitination are the most prominent examples of tagging for autophagosomal recycling [5]. εDifferent selective autophagy receptors exist depending on the substrate to be degraded. Protein aggregate degradation, aggrephagy is mediated by proteins such as p62, optineurin, NBR1 (neighbor of Brca1) and NDP52 (nuclear dot protein 52 kDa). For instance, NBR1 and p62 proteins act as cargo receptors for selective autophagy of ubiquitinated targets [6-8]. Organellophagy, the autophagic recycling of organelles can occur with the concerted action of the receptors and adaptors referred to above in combination with more specific ones, such as the BCL2 and adenovirus E1B 19-kDa interacting protein 3 (BNIP3), and FUN-14 domain containing protein 1 (FUNDC1) for mitophagy.

Mutations in autophagic receptors can lead to severe phenotypes such as metabolic disorders, neurodegenerative and age-related disease [9].

In mitophagy, there are several proteins on the mitochondria or targeting the mitochondria modulating mitochondrial degradation. Mutations in the PINK1 and Parkin proteins, which are involved in the ubiquitination of outer mitochondrial membrane proteins that are then recognized by autophagic adaptor proteins such as p62, OPTN and NDP52, cause Parkinson's disease [10]. Optineurin mutations have been associated with amyotrophic lateral sclerosis (ALS). Moreover, mutations in the PEX5 gene cause the fatal cerebro-hepato-renal Zellweger syndrome. PEX5 encodes a pexophagy-specific receptor, that is then ubiquitinated to interact with p62 and then transported to the autophagosome. These examples highlight the intricate relationship of autophagic receptors and substrates in orchestrating selective autophagy [11, 12].

1.2 *Caenorhabditis elegans* & autophagy

C. elegans is an easy-to-use invertebrate model organism used for investigation of a large variety of cellular processes. Its transparency, genetic amenability, cell traceability and our detailed knowledge of its anatomical features and developmental stages allow for *in vivo* physiological studies both at the organismal and the cellular level. Its short lifespan, reproducibility and growing in large numbers offers unique

experimental opportunity to investigate the coping molecular mechanisms against physiological stress such DNA damage and nutritional stress [13].

Proteins LGG-1 and LGG-2 are homologous to yeast Atg8/mammalian LC3B (cytosolic microtubule-associated protein 1 light chain 3-MAP1LC3). The transgenic reporter strain [$p_{lgg\text{-}1}$GFP::LGG-1; rol-6(su1006)] expresses GFP mainly in seam cells, hypodermis, and intestinal cells Autophagic receptors exist in selective autophagy as well (14). The *C. elegans* homolog of mammalian SQSTM1/ p62, SQST-1 (SeQue-STosome-related protein) has a dual role as an autophagic receptor, but also as an autophagic substrate being degraded via autophagy. Visualization of SQST-1 is challenging under physiological conditions at larval and adult stages, most probably due to the basal rate of basal autophagic flux. However, it is a suitable autophagy reporter under autophagy suppressed conidtions where SQST-1 levels are elevated in tissues such as the epidermis, neurons, and intestine [14]. Upon nutrient deprivation or starvation, *C. elegans* upregulates autophagy to cope with this unfavorable condition. Other assays that induce both general and selective macroautophagy are crowding, hypoxia, heat, and oxidative and DNA damage-induced stress.

Genetic manipulations that influence longevity have been repeatedly associated with autophagy, and in some cases, autophagy is required for their effects on life span.

For instance, the *eat-2(ad1116)* mutant is a feeding-defective dietary restriction genetic model which has been shown to have higher basal levels of autophagy ultimately extending lifespan [15]. Mutations in the gene encoding the insulin/IGF-1-like receptor abnormal Dauer Formation 2 (DAF-2) extend the life span and activate autophagy. This life span extension requires both the activity of DAF-16/FOXO and autophagy. Likewise, autophagy is required for life span extension by dietary restriction in *C. elegans*. Moreover, suppression of autophagy prevents life span extension by dietary restriction and TOR inhibition, which is known to mediate, at least in part, the beneficial effects of dietary restriction on longevity. Chemical suppression of autophagy has been widely used in higher eukaryotes. Cell culture experiments are usually conducted to investigate the effects of exogenous agents on autophagic responses, as there are no paracrine effects or boundaries that can affect the readout of the experiment. *In vivo* experiments need much higher chemical concentrations for longer periods of time. Bafilomycin A1 is a V-ATPase inhibitor that blocks the autophagic flux acutely by inhibiting lysosome acidification and autophagosome-lysosome fusion.

1.3 Autophagy in aging

Autophagy has been shown to be a mediator of longevity and healthspan in several cases. Both general autophagy and selective autophagy have been shown to pro-

mote lifespan extension [16]. Short and long-lived mutants transcriptome analysis in yeast reveals the importance of autophagy in fighting aging, while its amino acid deprivation-mediated lifespan extension cannot occur without autophagy [17]. In a similar fashion, *Caenorhabditis elegans* autophagy mutants for *unc-51, bec-1, atg-7, atg-12 and atg-18* have a shortened lifespan [18]. Autophagy gene expression is reduced in neurons of old *Drosophila melanogaster*, autophagy gene RNA levels are lower in older neurons, while loss of Atg8 decreases lifespan [19]. Complementarily, overexpression of Atg1 and Atg8 promotes lifespan extension. The master transcriptional factor regulator of autophagy, TFEB/HLH-30 has been shown to extend lifespan in the nematode [20]. In mice, increased Atg5 prolongs lifespan while aged brains demonstrate low levels of Atg5, Atg7 and Beclin-1 [1, 21, 22].

Cell signaling pathways that modulate autophagy levels and determine longevity include insulin/insulin-like growth factor (IGF-1) signaling. Lifespan extension due to low insulin signaling in *C. elegans daf-2* mutants is perturbed upon autophagy inhibition [23]. Moreover, a correlation between longevity and IGF1 mutations is evident in centenarians [24]. Inhibition, genetic or pharmacological, of another signaling pathway, the mammalian target of rapamycin (mTOR), by rapamycin, which mimics nutrient deprivation inducing catabolic processes such as autophagy while halting anabolic protein synthesis, has been shown to extend lifespan from single cell eukaryotes until mice [25, 26].

Resveratrol and spermidine are naturally occurring chemicals which have been shown to induce autophagy and extend lifespan. Importantly, dietary restriction has been shown to induce longevity and health span in all species tested and most importantly in humans. Autophagy is essential for dietary restriction-mediated longevity [27, 28].

Both general and selective autophagy defects are apparent in age-related pathologies. Tissue-specific autophagy gene knockout mice have been used instead of traditional knockouts that have developmental defects and postnatal lethality [1]. Autophagy gene conditional knockouts demonstrate age-related phenotypes. In the central nervous system, *Atg7* knockout neurons contain ubiquitin-positive inclusion bodies, uncoordinated movement and premature death [29]. In Huntington's or Alzheimer's disease, in which huntingtin or amyloid-beta protein aggregate respectively, pharmacological activation of autophagy ameliorates disease symptoms [30]. Defective mitophagy triggers mitochondrial reactive oxygen species accumulation, mitochondrial DNA damage, defective mitochondrial dysfunction, impaired stress resistance and leading to overall reduced cellular fitness and in a cell-specific context, neurodegeneration [9].

Macrolipophagy triggered by caloric restriction reduces lipid droplet storage, metabolic disease and age-related lipid deposition. Moreover, p62 absence can induce obesity, glucose and insulin intolerance accentuating its significance in metabolic health [31, 32].

1.4 The nucleus

The nucleus is the largest organelle of the cell, however, the mechanism(s) underlying its recycling in terms of receptors, substrates and particular signaling pathways are not well understood. The nucleus consists of a vast variety of macromolecules which can be exclusively nuclear or constantly interchange between the nucleus (nucleoplasm) and the cytoplasm through its phospholipid bilayer. The ER is continuous to the nuclear membranes, although quite different in protein composition [33]. The inner nuclear membrane consists mainly of the nuclear lamina, such as lamins, SUN proteins, emerin and HP1 which directly interacts with chromatin and affects its localization and thus gene expression. SUN proteins interact with nesprins (SYNEs), which are outer nuclear membrane proteins connecting the nucleus with the cytoskeleton. SUN proteins together with nesprins form the LINC complex (linker of the nucleoskeleton-cytoskeleton complex). Nesprins regulate nuclear migration, nuclear shape and nucleocytoplasmic shuttling. Nuclear compartments in the cytoplasm range from DNA, RNA, the nucleolus, nuclear bodies, and proteins regulating DNA replication, transcription.

1.5 Nucleophagy in yeast

Nucleophagy was initially described in *Saccharomyces cerevisiae*, in two forms, piecemeal macronucleophagy (PMN) and late nucleophagy (LN). Yeast perform mi-

cronucleophagy as well as macronucleophagy[34]. TORC1 (target of rapamycin complex 1) inactivation induces nucleophagy through the Nem1/Spo7-Pah1 axis, which properly localizes micronucleophagy component Nvj1 (nucleus-vacuole junction 1) and nucleophagy receptor Atg39 [35].

PMN occurs under basal conditions, mTOR inactivation after rapamycin treatment and short nutrient (nitrogen) deprivation. The lytic vacuole, the organelle which contains the degradative (lytic) enzymes, and the nucleus directly interact with the formation of tight nuclear-vacuole junctions (NVJ). Then, the outer nuclear membrane and nuclear ER form protrusions, transform into ER-derived vesicles which are then encircled by the lytic vacuole [36]. Subsequently, vesicles are pinched off the nuclei and nuclear-derived membranes fuse at multiple sites with the vacuole membrane for the release of autophagic substrates. The outer nuclear membrane nucleus to vacuole protein

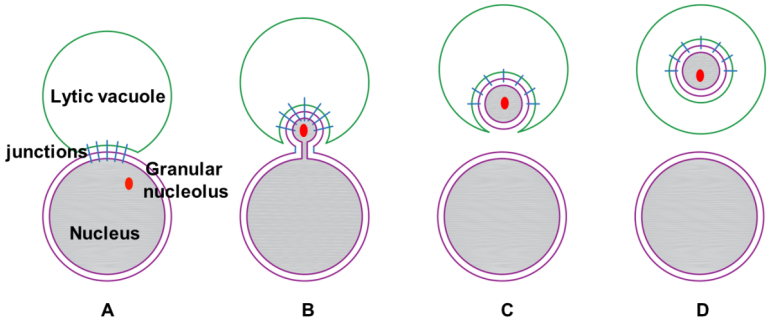

Figure 2. Yeast micronucleophagy. The nucleus (purple) directly interacts with the lytic vacuole (green) via tight junctions, bulges in and ultimately part of the nuclear membrane together with nuclear components such as the granular nucleolus, is encircled bu the vacuole and is pinched off to be degraded (41).

1 (Nvj1p) and vacuolar protein 8 (Vacp8) are selective autophagic receptors which mediate micronucleophagy, Autophagic substrates of PMN consists of nuclear envelope components, Cytoplasm-to-vacuole targeting pathway is performed by Vacp8 together with Apg13p [37].

Although initially suggested that core autophagic proteins are involved in this process, recent evidence shows that endosomal sorting complex proteins such as Vph1, Pho8 and Vps27 are required in microautophagy rather than macroautophagic proteins [38]. Non selective RNA degradation has been reported after nitrogen starvation, however whether the RNA is directly directed to the lytic vacuole from the nucleus or first transported to the cytoplasm to be degraded by general autophagy is unknown [39]. However, it is not known whether nuclear RNA is directly degraded or whether cytoplasmic RNA is recycled by general autophagy after transported to the cytoplasm. Autophagic cargo of PMN includes nuclear envelope components, the granular nucleolus with pre-ribosomes without nuclear pores, spindle pole bodies and RNA[40].

CLIP and cohibin mediate nucleolar protein degradation by restricting them from ribosomal DNA which is undegraded, by tethering them to the outer nuclear membrane,

and directing them proximal to NVJs 25. In this process, a protein complex Rpd3-Sin3 histone deacetylase (HDAC), and high-mobility group protein 1 (Hmo1) are responsible for ribosomal DNA condensation.

PMN and LN are almost invariably temporally and spatially mutually exclusive (table 1). Late nucleophagy is an example of macronucleophagy only induced after prolonged nitrogen starvation, and unlike PMN, causes nuclear morphology modifications, implying aggregation of nuclear cargo that is not degraded. They can be differentiated by two reporters Nvj1p-EYFP, for the former and n-Rosella for the latter [41]. LN requires Nvj1p, Vacp8 as well as other autophagic proteins, such as Vps34p, Vps15p, Atg6p, and Atg14p or Atg11p.

Another type ERphagy and nucleophagy has been also shown in yeast with the Atg39 receptor, found on the perinuclear ER, being required for macronucleophagy, while Atg40 mediates ERphagy and also contributes to macronucleophagy. These receptors are also substrates of macroautophagy. This type of macronucleophagy also degrades outer and. inner nuclear membrane proteins such as Hmg1, Src1, and nucleolar protein Nop1. No exact homolog has been found in mammals although functionally similar for theses nucleophagy receptors [42].

1.6 Interplay between autophagy and the nucleus in mammals

The crosstalk between autophagy and the nucleus in mammals has only recently been investigated. Acetylated LC3 pools are stored in the nucleus under normal conditions [43]. Under starvation, LC3 is deacetylated at K49 and K51 residues by Sirt1, to be transferred to the cytoplasm by the DOR protein. There, LC3B is embedded in autophagosomal membranes by lipidaton. It is still unknown whether LC3 localization in the nucleus has other functional purposes other than storage.

Moreover, other autophagic proteins, such as selective autophagy receptors are also localized in the nucleus, the function of which remains largely unexplored (Figure 2). p62 shuttles between the nucleus and the cytoplasm along with large autophagic adaptor protein ALFY. Together, they target ubiquitinated proteins to PML bodies found in the nucleus. Moreover, upon stress, ALFY becomes localized with p62 to ubiquitin-positive bodies in the cytoplasm [44]. Moreover, ATG5 and ATG7 localized in the nucleus modulate p53 induction and cell cycle progression as well as autophagy [45]. Atg7 modulates p53 activity to regulate cell cycle and survival during metabolic stress [46].

Table 1. Yeast nucleophagy

Factors	Piecemeal nucleophagy	Late nucleophagy	Mammalian nucleophagy
Macroautophagy genes	atg1, atg2, atg3, atg4, atg5, atg7, atg8, atg9,atg13, atg18, atg17, atg29, atg31	atg1, atg2, atg3, atg4, atg5, atg7, atg8, atg9, atg10, atg12, atg13, atg16, atg18, atg23, atg29, atg31	Atg7, Lc3
Receptor	Nvj1p, Vac8p	Atg39	-
Substrates	nuclear envelope components, granular nucleolus, pre-ribosomes, spindle pole bodies, RNA	nuclear envelope components, granular nucleolus, pre-ribosomes, spindle pole bodies, RNA, Hmg1, Src1, Nop1	Lamin A, Lamin B2
Pathway/Inducer	Short nitrogen starvation, TORC1 inactivation, Nem1/Spo7-Pah1 axis	Prolonged nitrogen starvation, TORC1 inactivation, Nem1/Spo7-Pah1 axis	DNA damage, Oncogenesis
Phenotype	-	Nuclear shape alterations	Cell death, neurodegeneration, senescence

Whole nuclei degradation has been shown in filamentous fungi. They consist of multinucleate cells called hyphae that divide from the hyphal tip. Basal cells 'eat' their nuclei among other selective modes of autophagy such as pexophagy and mitophagy (49). It is implicated that autophagosomes containing nuclei are different and specific as they are much bigger. Colony growth is inhibited upon perturbation of autophagy, indicating that autophagy and potentially catabolic products from nucleophagy are required for survival and proliferation under nutrient deprivation, given that nuclei contain phosphorus and nitrogen. Therefore, in this case, nucleophagy is most likely an energy source for survival.

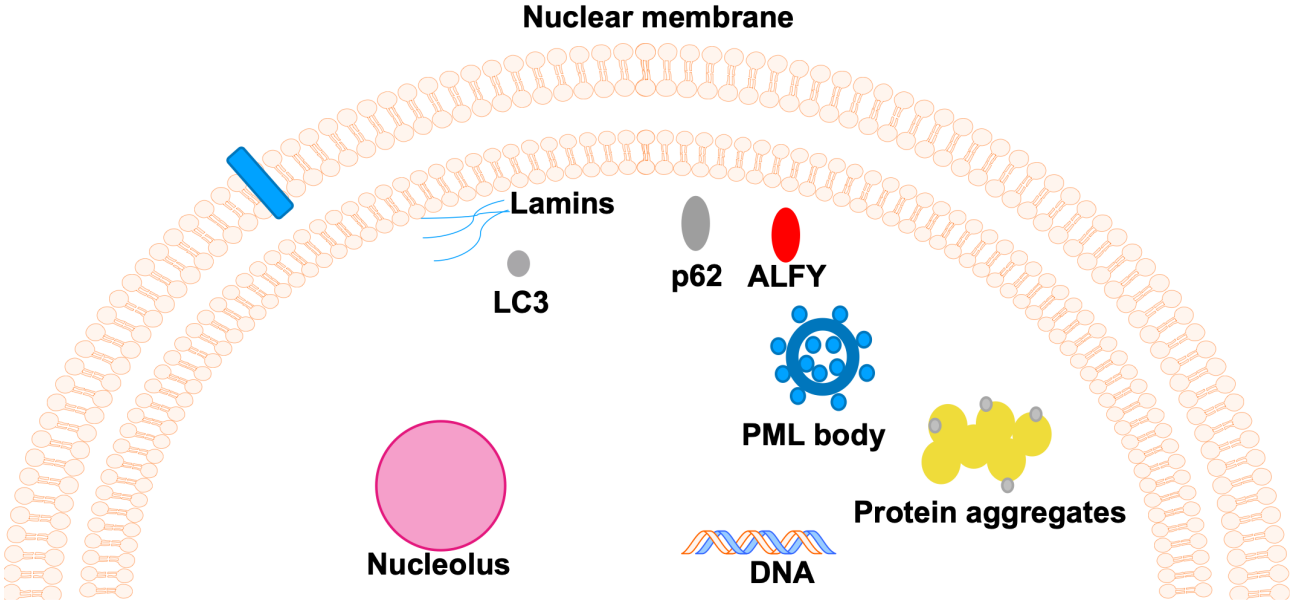

Figure 3. Schematic diagram of interplay between autophagy & the nucleus(50)

Nucleophagy has also been detected during cell differentiation of skin epidermal keratinocytes. As these cells moved from the epidermis to the granular layer, they change into corneocytes that are cells without a nucleus (51). Perinuclear LC3 positive vesicles containing p62 and HP1α are observed in close proximity to lamins. Nucleophagy is also apparent in transformed cells. Electron microscopy has revealed nuclear alterations in shape, size and patterns. Chromosomes, protein, and PML bodies are relocalized, while the nucleolus, becomes enlarged to satisfy the excessive protein synthesis needs of the cancer(52). The first undisputed example of mammalian nucleophagy was observed in mutated KRAS primary human cells (53).

Nuclear LC3 directly interacts with lamin B1 through its LIR sequence and together shuttled with heterochromatin to the cytoplasm for lysosomal degradation. In contrast to yeast, starvation or mTOR inhibition does not trigger this response, accentuating the specificity of iffernet modes of nucelopagy in different species. Genetic inhibition of this type of nucleophagy leads to premature senescence, although the exact mechanism has not yet been elucidated. Another context where lamin B has been detected to be an autophagic substrate is during photoaging (54).

Cellular DNA has been shown to cause autoimmune disorders when not degraded by transport to the cytoplasm and lysosomal degradation. A deficiency in the enzyme responsible for DNA degradation, Dnase2a or autophagy dysfunction causes extra-nu-

clear DNA aggregation which in turn triggers a severe inflammatory response through the STING DNA sensinsg pathway (55).

Dysfunctional selective autophagy in neurodegneration is prominent, where protein and organelle aggregation is a direct result of defective autophagy. Polyglutamine (PolyQ) diseases are triggered by expansion of CAG repeats in the genes encoding PolyQ proteins. Dentatorubral-pallidoluysian atrophy which causes ataxia, dementia and

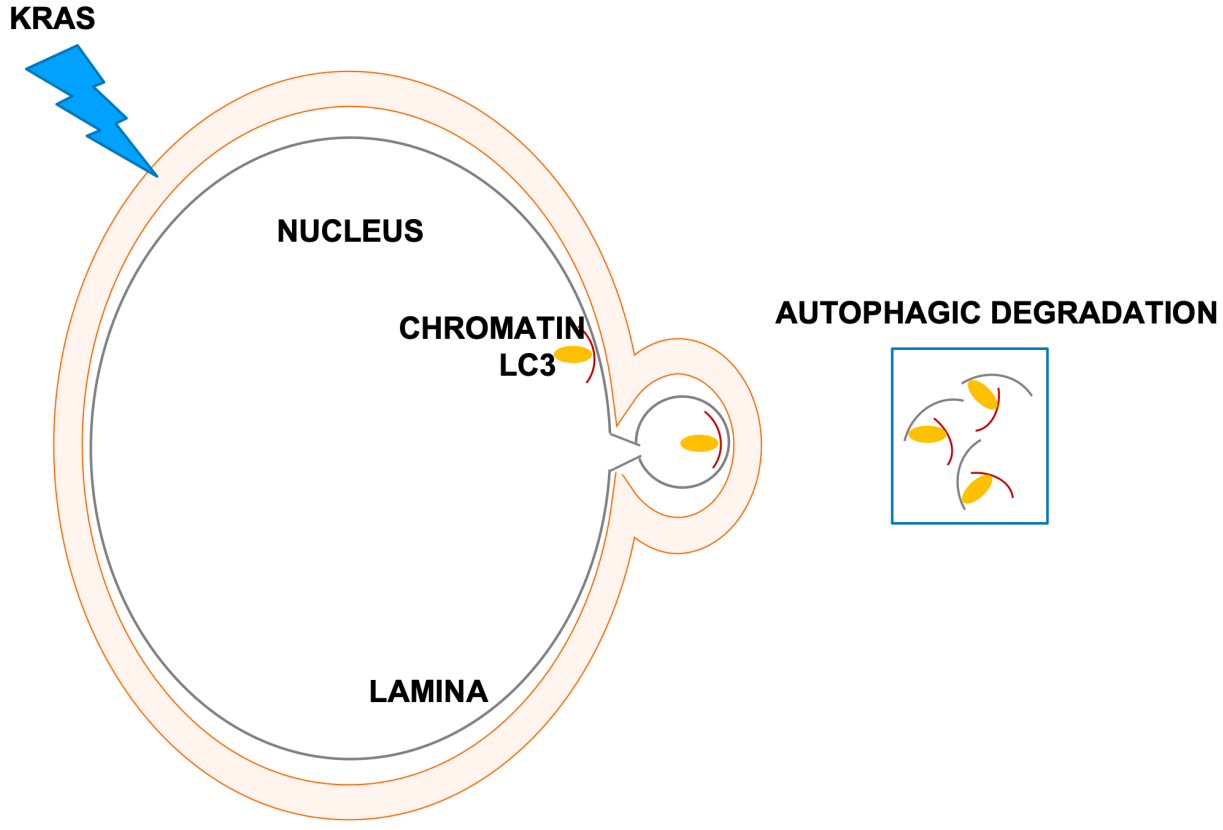

Figure 4. Schematic diagram of oncogenic nuclear autophagy(41)

epilepsy, is triggered by atrophin mutations, and demonstrates a peculiar pathological mode of nucleophagy (14, 56).

In this scenario, physiological autophagy is halted, while Golgi membrane degradation and nuclear breakdown is triggered via lamin B degradation and cell secretion. At the same time, there is reduction in autophagic flux, p62 increase and sing of DNA damage and senescence. Blockage of autophagy with concomitant activation of alternative degradative pathways causes nuclear morphology malformation and destruction and finally cellular atrophy. Apart from very specific examples such in the case of fungi, nucleophagy has been depicted in disease. Both in cancer and neurodegeneration, nucleophagy is activated to clear out nuclear DNA or protein aggregates. Therefore, we know that the nucleus protects genetic material and modulated its expression, thus, it is essential to better understand the effect of nucleophagy in maintaining nuclear homeostasis, both in physiology and pathology. Nucleophagy is potentially a protective mechanism against age-related disease.

1.7 Nuclear abnormalities in aging

In *C. elegans,* complete intestinal nuclear loss or reduced DNA copy number has been detected during aging (57). *Daf-2* long-lived animals show a delay in the presentation of reduction of DNA copy number implying that the insulin/IGF1 signaling pathway at least partially regulates the loss of nuclei (58). It is assumed, like in the case of fungi

referred to above, that autophagy degrades nuclei during aging, to supply nutrients. Nuclear morphology defects occur in malignancy which could be the result of DNA, nuclear protein or envelope protein accumulation. Nuclear envelopathies include mutations in genes encoding nuclear membrane proteins. Emery-Dreifuss muscular dystrophy and dilated cardiomyopathy, are caused by mutations in *LMNA, emerin* and *nesprin1/2* (59-61). Myocytes from such patients have enlarged nuclei. Senescence occurs upon nesprin perturbation, which is potentially attributed to the compartmentalization of the extracellular signal-regulated kinase 1/2 to PML bodies residing in the nucleus (62).

Nuclear inclusion body diseases are prominent in neurodegenerative diseases such as Huntington's disease, spinocerebellar ataxias (SCAs) and spinobulbar muscular dystrophy where mutant huntingtin, ataxin and androgen receptor aggregate respectively. Moreover, multiple muscle atrophy is presented with filamentous nuclear aggregates associated with the nucleolus or the inner nuclear membrane, while inefficient protein clearance can also cause neurological defects and neuronal cell death (67).

Concerning the nucleolus, its shape, size and composition is used as an aging biomarker. More generally, nucleolar size is predictive of organismal lifespan irrespectively of cell type in both *C. elegans* and mammalian cells. In *C.elegans, daf-2, eat-2, ife-2* and *glp-1* long-lived mutants contain. cells with smaller nuclei compared to those of

their wild type counterparts. The NCL-1 protein the translational repressor of fibrillarin1. Inhibition of *ncl-1* expression results in fibrillarin-1 derepression and lifespan shortening. Complementarily, *fib-1 RNAi* extends the lifespan of wild type worms. Enlarged nucleolar size is not merely an aging biomarker but actively contributes to the aging process. Signaling pathways extend lifespan, at least partially ,through negatively modulating nucleolar expansion and ribosomal biogenesis. Similarly, in aging syndromes such as Hutchison-Gilford progeria syndrome, cells demonstrate larger nucleoli, implying increased ribosome biogenesis and protein translation rates (65). Progerin which is a mutant form prelamin A, causing progeria syndrome also increases nucleolar size. This protein is degraded and symptoms are ameliorated by mTOR inhibitor and autophagy inducer rapamycin (66).

The germline anatomy of the nematode is well-characterized (Figure 5). The adult hermaphrodite contains two U-shaped tubular arms [47] with a distal to proximal polarity from germ cell mitosis, to meiosis followed by gametogenesis. The distal end contains the distal tip cells which are proliferative. Moving proximally, germ cells undergo meiosis. At the loop region, germ cells undergo programmed cell death, apoptosis with the aid of the somatic gonad, the gonadal engulfing sheath cells. This ultimately leads to gamete production.

Figure 5. *C. elegans* germline

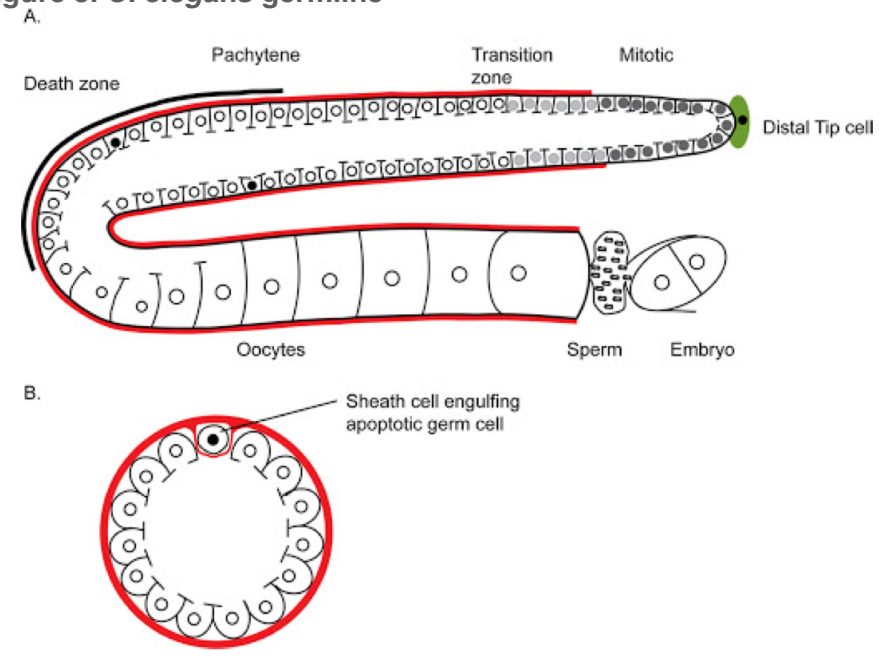

Biomarkers of reproductive aging include germ cells as well as oocytes with larger nucleoli, which contributes to lower oocyte quality and decreased fertility (63, 64). In *C. elegans,* the mature oocyte which is ready to be fertilized physiologically loses nucleolus while transcription is halted [48]**.** Evident nucleoli in the last oocyte (-1) are associated with lack of maturation, low quality or aged oocytes (Figure 5). Low quality oocytes are also usually smaller in size and not stacked in a linear fashion. Moreover, aberrant multinuclear germ cells that are not cleared out by physiological apoptosis form multinucleate oocytes. Similarly, in mammals, germline aging is synonymous to poor oocyte quality which leads to infertility, miscarriages and birth defects. More specifically, more prominent and dense fibrillar centers as well as double fibrillarin expression are

evident [49]. Increased fibrillarin expression is coupled with increased ribosomal production (proteins and rRNA) and protein translation discrepancies.

The relationship between somatic and germline aging is highly controversial. The theory of the disposal soma [50]. This theory supports that organismal energy expenditure is dedicated to proofreading, to prevent germline damage, that ultimately ensures germline stability for the evolution of the species. In parallel, an entry saving strategy is employed in the soma, where error regulation is not highly controlled which causes gradual defect accumulation in somatic tissues [51]. Importantly, recently, this crosstalk between germline is soma has been shown to be bidirectional. Specifically, DNA damage in germ cells activates ERK/MPK signaling which in turn causes peptide secretion to the soma. The soma then upregulates proteostasis and global stress resistance to delay somatic aging when the germline is compromised and until it is repair [52]. More recently, germline mutation rates have been directly associated to both germline and somatic aging [53].

1.8 Aim

Gradual destruction of nuclear architecture is a common denominator of aging and variable age-related pathologies, in diverse species. Progeroid syndromes and aging-related diseases are associated with nuclear abnormalities and aggregation In aging, cells harbor expanded nucleoli, while on the other hand, longevity and lifespan-ex-

tending interventions have been associated with small nucleolar size. The mechanism that causes these alterations remains undiscovered. In addition, it is still uncertain to what extent these phenotypes are merely byproducts of the aging process or have a functional, causal role in senescence. Moreover, the contribution of signaling pathways that control lifespan and nuclear morphology during both somatic & reproductive aging is not well understood. Examination of the involvement of nuclear material-selective autophagy, and nuclear autophagic substrates in the preservation of nuclear and nucleolar homeostasis will be performed in this study. We will use both *C. elegans* and mouse exploiting each model's experimental advantages.

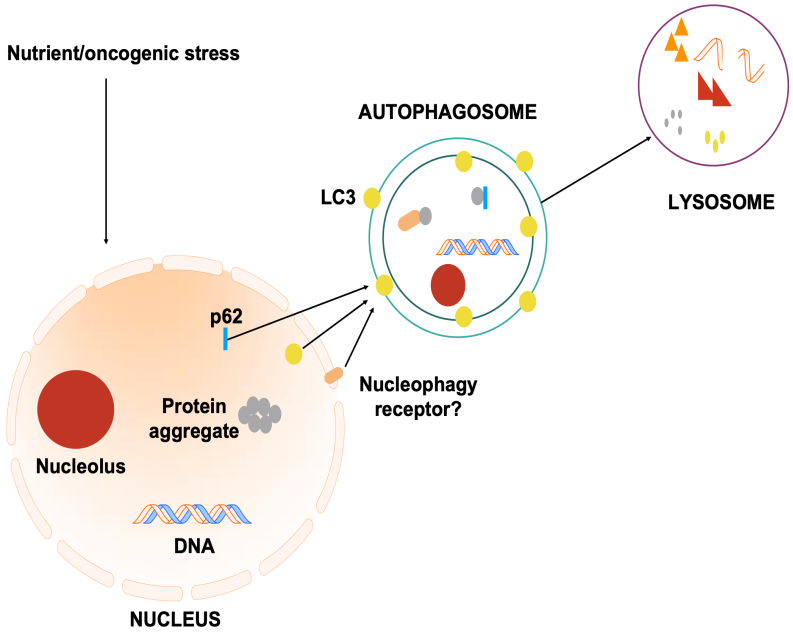

Figure 6. Potential Nucleophagy mechanisms(41)

2. Materials & Methods

Ethics statement. All mouse experiments were performed according to National and European guidelines for the Care and Use of Laboratory Animals. Protocols were approved by the Foundation for Research and Technology-Hellas (FORTH) Ethics Committee (FEC).

2.1 *Caenorhabditis elegans* strains.

Strains were maintained at 20°C unless otherwise noted. The following strains were used in this study: N2: wild-type Bristol isolate, CB3339: anc-1(1753),DA465: *eat-2(ad465), ccIs4810 [(pJKL380.4)* p$I_{mn\text{-}1}$LMN-1:GFP + (pMH86) dpy-20(+)],COP262: *knuSi221 [*p$_{fib\text{-}1}$FIB-1::GFP*; unc-119(+)], HZ*589: *him-5(e1490), bpIs151* [p$_{sqst\text{-}1}$SQST-1::GFP, unc76(+)], HZ946: *rpl-43(bp399)*, bpIs151 [p$_{sqst\text{-}1}$SQST-1::GFP, unc76(+)], bpIs168[p$_{nfya\text{-}1}$DFCP1::GFP; unc-76(+)], and *atg-2(bp576),*bpIs168[p$_{nfya\text{-}1}$DFCP1::GFP; unc-76(+)], KX15Ex[p$_{ife\text{-}2}$GFP, pRF4], OD95 ltIs37[(pAA64) p$_{pie\text{-}1}$::mCherry::his-58+unc-119(+);ltIs38 p$_{pie\text{-}1}$::GFP::PH(PLC1delta1)], WS4581 *opIs263*[p$_{rpa\text{-}1}$::RPA-1::YFP + unc-119(+)], AM141:rmIs133 [p$_{unc\text{-}54}$::Q40::YFP], JJ1850: uIs178[his-72(1kb 5' UTR)::his-72::SRPVAT::GFP::his-72], UD626: anc-1(yc72[mKate2::anc-1b], UD612: anc-1(yc68[GFP:anc-1b].

2.2 Molecular cloning.

anc-1, bec-1, daf-2, lgg-1, bec-1, ced-3, ced-4, ced-9, ife-2 RNAi constructs were engineered by PCR amplification of genomic DNA, using the following primer sets respectively:
FW: 5'-AAGAGTTGAGACGTGCTCTCC-3',

RV:5'-ACAGGATCATCGATTGTGTCCAG-3',

FW: 5'-GCTCTAGAGTTATCACAGAAGCTCTG-3',

RV:5'-GCTCTAGAGTTATCACAGAAGCTCTG-3',

FW: 5'-CGGGATCCTGTGCCCACGTGGAGCTT-3',

RV: 5'-CCGCTCGAGTGAATAGCGTCCGAA TCGA-3'

FW: 5’-GGAATTCAAGTGGGCTTACAAGGAG-3’

RV: 5’-GGAATTCGTCTTCTTCGTTTATTCATG-3’

FW: 5’-GCTCTAGAGTTATCACAGAAGCTCTG-3’

RV: 5’-CGGGATCCGTCCATACAATGCGTACG-3’

FW: 5’-GGATCCATGATGCGTCAAGATAGAAG-3’

RV: 5’-AAGCTTTGCTGAATGAGCGATTACGAC-3’

FW: 5’-AAGCTTTGCTGAATGAGCGATTACGAC-3’

RV: 5’-GGATCCAGCTCGGCCGTGTAGAAACAG-3’

FW: 5’-ATGACACGCTGCACGGCGG-3’

RV: 5’-CTTCAAGCTGAACATCATCCGCCC-3’

FW: 5’-CGGGATCCAGCAAGTAATGTCCGAAG-3’

RV: 5’-AACTGCAGCATTTCAACAAGTGAAGAAC-3’

The resulting fragments were subcloned into the pL4440 plasmid vector. The plasmids constructed were then individually transformed into HT115(DE3) *Escherichia coli* bacteria. Bacteria carrying an empty plasmid vector were used as control.

2.3 Stress assays

Synchronous populations of worms were generated by treating gravid adults with bleaching solution (H_2O:Bleach:5N NaOH 7:2:1). Animals were washed 3 times in M9 buffer and then incubated in M9 buffer on a rotor. On day 5 and day 10, 30µl of M9 was placed on an NGM plate and after 1 hour, the percentage of alive L1 (larvae stage 1)

worms was measured. For heat stress day 1 adult animals were placed in a 37°C incubator for 1 hour and survival was scored at day 2 and day 4 of adulthood. Chloroquine (Biovision, 1825) was added on plates at 5µm concentration 3 hours before imaging.

For UV-C induced DNA damage, day 1 worms were plated on UV-killed OP50 bacteria and treated with either 200J m^{-2} or 200J m^{-2} UVC irradiation using an ultraviolet crosslinker (BIO-LINK-BLX-E365, Vilber Lourmat) (83). 1 day later worms were scored for survival. For DIC and fluorescence microscopy of RPA-1::YFP worms, 16-18 hours after UV-C treatment, worms were gently washed once from bacteria using M9. Worms were then immobilized using 15µl 20mM levamisole and mounted on slides. Microscopic examination of cell or neuron corpses were detected at 40X magnification using DIC with a Zeiss AxioImager Z2 epifluorescence microscope.

2.4 Egg laying assay

L4 worms from each strain (10 worms/per strain) were separately plated on NGM plates at 20°C and 25°C. Eggs were counted and directly removed for the next three days. 10 larvae from the next generation, offspring, were then transferred from each plate of each strain to measure their egg laying capacity. This was repeated until no eggs were detected in the plates of *anc-1* mutant worms placed at 25°C.

2.5 Fluorescent recovery after photobleaching (FRAP)

Day 1 adult nematode worms were treated with RNAi for 24 hours or with protein translation inhibitor cycloheximide (500µg/ml) 2 hours prior to. photobleaching. Photobleaching was performed using an epifluorescence microscope for 7 minutes (ZEISS, model:Axioskop 2 Plus). Images were captured immediately before, immediately after, and every hour for the next 6 hours after photobleaching. The experiments were performed four times and a representative regression analysis is presented, illustrating the general trend, with the best fit line and its respective equation and R^2.

2.6 Lifespan assays

Lifespan assays under *RNAi* were performed at 20^{o}C unless otherwise noted. Synchronisation of animal populations was performed as referred to above in the survival assay, on RNAi plates containing 2mM IPTG and seeded with HT115(DE3) *E. coli* bacteria, transformed with the pL4440 plasmid vector. Next generation L4 worms were transferred onto NGM plates, seeded with HT115(DE3) *E. coli* bacteria, transformed with either the pL4440 plasmid vector, or the specific test RNAi plasmid construct. 20 animals were used per plate for a total of 200 individuals per experiment. Animals were transferred to fresh plates every 2-4 days. Touch-provoked movement and pharyngeal pumping was assessed until death. Animals which died due to gonad extrusion or internal egg hatching were removed. Survival curves were repeated at least

twice and representative graphs are shown here. Survival curves were drawn using the product-limit method of Kaplan and Meier. The log-rank (Mantel–Cox) test was used to evaluate differences between survivals and determine P values. We used the Prism software package (GraphPad Software, San Diego, USA) for statistical analysis and to determine lifespan values.

2.7 Mouse Models

All animal protocols were approved by the FORTH Ethics Committee (FEC). All mice were maintained in a pathogen-free environment and housed in clear shoebox cages, in groups of five animals per cage with constant temperature and humidity and a 12 hr/12 hr light/dark cycle. All animals used were male mice of C57BL/6 genetic background. Adult animals were used as indicated in the text. Food deprivation was initiated in the morning, for a total duration of 24 hrs, with free access to water.

2.8 Quantitative RT-PCR

For mRNA quantification, total RNA isolation from heart, liver, kidney and different brain areas was performed using the Trizol reagent (Thermo Fisher Scientific, USA). cDNA synthesis was performed using the iScript kit (Biorad, USA). qPCR was performed with the Eva Green qPCR Kit (Biotium, USA). All kits were used following the manufacturer's instructions. The following oligonucleotides were used for mRNA quantification:

18S rRNA, FW: 5'-GTAACCCGTTGAACCCCATT-3'and

RV: 5’-CCATCCAATCGGTAGTAGCG45S-3’

45S rRNA, FW:5’-GATGTGTGAGGCGCCCGGTT-3’ and

RV: 5’-GTATGCAACGCCACCGGCCA-3’,

LC3b: FW: 5’-CGTCCTGGACAAGACCAAGT-3’ and

RV: 5’-ATTGCTGTCCCGAATGTCTC-3’,

nesprin 2, FW: 5’-CGAGCTGGAAGCTCTGAAGT-3’ and

RV: 5’-ATGGAGTCTATTTTGGAGTTCTGTG-3’, and

for HMBS, FW: 5’-GATGGGCAACTGTACCTGACTG-3’ and

RV: 5’-CTGGGCTCCTCTTGGAATG-3’

2.9 Western Blotting and immunoprecipitation

Kidney, liver, hippocampus, pancreas and cortex regions were isolated and immediately processed for protein analysis by western blot. Tissues were collected in ice-cold PBS and lysed with sonication in RIPA buffer (500 mM Tris-HCl pH 7.2, 1 M NaCl, EDTA, Triton 100-X, Na-deoxycholate, 10% SDS), supplemented with protease and phosphatase inhibitors (Roche, Basel, Switzerland) and β-mercaptethanol placed for 20 min on ice, followed by a 20-minute centrifugation at 14,000 rpm, and addition of 6X Laemmli buffer. For co-immunoprecipitation experiments, overnight preclearing was performed with protein lysate and protein G agarose beads diluted in RIPA buffer on a moving rotor at 4^{o}C. The next day, the protein lysate was transferred to a clean tube,

with fresh beads and the antibody of interest of control IgG of the same species was added overnight on a moving rotor at 4°C. The next day, 3 washes with RIPA were performed followed by laemmli addition, 95°C, 10 minute incubation followed by supernatant transfer without the beads in a new tube. *C. elegans* proteins were extracted from at least 100 worms/strain/condition using 1XRIPA and 6X Laemmli buffer, 5 min vortexing, followed by 10 min incubation at 95°C. Samples were run on 10-15% polyacrylamide gels, and transferred to a 0.2μm nitrocellulose membrane (Millipore, USA). After blocking for 1 hr at RT in 5% non-fat milk or BSA, membranes were incubated overnight with primary antibodies, at 4°C. The primary antibodies used for each target protein were as follows for SYNE-1 (Abcam-ab5250, UK), for nesprin 2 either SYNE-2 (SIGMA-HPA003435, USA) or nesprin 2 (ThermoFisher, K20-478-5, USA), for LC3B (Santa Cruz Technology, USA), LC3B (Cell Signaling #2775, Netherlands) for p62 (Progen-GP62-c, Germany), for lamin B (Santa Cruz Technology-sc-6216, USA), β-tubulin (Abcam-ab6046, UK),, α-tubulin (DSHB-12G10, USA), actin (SIGMA-MAB1501, Germany) for *C. elegans* fibrillarin (Novus Biologicals NB300-269, USA), and for mouse fibrillarin (SIGMA SAB4300633, USA) GFP (Minotech, Greece), mTOR, phosphor-mTOR (Cell Signaling #9862, Netherlands). After three washes in PBS-Tween-20 (100 mM, 0.5N NaCl, 0.1% Tween-20) or TBS-Tween-20, membranes were incubated for 1hr at RT, in the corresponding secondary HRP-conjugated antibodies (Abcam, UK). Development of blots was performed by chemiluminescence

(pico and femto supersignal chemiluminescent substrate, Thermo Fisher Scientific, USA), according to the manufacturer's instructions. The Fiji (ImageJ) software package (http://rsb.info.nih.gov/ij/) was used to measure the relative mean pixel intensity after subtracting the background and normalized to α-tubulin, β-tubulin or actin according to the loading control used in each experiment. Mean values were compared using unpaired t-tests. Error bars indicate standard deviation. Each assay was repeated at least three times. We used the Prism software package (GraphPad Software, San Diego, USA) for statistical analyses.

2.10 Neuronal and mouse embryonic fibroblast (MEF) cultures

Cortices of E16.5 mice (mixed sex) were dissected treated with 0.5% trypsin for 15 minutes at 37^{o}C with simultaneous mechanical dissociation. Following centrifugation, cells were plated on 24-well plates with 13mm coverslips treated overnight with 1X Poly-L-ornithine hydrochloride (Sigma P2533), followed by 3 hours of laminin (Thermofisher-230117015) for 5 days. Cells were cultured in neurobasal media (GIBCO) supplemented by N2 B27 L-glutamine (200 mM) (Thermofisher) and pen/strep (Thermofisher) and cultured for 5 days. Cells were treated with ULK1 inhibitor SB0206965 (1μm) (Cayman).

MEFs were isolated from E13.5 mice (mixed sex), treated with 0.5% trypsin for 10 minutes. Cortices of E16.5 mice (mixed sex) were dissected, treated with 0.5%

trypsin for 15 minutes at 37^{o}C, with simultaneous mechanical dissociation. Following centrifugation, cells were plated on 24-well plates, with 13mm diameter round cover-slips, treated overnight with 1X Poly-L-ornithine hydrochloride (Sigma P2533), followed by 3 hrs of laminin treatment (Thermofisher-230117015, USA), for 5 days. Cells were cultured in neurobasal media (N2B27, GIBCO), supplemented with L-glutamine (200 mM; Thermofisher, USA) and penicillin/streptomycin (Thermofisher, USA), and cultured for 5 days. Cells were treated with the ULK1 inhibitor SB0206965 (1μM; Cayman, USA) and bafilomycin A1 (50nM; SIGMA, USA), under starvation conditions, in Enhanced Balanced Salt Solution (EBSS, GIBCO, USA) for 3 hrs.

2.11 Immunostaining

Cultured cells (neurons and MEFs) were washed with PBS and fixed for 15 min in 4% paraformaldehyde (PFA), in PBS. Following fixation, cells were washed with PBS and incubated for 1 hr in blocking solution, containing 10% fatal calf serum, 0.2% Triton-X in PBS. Cells were then incubated overnight at 4^{o}C, in blocking solution, containing primary antibody for LC3 (1:1000, rabbit polyclonal, Cell Signaling, Netherlands), Ne-sprin 2 (1:1000, mouse poluclonal, Abcam, UK), DFCP1 (Santa Cruz Technology-515049, USA), LAMP1 (Santa Cruz Technology-1D4B), p62 (1:1000, guinea pig. Progen-GP62-c, Germany)Coverslips were then washed with PBS, followed by secondary antibody staining (Abcam, UK), for 1hr, at room temperature. Cells were

rinsed in PBS and incubated with the following secondary antibodies: anti-rabbit Alexa 488, anti-mouse Alexa 594, and anti-guinea pig Alexa 647 (Abcam, UK). Mounting medium with H-1800-10 VECTASHIELD Vibrance Antifade Mounting medium with DAPI (Vector Laboratories, Greece) was used to mount coverslips on slides and stain nuclei.

2.12 Confocal microscopy

Confocal images of fluorescently labelled proteins were captured using a 40X objective lens on a LSM 710 NL multi-photon confocal microscope (Zeiss). Puncta number, size and pixel intensity was performed using Fiji (ImageJ) after subtracting any background setting the appropriating thresholds. Nuclear pixel intensity was determined by DAPI boundaries in mammalian cells. Area of interest used to measure all variables was kept constant in FIJI.

2.13 Quantification & Statistics

Quantification after imaging was performed using FIJI, while statistical analyses and graph design was done using Prism (Graphpad).

Acknowledgements Some nematode strains used in this work were provided by the *Caenorhabditis* Genetics Center, which is funded by the National Center for Research Resources (NCRR) of the National Institutes of Health (NIH), and S. Mitani (National

Bioresource Project) in Japan. A. Fire for plasmid vectors, H. Zhang for kindly providing us with the *bpIs168*[$p_{nfya\text{-}1}$DFCP1::GFP*; unc-76(+)*], *atg-2(bp576),bpIs168*[$p_{nfya\text{-}1}$DFCP1::GFP*; unc-76(+)*], David Starr for providing as the ANC-1B reporter strains and J. Chen for the *nesprin2*$^{-/-}$ mice.

3. Results

3.1 Autophagic regulation of nuclear components

Our first question was whether ANC-1 affects nuclear patterns. We aimed to detect regulators of nuclear size/morphology that could potentially be nuclear autophagy receptors. Previous studies have implicated two nuclear envelope proteins, nesprin 1 and nesprin 2, as modulators of nuclear size in eukaryotic cells. These are outer nuclear membrane proteins which contain actin binding domains (the giant isoforms), multiple spectrin repeats and are embedded in the outer nuclear membrane (KASH domains).

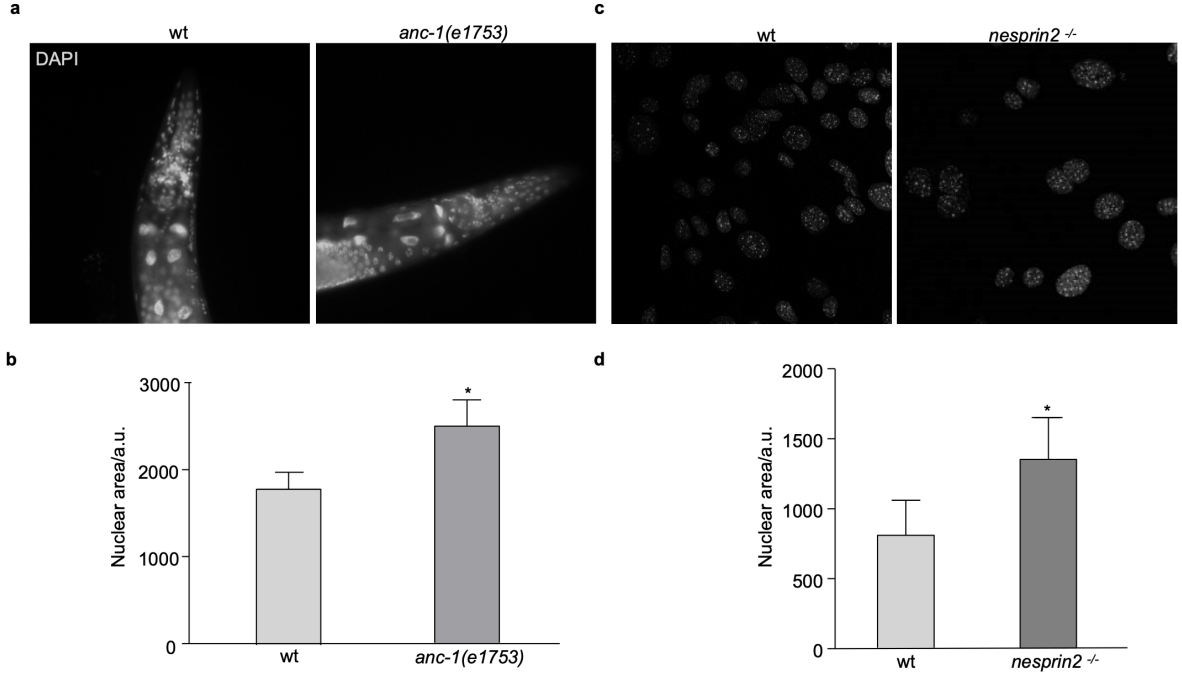

Figure 7. Nuclear size regulation by ANC-1/Nesprin 2. a) Imaging of day 2 worms after DAPI staining. b) Measurement of nuclear area using FIJI. c) Confocal imaging of wt and *nesprin 2*$^{-/-}$ MEFs stained with DAPI. d) Measurement of nuclear area using FIJI. All statistical analyses were performed using the unpaired t-test (*p<0.05,**p<0.005, ***p<0.001).

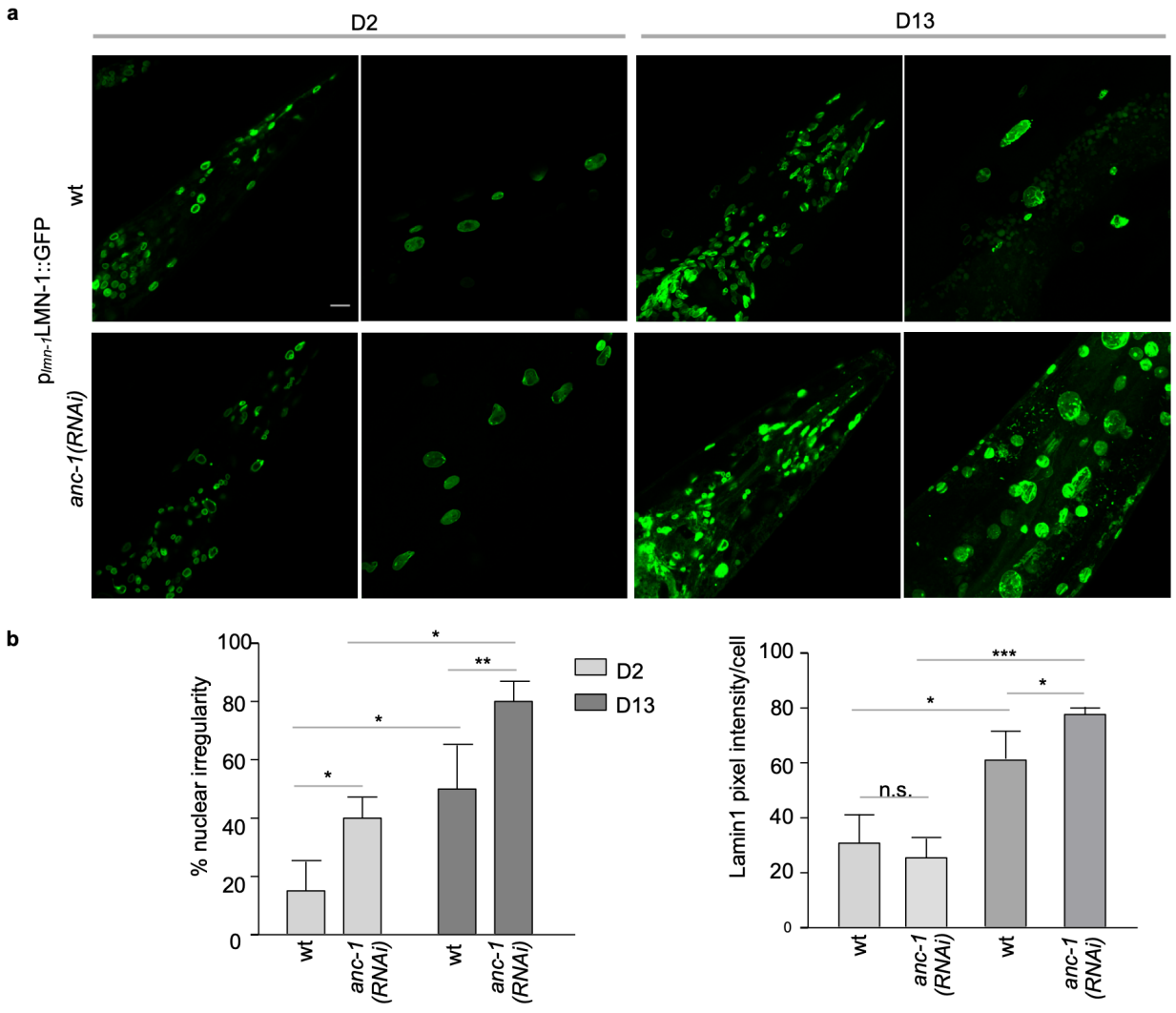

Figure 8. Autophagy regulates lamin abundance through ANC-1. a) Confocal imaging of control (wild type; wt) and *anc-1(RNAi)* nematodes, of D2 young adults or D13 aged adults expressing the p*lmn-1*LMN-1::GFP reporter gene. b) Quantification of irregular nuclei in the head region (micronuclei, irregular shape, lamin aggregation) and measurement of Lamin-1 pixel intensity in cells from the head and intestine of the worm. All statistical analyses were performed using the unpaired t-test (**p*<0.05,***p*<0.005, ****p*<0.001). Scale bar indicates 10um.

ANC-1 is the nematode orthologue of nesprin1/2. *Anc-1(RNAi)* & *anc-1* mutants as well as n*esprin 2*$^{-/-}$ MEFs were used to identify nuclear size and lamina alterations. DAPI staining revealed increased nuclear size in the absence of ANC-1/Nesprin 2, illustrating its regulatory role in nuclear dynamics (Figure 7a & b).

During aging and in progeria syndromes, significant nuclear lamina alterations occur. By using the by using the p$_{lmn-1}$LMN-1::GFP translational reporter worm strain, we detected nuclear lamina pattern changes in the absence of ANC-1, both in young and old adults, while lamin 1 accumulation was more severe after *anc-1* RNAi knock-down of day 13 worms. Moreover, lamin 1 abundance increases during aging, day 13 versus day 2, and this phenotype is exacerbated in the absence of ANC-1.Thus, ANC-1

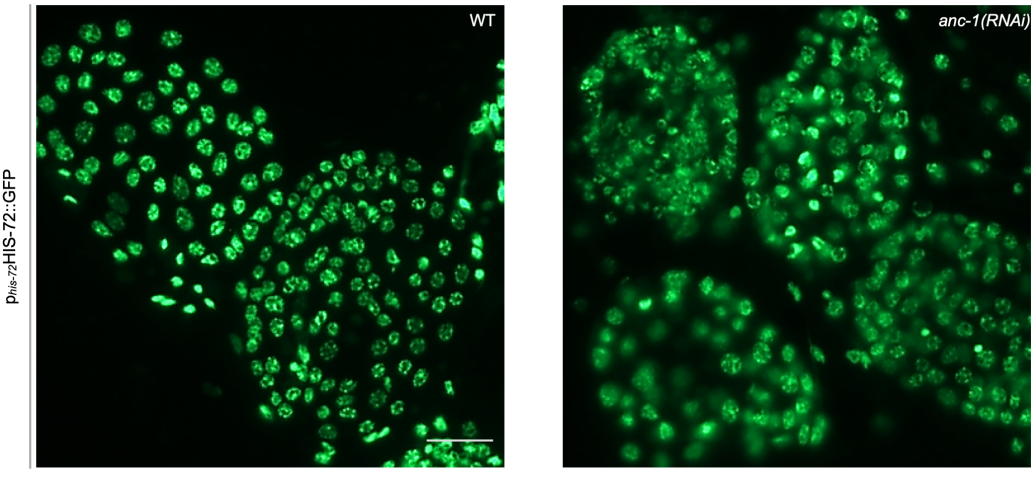

Figure 9. ANC-1 regulates histone localization. a) Epifluorescence. imaging of eggs of control (wild type; wt) and *anc-1(RNAi)* treated nematodes, of p$_{his-72}$HIS-72::GFP reporter gene. Scale bar indicates 5um.

regulates lamin 1 abundance during aging (Figure 8a & b). Additionally histone dynamics are altered in the absence of ANC-1 (Figure 9).

Wild type and *nesprin 2*$^{-/-}$ MEFs were imaged to detect lamin B abundance and pattern at basal autophagic levels and after autophagic flux perturbation by bafilomycin A1 (bafA1). Indeed, nesprin regulation of lamin B abundance is conserved in mammals at basal autophagic conditions (Figure 10a). Lamin B2 has been shown to be a sub-

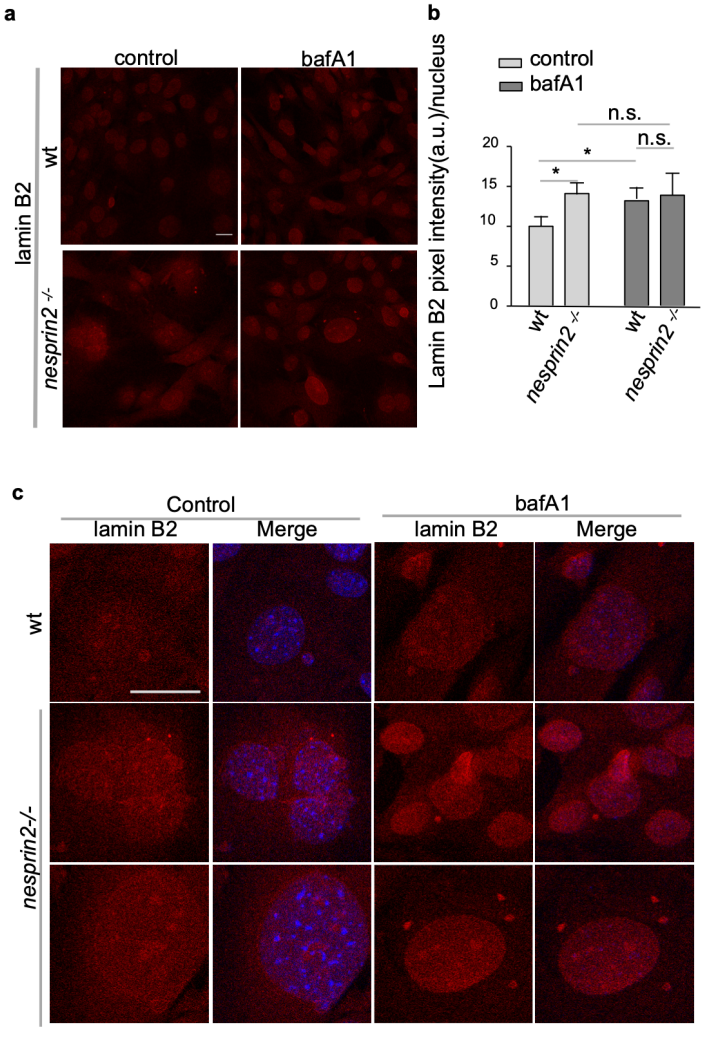

Figure 10. Autophagy regulates lamin abundance through nesprin 2. a) lamin B2 immunostaining of control and bafilomycin A1 (bafA1)-treated wt and *nesprin2*$^{-/-}$ MEFs. b) Quantification of lamin B2 pixel intensity per nucleus. c) Percentage of cells with lamin B puncta (red) outside the nucleus d) control & bafilomycin A1 (bafA1) - treated wt and *nesprin 2*$^{-/-}$ MEFs stained with lamin B and DAPI in control & bafA1-treated cells. All statistical analyses were performed using the unpaired t-test (*p<0.05,**p<0.005, ***p<0.001). Scale bar indicates 20um.

strate of autophagy in cancer cells. BafA1 increases lamin B2 abundance in wild type cells, while there is no additive effect in lamin B abundance in the absence of nesprin 2. Therefore Lamin B2 degradation is mediated by autophagy and regulated, at least partially, through nesprin 2. Moreover, nesprin 2 absence causes nuclear abnormalities such as micronuclei (Figure 10b). Thus, the role of nesprin family members in maintaining nuclear architecture is evolutionarily conserved from nematodes to mammals.

3.2 ANC-1/Nesprins are autophagic substrates

Mammalian nesprins and ANC-1 contain potential LC3-interacting region (LIR motifs), typical of autophagy substrates and receptors. Therefore, we hypothesized that ANC-1/nesprins themselves are regulated by selective autophagy, thereby contributing to nuclear morphology homeostasis. We uninhabited autophagy by both generic and

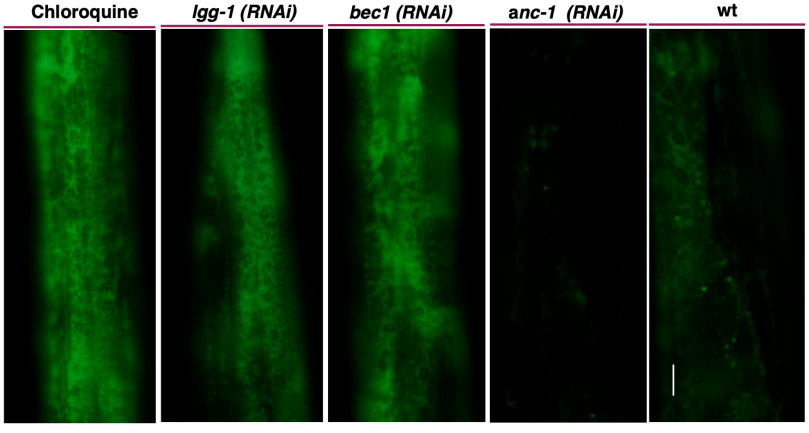

Figure 11. ANC-1 is an autophagic substrate *in vivo*. a) Epifluorescence imaging of day 2 GFP-ANC1B worms treated *anc-1(RNAi), bec-1(RNAi), lgg-1(RNAi)* and 5uM chloroquine. Scale bar indicates 20um.

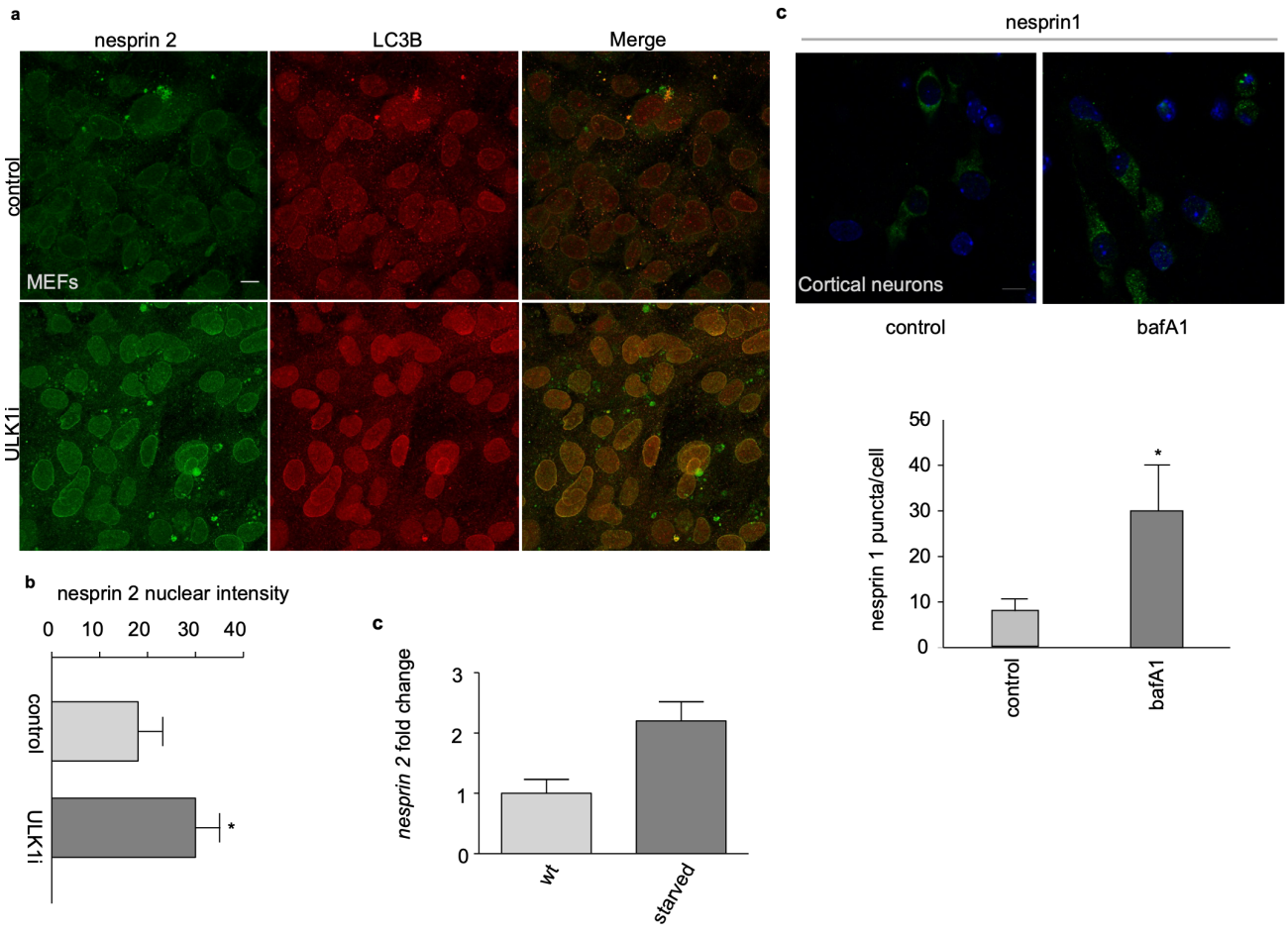

Figure 12. Autophagy regulates nesprins *in vitro*. a) Immunofluorescence imaging of E14.5 MEFs, treated with the ULK1 inhibitor SBI-0206965 (ULK1i), followed by nesprin 2 (green), and LC3B (red) antibody b) Quantification of nesprin 2 nuclear intensity (left) and *nesprin 2 r*elative RNA levels in control and starved (2hrs) conditions using quantitative real time PCR c) immuofluorescence imaging of control & bafA1-treated (2hrs) wt E16.5 cortical neurons, stained with nesprin 1 antibody (green) and DAPI &d) puncta measurement. All statistical analyses were performed using the unpaired t-test (*p<0.05,**p<0.005, ***p<0.001).

a

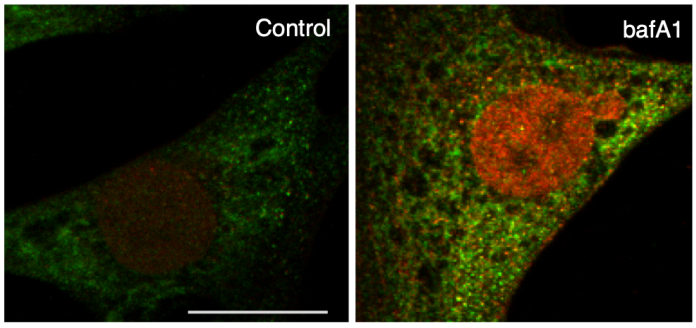

b

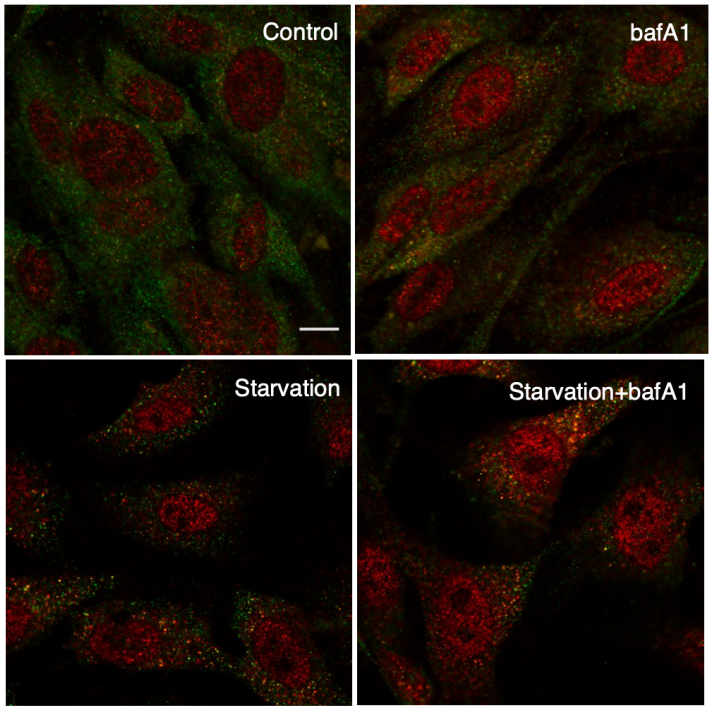

Figure 13. Autophagy regulates nesprins *in vitro*. a) Confocal imaging after immunofluorescence staining nesprin 2 (red) & LC3B (green) staining of control & bafA1-treated MEFs. Scale bar indicates 20μm b) Confocal imaging after immunofluorescence staining of nesprin 1 (red) & LC3B (green) staining of control, bafA1, starvation & starvation+bafA1-treated MEFs. Scale bar indicates 10μm.

chemical means in the GFP::ANC-1B translational reporter strain. We showed that in the absence of either autophagy initiator BEC-1 or autophagosomal membrane protein LGG-1, GFP levels dramatically increase. Moreover, 5μm chloroquine treatment of the worms by adding it on the plate, which blocks autophagosom-lysosome fusion, caused similar GFP accumulation (Figure 11). Thus, ANC-1 is an autophagic substrate.

To test this hypothesis in mammals, we firstly examined whether nesprins are substrates of autophagy *in vitro,* by using both MEFs and embryonic cortical neurons Treatment of E14.5 MEFs with selective ULK1 inhibitor, ULK1i, leads to an increase in nesprin 2 aggregation in the nucleus (Figure 12a & b). Similarly, treatment of E16.5 neurons with bafA1 increases nesprin 1 puncta (Figure 11c&d). Both nesprin 1 & nesprin 2 costaining with LC3B reveals increased nesprin 1 & 2 expression as well as increased colocalisation of LC3B and nesprins upon autophagic flux inhibition, as well as autophagy induction for nesprin 1 & LC3B underlining that nesprins are autophagic substrates (Figure 14). Taken together, these experimental data suggest that nesprins are nuclear autophagy substrates.

To further substantiate this finding i*n vivo*, autophagy was physiologically induced by subjecting young male mice, to avoid female hormonal alterations' effects, to food deprivation. Quantification of relative nesprin 2 and nesprin 1β protein levels in the kidney and brain, cortex, respectively due to their relative abundance, reveals substantial reduction in both proteins, illustrating that they are *in vivo* autophagic substrates (Figure 13a & b). Indeed, we examined whether nesprins directly interact with the core autophagic machinery. We find that nesprin 2 directly interacts with the autophagosomal membrane protein LC3B in the mouse kidney (Figure 14c) while Nesprin 1 interacts with LC3B, p62 and DFCP1 (Figure 14d). Thus, nesprins 1 and 2

associate with autophagic machinery components and are specifically targeted by autophagy under conditions of nutrient stress.

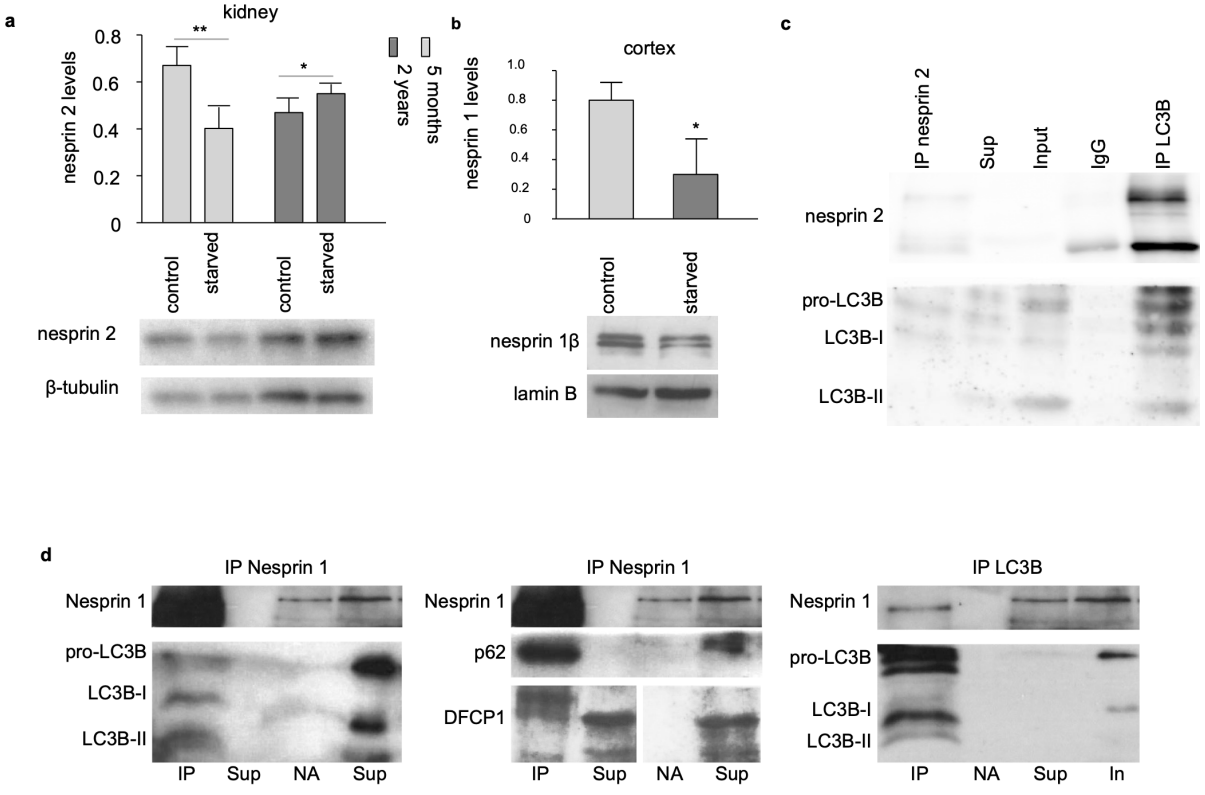

Figure 14. Autophagy regulates nesprins *in vivo*. a) Western blot analysis & quantification of nesprin 2 kidney protein levels in control and food deprived (24h starvation) 5-month and 2-year old mice normalized to β-tubulin b) nesprin 1β protein levels in the cortex of 9-week old male mice normalized to lamin B c) Immunoprecipitation (IP) of mouse nesprin 2 (kidney) & LC3, followed by western blot with mouse nesprin 2 and rabbit LC3 (left panel), IP of rabbit nesprin1 and LC3 (cortex) followed by western blot with rabbit LC3B and rabbit (middle panel), IP nesprin 1 (cortex) followed by western blot for mouse guinea pig p62 and mouse DFCP1 (sup: IP supernatant, IgG: mouse IgG antibody control, in: input protein). All statistical analyses were performed using the unpaired t-test (*p<0.05,**p<0.005, ***p<0.001).

3.3 Autophagic regulation by nesprins

We next investigated whether there is cross-regulation between autophagy and nesprins, as it is the case with autophagic substrates/receptors and the autophagic pathway as a negative feedback loop mechanism. We examined several steps in the autophagic pathway, from omegasome and autophagosome formation to autophagosome/lysosome degradation.

We first used the nematode translational reporters for autophagic protein components. $p_{nfya\text{-}1}$DFCP1::GFP animals where the omegasome double FYVE domain-containing, PI(3)P-binding protein DFCP1protein is detected. The worms were treated with *anc-1* RNAi*,* which encodes the nematode nesprin 1/2 orthologue, from L4 to D2 adults, which caused accumulation of DFCP1::GFP puncta, which represents early autophagic structures in somatic tissues (Figure 15a & b) (68). Notably, there is no additive effect in *atg-2(bp56);*$p_{nfya\text{-}1}$DFCP1::GFP where ATG-2, a pre-autophagosomal protein is depleted, as DFCP1::GFP puncta do not further increase, indicating that both ANC-1 and ATG-2 function in the same autophagic pathway (Figure 15a & b). Similarly, when *anc-1* was knocked down in $p_{lgg\text{-}1}$GFP::LGG-1 worms, we observed an increase in LGG-1 puncta, the nematode Atg8/LC3 protein homologue, (Figure 15a & b). Therefore, ANC-1 is required for initiation of basal autophagy. We then assessed the requirement of ANC-1 under low insulin/IGF-1 signaling, known to induce autophagy in *daf-2* insulin/IGF-1 receptor mutant nematodes. ANC-1 deficiency both dramatically increases while

simultaneously expanding autophagosomal puncta, indicating that either autophagosomes become larger or coalesce with each other (Figure 15 a, b). Western blot analysis of LGG-1-II/I relative protein ratio is increased in the absence of ANC-1, which indicates increased incorporation of LGG-1 into autophagosomal membranes. Autophagic flux perturbation is illustrated by accumulation of the lipidated membrane LGG-1-II form and coupled with accumulation of SQST-1, the *C. elegans* orthologue of p62 (Figure 15c & d) upon ANC-1 depletion. All in all, these observations illustrate ANC-1's role in promoting autophagosomal structure formation, while its perturbation blocks autophagosomal progression.

This novel function of ANC-1 as an autophagy regulator is conserved in the mouse. To this end, we evaluated DFCP1, LC3B, p62 and LAMP1 protein levels, pattern and localization in starvation conditions conditions in MEFs derived from wild type and *nesprin 2*$^{-/-}$ mice. Omegasome marker, DFCP1, demonstrates an increased puncta area, but not number, in the absence of nesprin 2 when autophagic flux is inhibited during starvation-induced autophagy (Figure 16a & b). This finding together with the increased area of LAMP1 puncta, which represents lysosomes as well as endosomes, illustrates a defect in autophagosomal maturation and immature autophagy-related structure accumulation (Figure 16a & b).

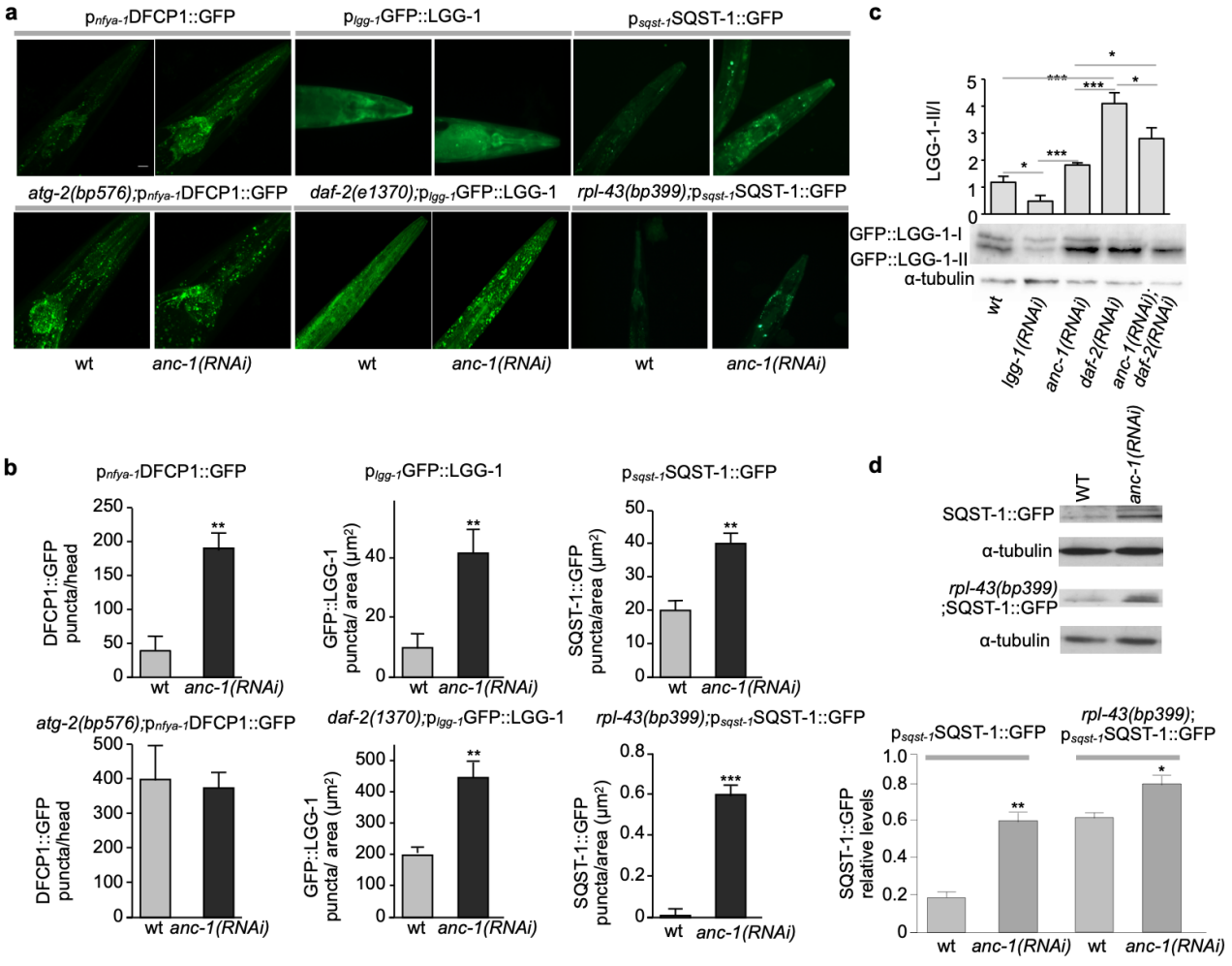

Figure 15. ANC-1 regulates DFCP1, LGG-1 & SQST-1 abundance. a) Representative, anterior head region images of wild type nematodes, in addition to *atg-2(bp576)*, *daf-2(1370)*, and *rpl-43(bp399)* mutants, expressing the indicated reporter genes (p_{nfya-1}DFCP-1::GFP, p_{lgg-1}LGG-1::GFP and p_{sqst-1}SQST-1::GFP), subjected to *anc-1* RNAi-mediated silencing. b) Quantification of GFP fluorescence in nematodes imaged above, appropriately measured and adjusted for each reporter fusion protein and genetic background, as indicated (puncta per area, puncta area, n>80) c) Western blot analysis and quantification of GFP::LGG-1-II/I ratio in *lgg-1*, *anc-1, daf-2, anc-1;daf-2* RNAi-silenced D2 adult nematodes normalized to α-tubulin. d) Western blot analysis and quantification of in p_{sqst-1}SQST-1::GFP and *rpl-43;* p_{sqst-1}SQST-1::GFP RNAi-silenced D2 adult nematodes normalized to α-tubulin. All statistical analyses were performed using the unpaired t-test (*p<0.05,**p<0.005, ***p<0.001). Scale bar indicates 20µm.

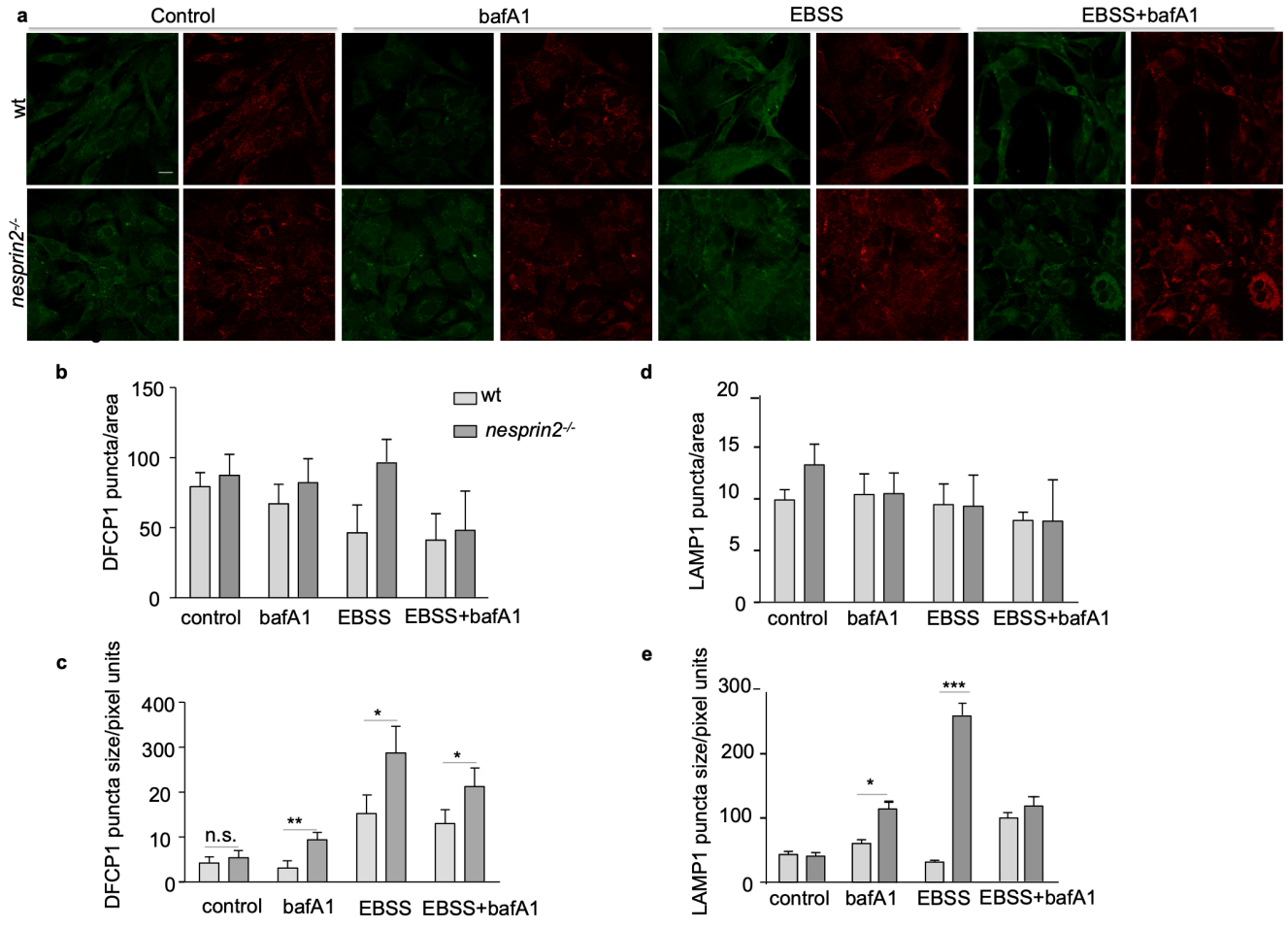

Figure 16. Nesprin 2 regulates DFCP1 puncta size. a) Immunofluorescence imaging of control and starved (2 hours EBSS) wt and *nesprin 2*$^{-/-}$ E14.5 MEFs with or without bafilomycin A1 (bafA1) followed by DFCP1 (green) & LAMP1 (red) antibody staining b & d) b) Quantification of DFCP1 & LAMP1 puncta/area, LAMP1 puncta size/pixel units (>0.01 square inches), using FIJI. All statistical analyses were performed using the unpaired t-test (*$p<0.05$,**$p<0.005$, ***$p<0.001$). Scale

Immunofluorescence imaging revealed that LC3B is more abundant in *nesprin 2*$^{-/-}$ MEFs, which is due to autophagic flux inhibition as there is no difference in LC3 puncta

between control and bafilomycin A1-treated cells (Figure 17). Similarly, the LC3B-II/I ra-

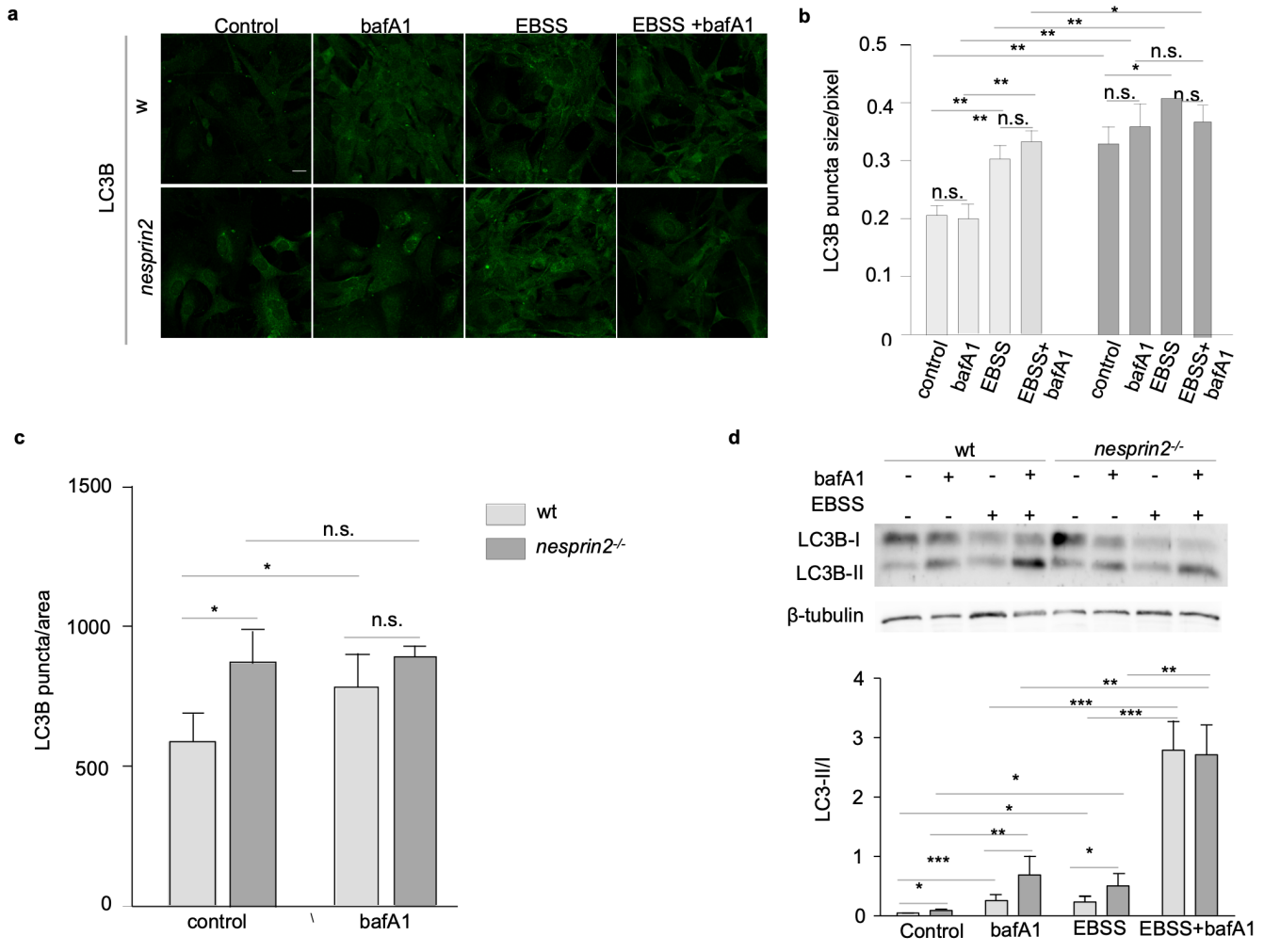

Figure 17. Nesprin 2 regulates LC3B. a) Immunofluorescence imaging of wt and *nesprin 2*$^{-/-}$ E14.5 MEFs of control, bafA1, starved (EBSS) & starved (EBSS)+ bafA1-treated (2 hours) and LC3B (green) b) Quantification of LC3 puncta size after control, bafA1, starved (EBSS) & starved (EBSS)+ bafA1-treated (2 hours) using FIJI c) Quantification of LC3 puncta size in control and bafA1 treated cells using FIJI d) Western blot analysis of LC3BI & II of control and starved (2 hours EBSS) wt and *nesprin 2*$^{-/-}$ E14.5 MEFs with or without bafilomycin A1 followed by quantification of the LC3II/I ratio normalized to β-tubulin. All statistical analyses were performed using the unpaired t-test (*p<0.05,**p<0.005, ***p<0.001). Scale bar indicates 20µm.

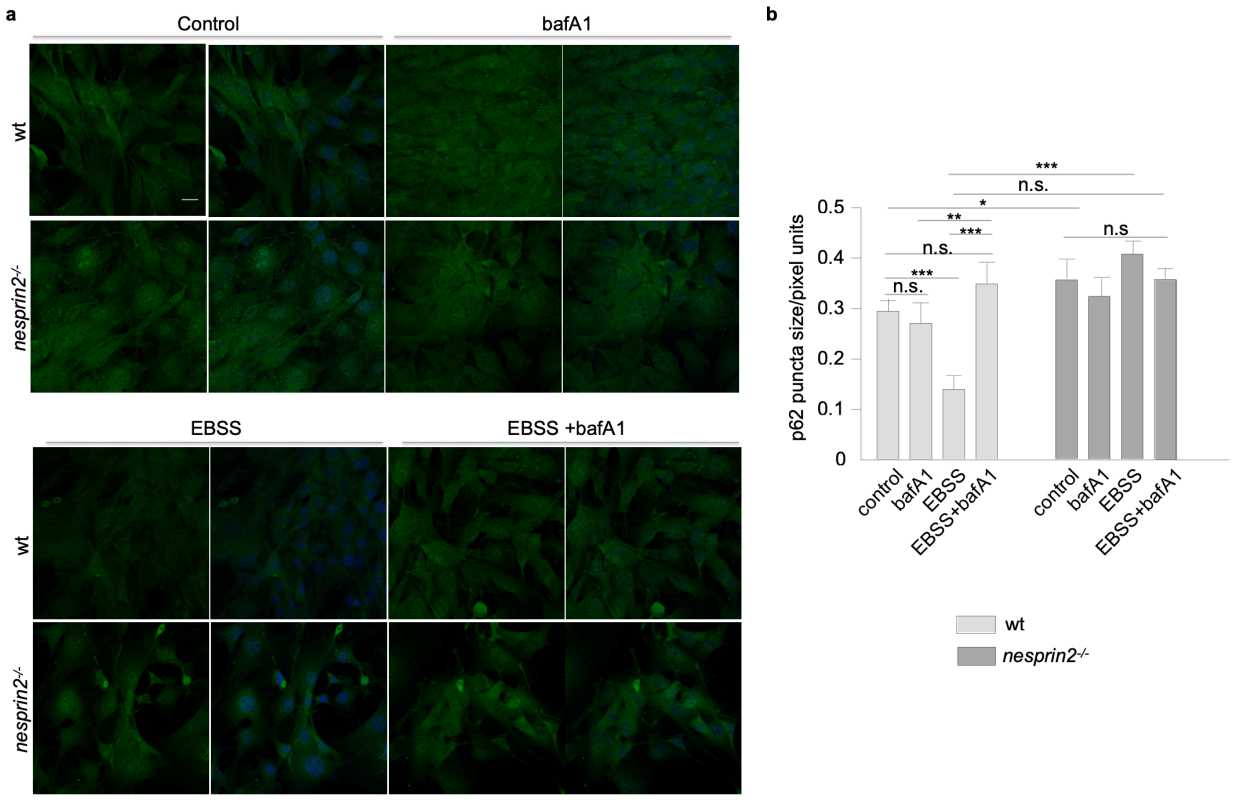

Figure 18. Nesprin 2 regulates p62 localization via autophagy. a) Immunofluorescence imaging of wt and *nesprin 2*$^{-/-}$ E14.5 MEFs of control, bafA1, starved (EBSS) & starved (EBSS) +bafA1-treated (2 hours) after LC3B staining (green) b) Quantification of p62 puncta size using FIJI in wt & *nesprin 2*$^{-/-}$ E14.5 MEFs using FIJI. All statistical analyses were performed using the unpaired t-test (*p<0.05,**p<0.005, ***p<0.001). Scale bar indicates 20μm.

tio is higher in *nesprin 2*$^{-/-}$ MEFs compared to wild type cells, in (i) basal (control & bafilomycin treatment) and (ii) starvation-induced autophagy (EBSS) while the ratios are the same after bafilomycin treatment during induced autophagy (EBSS+bafilomycin A1)

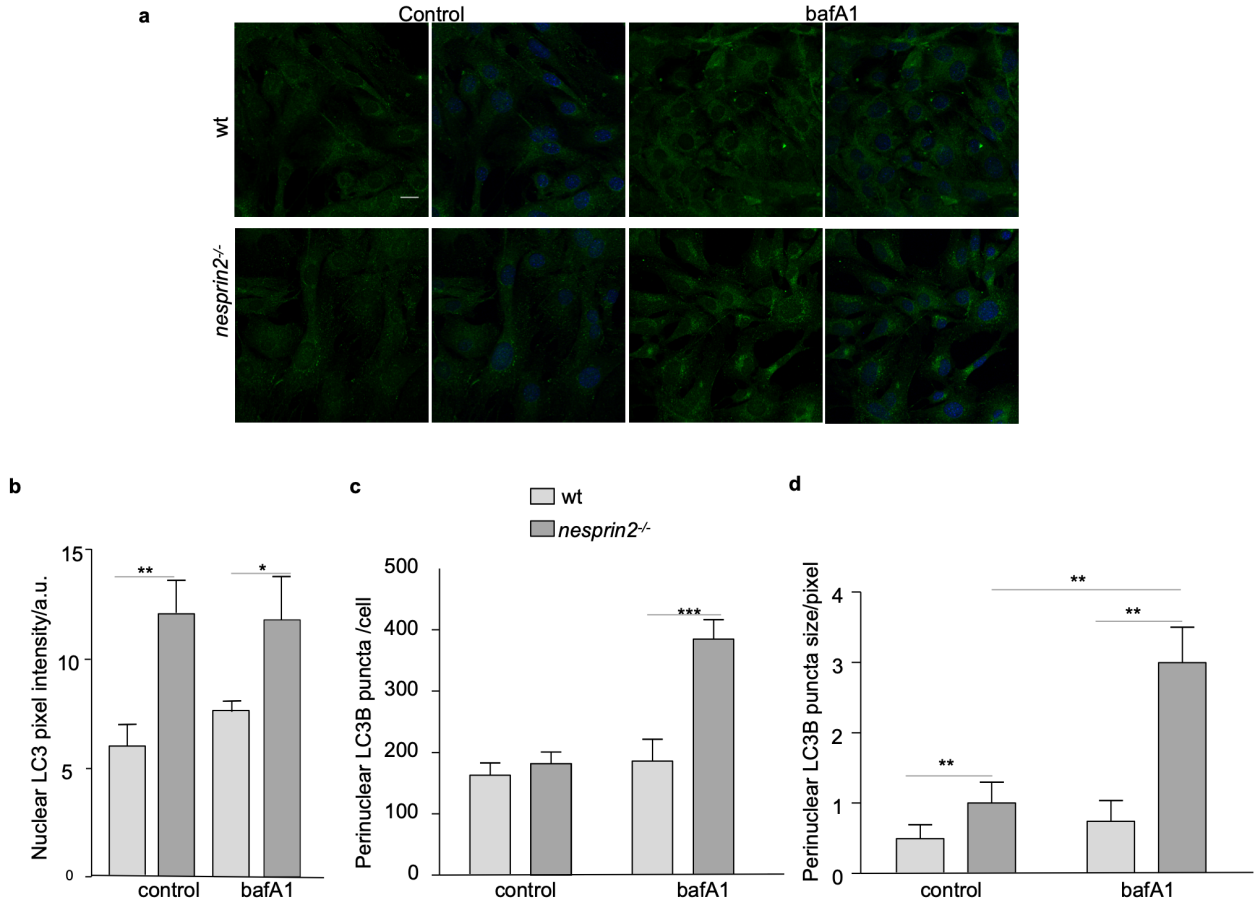

Figure 19. Nesprin 2 regulates LC3B localization. a) Immunofluorescence imaging of wt and *nesprin 2*$^{-/-}$ E14.5 MEFs of control, bafA1, starved (EBSS) & starved (EBSS)+ bafA1-treated (2 hours) after LC3B staining (green) b) Quantification of nuclear LC3 pixel intensity c) peri nuclear LC3B puncta/cell d) perinuclear LC3B puncta size using FIJI. All statistical analyses were performed using the unpaired t-test (*p<0.05,**p<0.005, ***p<0.001). Scale br indicates 20µm.

further showing nesprin 2 function in autophagy induction (Figure 17) Moreover, LC3 puncta size is also significantly larger in all conditions observed when nesprin 2 is depleted, indicative of autophagosome aggregation (Figure 17).

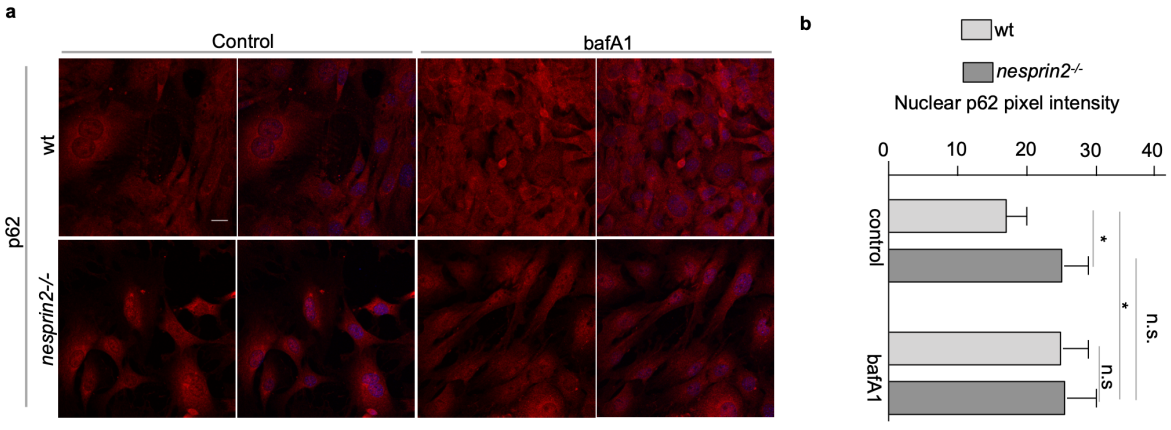

Figure 20. Nesprin 2 regulates p62 abundance via autophagy. a) Immunofluorescence imaging of p62 in control & bafA1 treated wt and *nesprin 2*$^{-/-}$ E14.5 MEFs b) Quantification of nuclear p62 pixel intensity using FIJI. All statistical analyses were performed using the unpaired t-test (*p<0.05,**p<0.005, ***p<0.001). Scale bar indicates 20µm.

P62 protein levels are indirect read out of autophagic flux, as it is an autophagic substrate. p62 puncta size increases in basal and autophagy-inducing conditions in the absence of nesprin 2, highlighting the failure of p62 aggregates from being degraded by starvation-induced autophagy (Figure 18). Interestingly enough, we detected increased nuclear and perinuclear enlarged LC3B puncta accumulation as well as nuclear p62 aggregation in the absence of nesprin 2 (Figure 19 & 20). Thus, nesprin 2 modulates autophagy by regulating autophagic proteins' subcellular localization.

Nesprin polymorphisms have been linked to cerebellar ataxias due to expanded CAG repeats which causes protein aggregation [54]. An *in vivo* nematode model for polyglutamine disease is a strain which expresses 40 repeats of glutamine p*unc-54*Q40::YFP. In the absence of ANC-1, day 1 adults have significantly increased Q40 puncta. There is no additive effect when both ANC-1 and autophagy proteins are ablat-

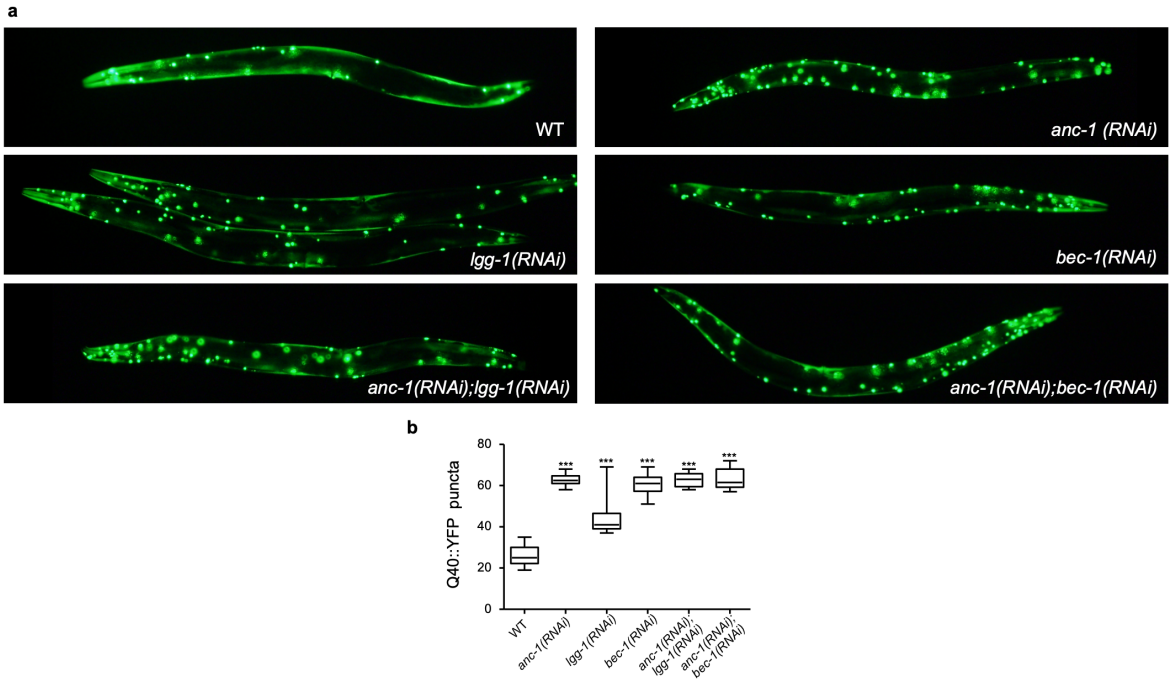

Figure 21. ANC-1 clears protein aggregates through autophagy. a) Epifluorescent microscopy of day **1** p*unc-54*Q40::YFP worms treated with control (WT), *anc-1 (RNAi), lgg-1RNAi), bec-1(RNAi), anc-1(RNAi);lgg-1(RNAi), anc-1(RNAi);bec-1(RNAi)*. b) Q40::YFP puncta/worm in control (WT), *anc-1 (RNAi), lgg-1(RNAi), bec-1(RNAi), anc-1(RNAi);lgg-1(RNAi), anc-1(RNAi);bec-1(RNAi)*.All statistical analyses were performed using the unpaired t-test (**p*<0.05,***p*<0.005, ****p*<0.001). Scale bar represents 20μm.

ed (LGG-1 & BEC-1) suggesting that ANC-1 acts through autophagy to clear out protein aggregates (Figure 21).

3.4 Nucleolar size regulation by nesprins

Nucleolar size has recently not only arisen as a biomarker of aging, but a determinant of longevity. Conditions of low insulin/IGF-1 signaling and dietary restriction decrease nucleolar size and delay the aging process. However, the mechanism(s) underlying and nucleolar size modulation remained elusive. Outer nuclear membrane proteins nesprins regulate nuclear size and autophagy components under conditions of low insulin/IGF-1 signaling and nutrient stress restriction.

Thus, we investigated whether nesprin-mediated autophagy modulates the nucleolus and specifically fibrillarin, a methyltransferase which regulates the maturation of rRNA [55]. Firstly, we show that fibrillarin is a substrate of basal autophagy, as bafilomycin A1 treatment increases fibrillarin expression & its punctum area (Figure 22). Moreover, in the absence of nesprin 2 , fibrillarin levels & its punctum area are increased compared to wild type under basal conditions, which has no additive effect upon bafilomycin treatment. Therefore, nesprin through autophagy regulates fibrillarin abundance. We confirmed these results by western blotting, as fibrillarin is degraded by sravratoin induce autopahgy which is blocked in the absence of nesprin 2. Particularly,

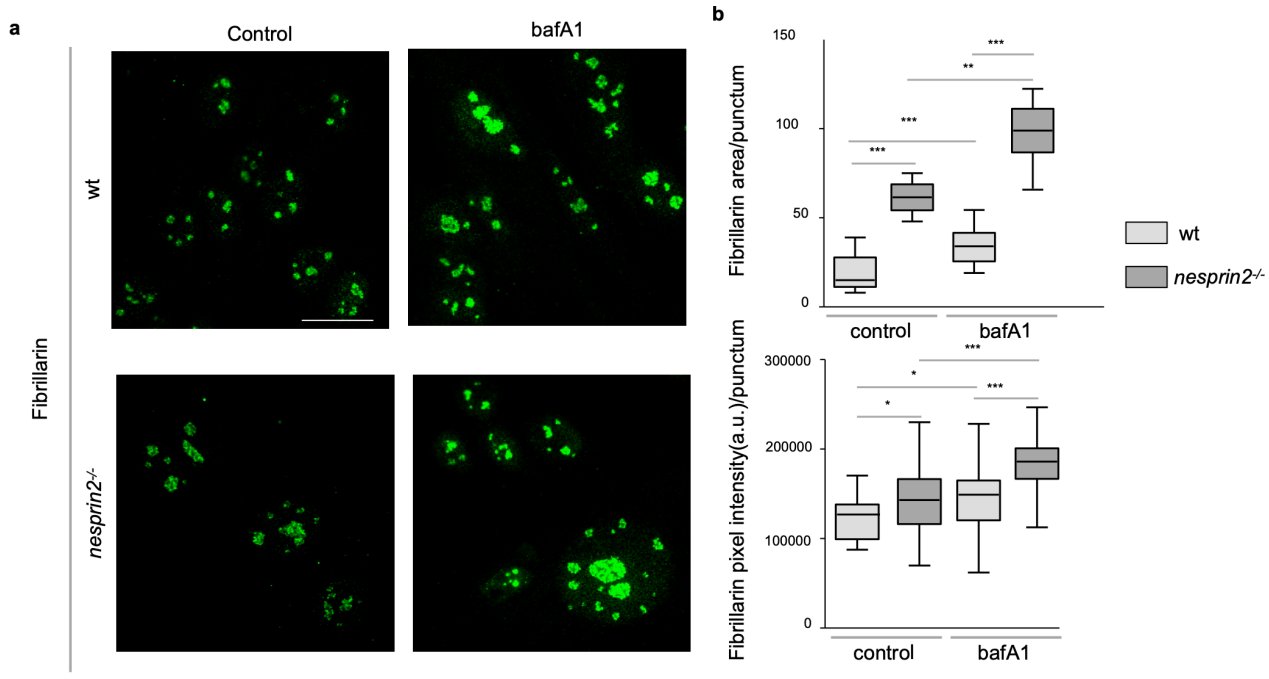

Figure 22. Autophagy through nesprins regulate nucleolar components and ribosomal biogenesis. a) Immunofluorescence imaging of wt and *nesprin 2*$^{-/-}$ E14.5 MEFs with or without bafilomycin A1 (bafA1) following immunostaining with fibrillarin b) Nucleolar area and pixel intensity, using fibrillarin staining as boundaries, was measured.All statistical analyses were performed using the unpaired t-test (*p<0.05,**p<0.005, ***p<0.001). Scale bar indi-

depletion of nesprin 2 and blockage of basal autophagic flux by bafA1 in MEFs causes accumulation of fibrillarin and increased fibrillarin puncta area (Figure 22). Complementarily, western blot analysis further accentuates the autophagic role of nesprin 2 in controlling fibrillarin abundance under control and starvation-induced conditions in nesprin 2-depleted MEFs (Figure 23a&b). Nesprin 2 also specifically monitors the expression of the pre ribosomal 45S rRNA, precursor of 18S, 28S and 5.8S rRNAs, without affecting

gene expression of autophagic genes such as LC3B (Figure 23c). This further indicates nucleolar dysfunction.

To monitor the physiological significance of nesprin-mediated effects on the nucleolus, *in vivo*, we observed nucleolar structure alterations in *C. elegans*, using a

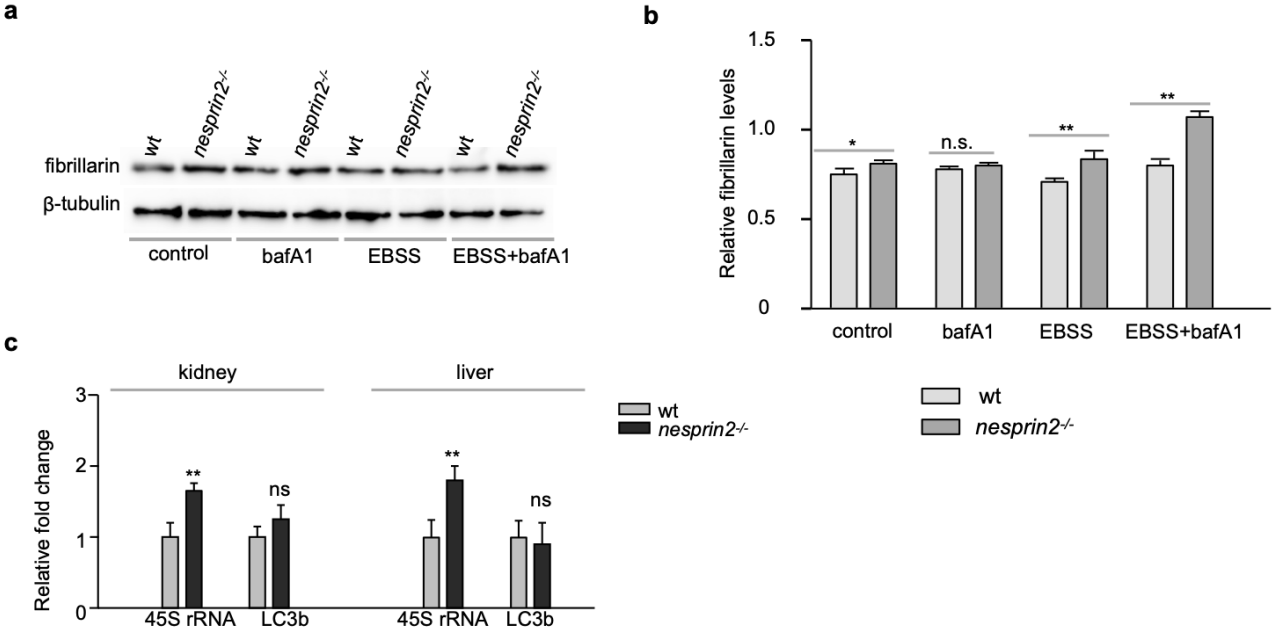

Figure 23. Autophagy and nesprins regulate nucleolar components and ribosomal biogenesis. a, Western blot analysis of fibrillarin in wt and *nesprin 2*$^{-/-}$ E14.5 MEFs with or without bafA1 under control and nutrient deprived (EBSS for 2 hrs). b, Quantification of fibrillarin protein levels in conditions mentioned above normalized to β-tubulin c, Relative quantification, of kidney and liver *18S rRNA, 45S rRNA* and *LC3b* transcript levels, in wt and *nesprin2*$^{-/-}$mice, by qPCR, normalized to the hydroxymethylbilane synthase (HMBS) transcript levels All statistical analyses were performed using the unpaired t-test (*p<0.05,**p<0.005, ***p<0.001).

fibrillarin-1 GFP reporter fusion. Remarkably, ANC-1 deficiency causes significant nucleolar enlargement, in wild type animals, which is recapitulated by depletion of the *C. elegans* beclin orthologue BEC-1 (Figure 24a&b). No further increase observed by simultaneous knockdown of both ANC-1 and BEC-1, while either *anc-1* or *bec-1* knockdown is fully epistatic to DAF-2 deficiency, suggesting that they function in the same signaling pathway to modulate nucleolar size. . Additionally, endogenous fibrillarin protein levels are higher in *anc-1* mutant animals (Figure 24c). Of note, ANC-1 is localized in nucleoli as shown by the GFP::ANC-1 translational reporter distinct pattern (Figure 24).These observations indicate that ANC-1 together with autophagy contribute downstream of insulin/IGF-1 signaling to preserve nucleolar morphology, in *C. elegans*.

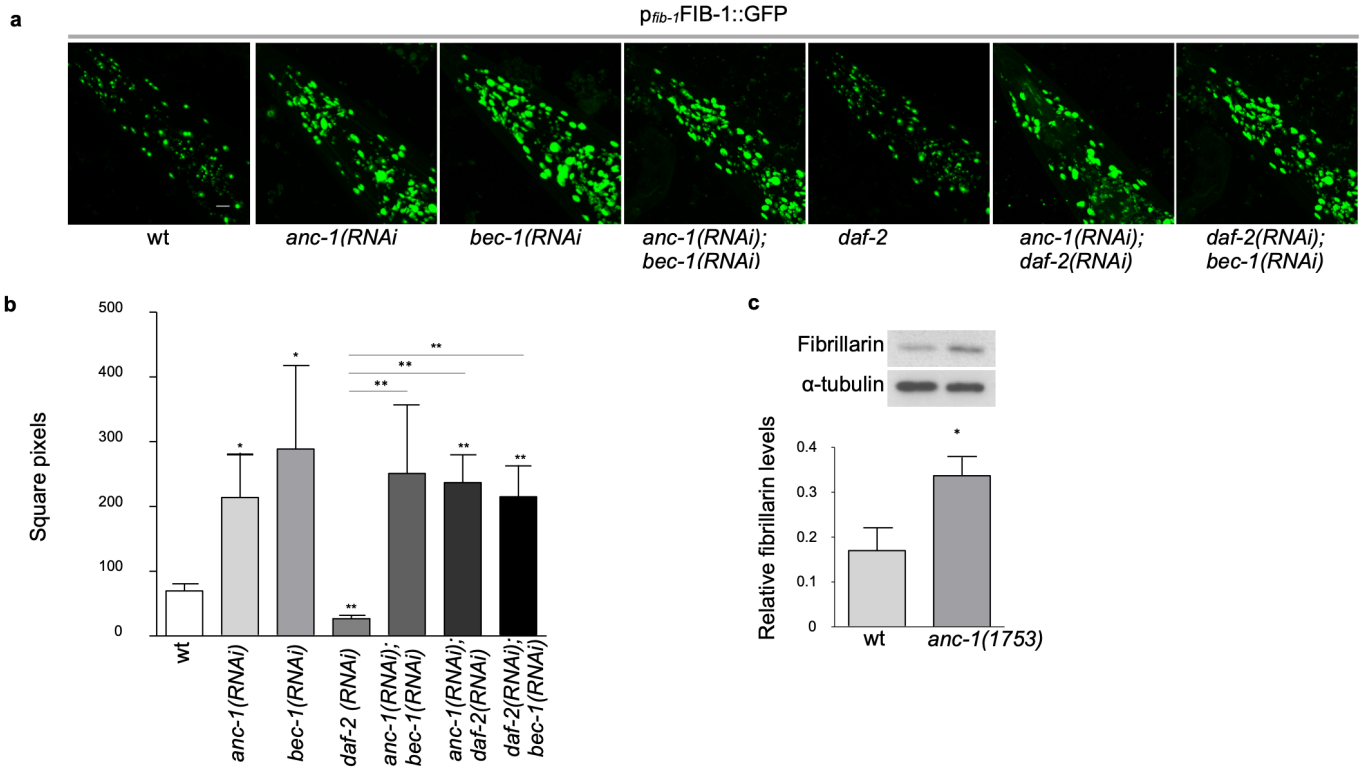

Figure 24. Nucleolar regulation by autophagy. a) Confocal microscopy imaging of day 3 adult nematodes expressing the p*fib-1*FIB-1::GFP D3 reporter fusion protein, subjected to RNAi-mediated silencing of the indicated genes, compared to wt. Scale bars, 20μm. b) Quantification of pixel area of FIB-1::GFP fluorescence c) Western blot analysis of endogenous fibrillarin-1 levels, in day-4 adult wt nematodes and *anc-1(e1753)* mutants. All statistical analyses were performed using the unpaired t-test (*p<0.05,**p<0.005, ***p<0.001). Scale bar indicates 20μm.

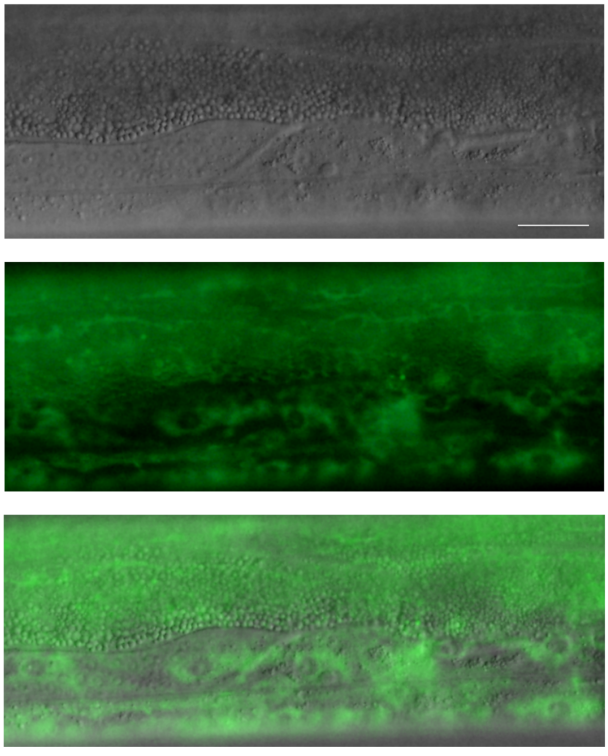

Figure 25. ANC-1 localises at nucleoli. Epifluroescence & DIC microscopy of GFP::ANC-1 worms indicates strong nucleolar localization of ANC-1. Scale bar indicates 20μm.

3.5 ANC-1 regulates lifespan under low insulin conditions & caloric restriction

Given that nesprin 1 and 2 protein family members are required for auotphagic recycling of nucleolar components, under both basal and nutrient stress conditions in diverse organisms, we examined whether nesprins also contribute to stress survival and lifespan extension. Indeed, ANC-1 is required for survival under conditions of complete starvation conditions as *anc-1* mutants display reduced survival compared to control after 5 days of starvation and no survival after 10 days (Figure 26a).

We specifically investigated the lifespan effects of low insulin/IGF-1 signaling and dietary restriction conditions under which nucleoli are smaller. Remarkably, knockdown of *anc-1* significantly shortens the lifespan of long-lived DAF-2-deficient nematodes, to a similar extent to *bec-1* knockdown (Figure 26b). Hence, ANC-1 functions to maintain nucleolar homeostasis and promote longevity under low insulin/IGF-1 signaling conditions. On a similar note, ANC-1 ablation in long-lived EAT-2-deficient animals, which have a defective feeding behavior and hence are calorically restricted**,** shortens lifespan (Figure 26c) [56]. ANC-1 confers other types of stress resistance such as to heat and DNA damage (Figure 27). Thus, our findings further suggest that autophagy

besides contributing to organismal longevity contributes to reproductive capacity potential.

We then hypothesized that these alterations in the nucleolus, which controls protein translation, would affect signaling pathways regulating protein translation as well as protein translation rates. FRAP analysis of transcriptional p*ife-2*GFP treated with *anc-1 (RNAi)* and translational inhibitor chemical cycloheximide revealed a very small increase in rate of translation when slopes of the best fit line of fluorescent recovery were drawn (Figure 28a). Similarly, a slightly but not significant increase in mTOR signaling was observed (Figure 28b, c & d).

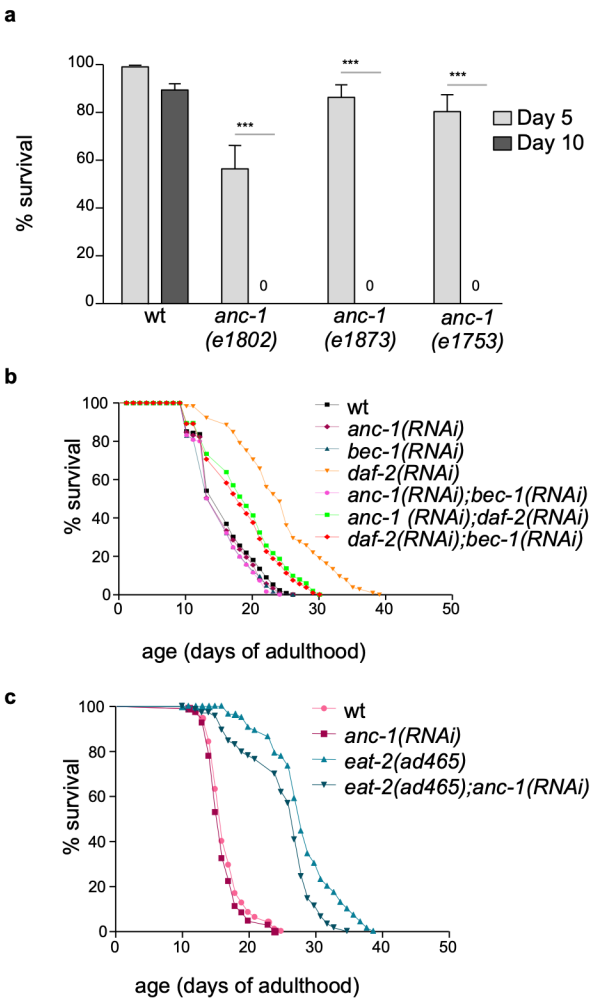

Figure 26. Nucleolar regulation by autophagy and ANC-1 regulate aging. a) Survival assay of wt nematodes, *anc-1(e1802)* mutants, *anc-1(e1873)* & *anc-1(e1753)* mutants after 5 & 10 days of starvation b) RNAi-mediated knockdown of either *anc-1* or *bec-1* shortens the lifespan of long-lived, DAF-2-deficient nematodes (*daf-2(RNAi)*). b) RNAi-mediated knockdown of *anc-1* shortens the lifespan of long-lived, EAT-2-deficient nematodes. Survival curves were drawn using the product-limit method of Kaplan and Meier. The log-rank (Mantel–Cox) test was used to evaluate differences between survivals and determine P values. We used the Prism software package (GraphPad Software, San Diego, USA) for statistical analysis and to determine lifespan values.

3.6 ANC-1 promotes germline immortality.

Besides organismal aging, reproductive aging has emerged as a major issue nowadays as infertility in women is a major medical, economic and social issue. The

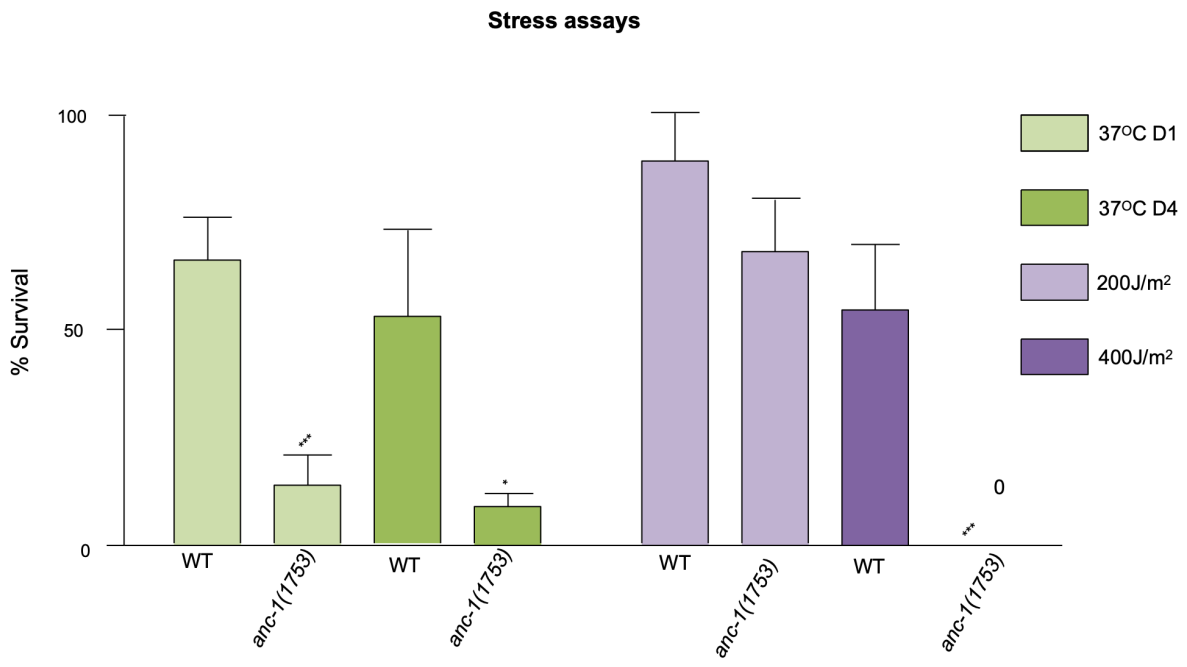

Figure 27. ANC-1 is required for acute heat & DNA damage stress survival. %Survival of WT & *anc-1(1753)* after acute heat stress (37 degrees celsius) at day 1(D1) and day 4(D4) of adulthood. UV-C induced DNA damage (200J/m^2 & 400J/m^2) at day 1 of adulthood. All statistical analyses were performed using the unpaired t-test (*p<0.05,**p<0.005, ***p<0.001).

nematode, albeit having major differences compared to the human female reproductive system, can be used as a simple fertility model organism. The intertwined relationship of somatic and germline aging has long been debated. In *C. elegans,* mutant strains which affect fertility, and have a mortal germline, include the *mrt-2* mutants which accumulate double strand breaks in their DNA both under basal conditions and after DNA damage [57]**.** Accumulation of damage across generations gradually leads to sterility. The experimental setup for fertility assays in *C. elegans* includes measurement of their egg laying capacity at 25°C, considered to be a mild prolonged stress for multiple gen-

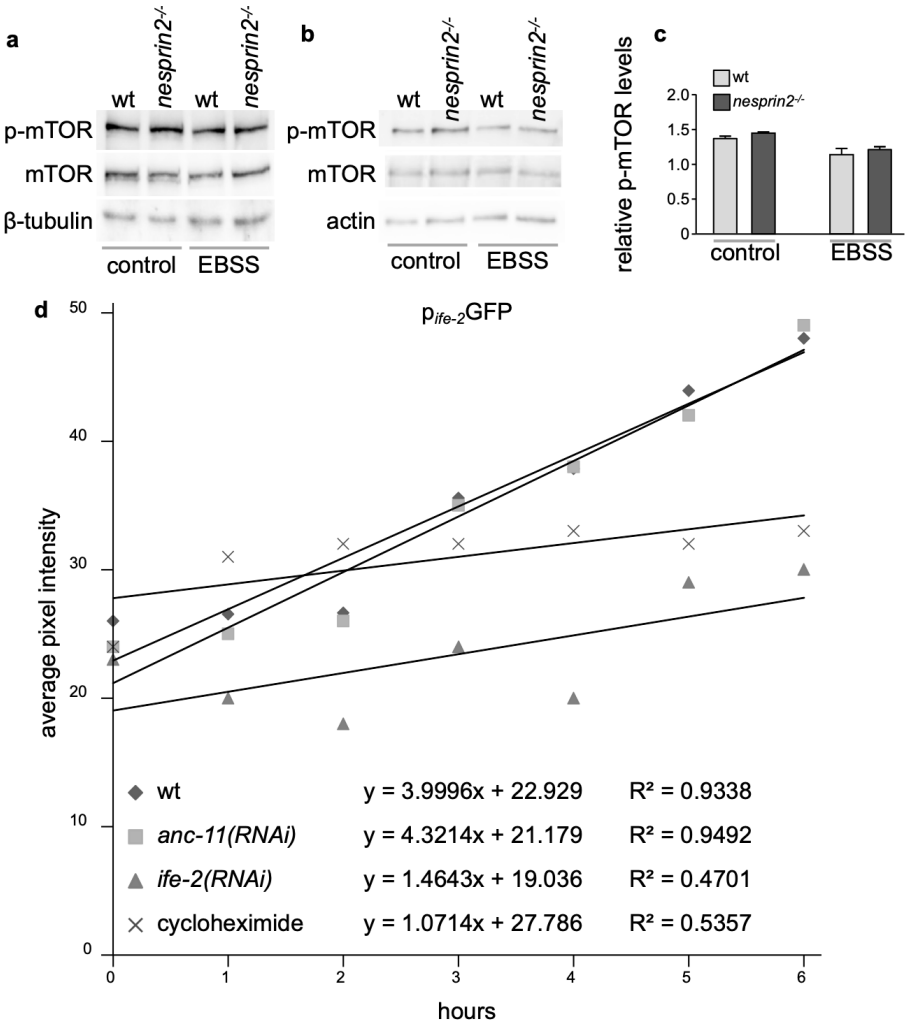

Figure 28. ANC-1/nesprin 2 mildly affects protein translation a) FRAP analysis of wt, *anc-1(RNAI), ife-2(RNAi)* & cycloheximide-treated transcriptional reporter p*ife-2*GFP nematode worms after epifluorescent imaging before, immediately after and every 1hr for 6hrs of photobleaching. The best fit line illustrates the recovery rate, while the slope is the quantification of the recovery rate. b & c) Western blot analysis of total mTOR and phosphorylated mTOR (p-mTOR) of two independent experiments. d) Quantification of the average p-mTOR of the two individual experiments compared to total mTOR and normalized to β-tubulin. All statistical analyses were performed using the unpaired t-test (*p<0.05,**p<0.005, ***p<0.001).

erations to detect gradual reduction of offspring until sterility.

Using this experimental design, it was shown that there is an initial decline in viable offspring in the absence of ANC-1 which ultimately leads to a mortal germline after 5 generations (Figure 29a). Moreover, irregular oocyte shape and size (purple dashed shape), oocyte stacking in a non-linear fashion as well a mutlinuclearity are characteristic of aging germlines which produce low quality oocytes (Figure 29b).

Moreover, in the gonad, physiologically, small sized proliferating germ cells contain large nucleoli while, as they enter meiosis and differentiate into oocytes, nucleolar size is decreased. The most proximal oocyte, which will be fertilized, has no nucleolus. This process of regulating nucleolar size in the gonad is integral to germ cell differentiation and healthy oocyte production. Interestingly enough, in the absence of ANC-1, proliferating germ cells have both larger nuclei as well as nucleoli (Figure 30a,b,c & d), while proximal oocytes fail to eliminate their nucleoli (Figure 31a & b).

In order to better detect gonad anatomical abnormalities, the OD95 strain was used where both the plasma membrane, PLC1-delta1 (green), and the nucleus by means of histone 58 (red) are detected. Tumour-like structures are evident in *anc-1(RNAi)* treated worms after 5 generations as detected by dashed yellow lines in

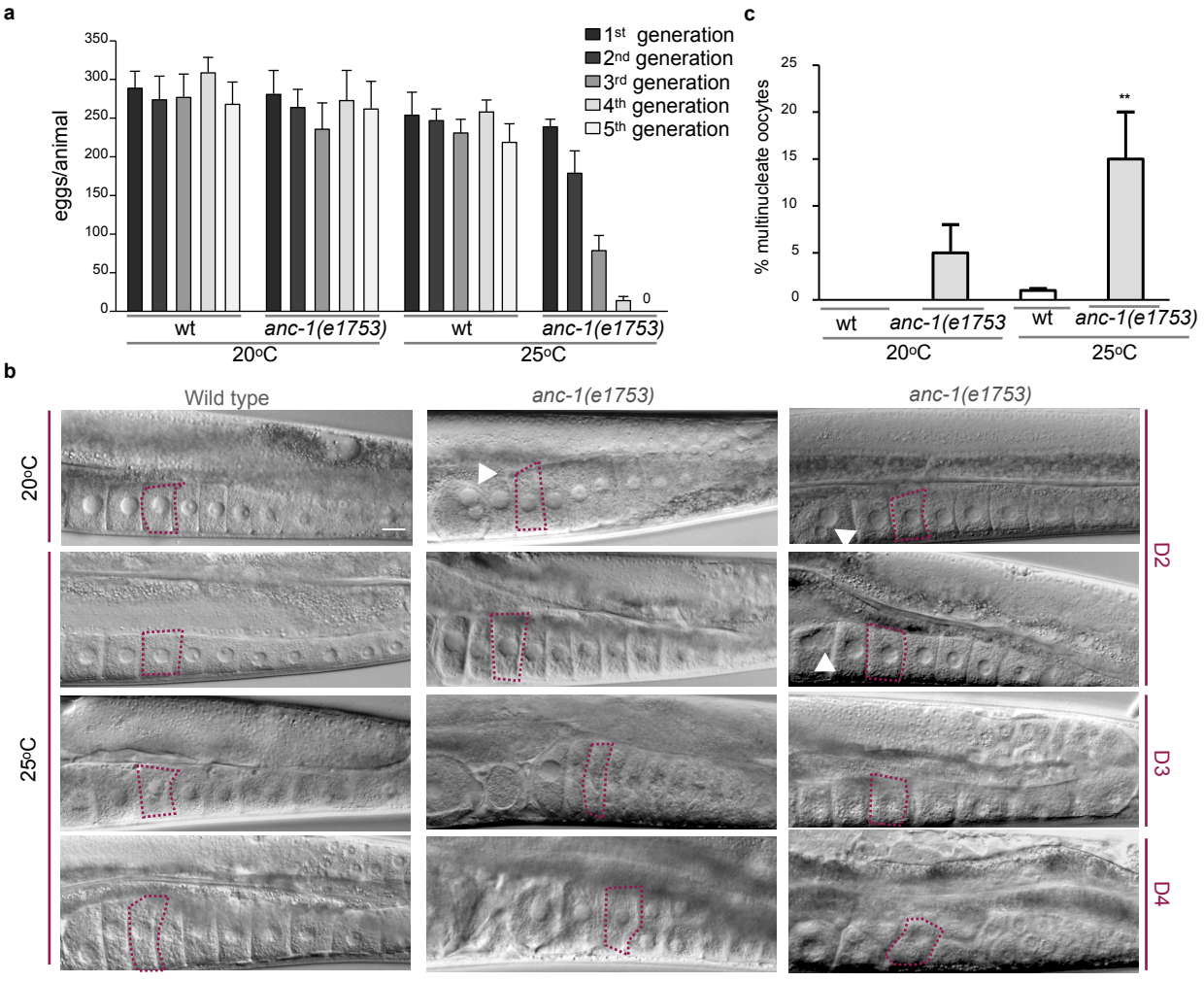

Figure 29. ANC-1 safeguards germline anatomy & immortality a) Egg laying capacity of wt and *anc-1(e1753)* mutants at 20 & 25 degrees Celsius. b) % of gonads with multinucleate oocytes in wt and *anc-1(e1753)* mutants at 20 & 25 degrees Celsius c) DIC microscopy of wild type and *anc-1(e1753)* mutant germlines at day 2 (D2), day (3) & day 4 (D4) of adulthood (20 & 25 degrees Celsius). Arrowheads indicate multinucleation; dashed purple line indicate oocytes.Scale bars represent 20µm. All statistical analyses were performed using the unpaired t-test (*p<0.05,**p<0.005, ***p<0.001).

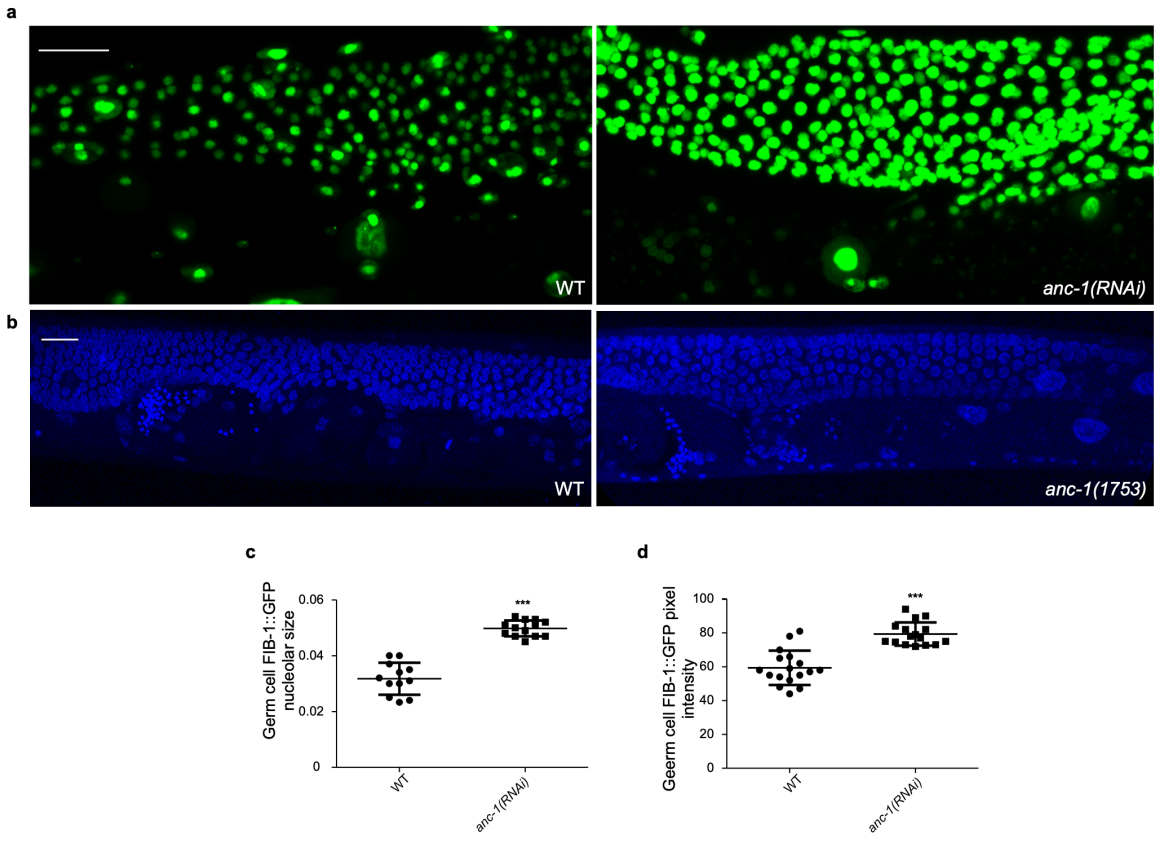

Figure 30. ANC-1 regulates nucleolar size in germ cells. a) Confocal microscopy of Germlines of day 2 WT & *anc-1(RNAi)*-treated FIB-1::GFP worms b) Confocal microscopy of DAPI-stained germlines of day 2 WT and *anc-1(1753)* worms. c) & d) Nucleolar germ cell size and pixel intensity as determined by FIB-1::GFP using Fiji. All statistical analyses were performed using the unpaired t-test (*p<0.05,**p<0.005, ***p<0.001). Scale bar indicates 20µm.

whole worm images (Figure 32a). Moreover, the proliferative and meiotic zone area is increased in the absence of ANC-1 in a similar manner as when pro-apoptotic CED-4 is ablated, the APAF-1 orthologue in worms (Figure 33). In the absence of pro-survival BCL2 orthologue, CED-9, germline area shrinks. Moreover, knockdown of ANC-1 caus-

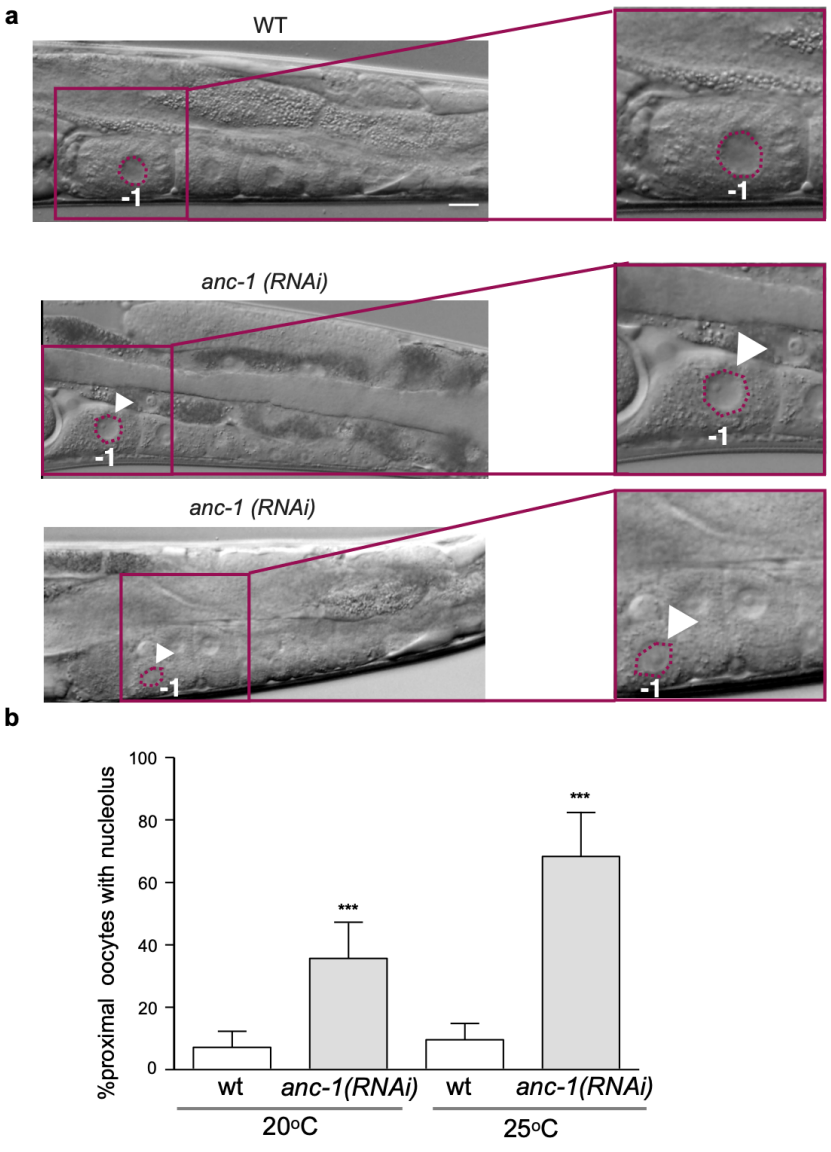

Figure 31. ANC-1 regulates nucleolar elimination in the proximal oocyte. DIC microscopy of wild type and *anc-1(RNAi)* germlines of day 2 adult worms (25 degrees Celsius). Arrowheads indicate nucleolar presence at the proximal oocyte annotated as '-1'; dashed purple circle indicates the nucleus of the proximal oocyte. Purple squares indicate the area which is enlarged on the right.; dashed purple line indicate oocytes.Scale bars represent 20µm. All statistical analyses were performed using the unpaired t-test (* $p<0.05$, ** $p<0.005$, *** $p<0.001$).

es germ cell accumulation at the apoptotic turn (yellow dashed line square) with increased oocyte production. This could be due to either an increased proliferative activity of the cells or an apoptotic defect. Additionally, multinuclearity, another characteristic of cancer like is evident (white arrowheads).

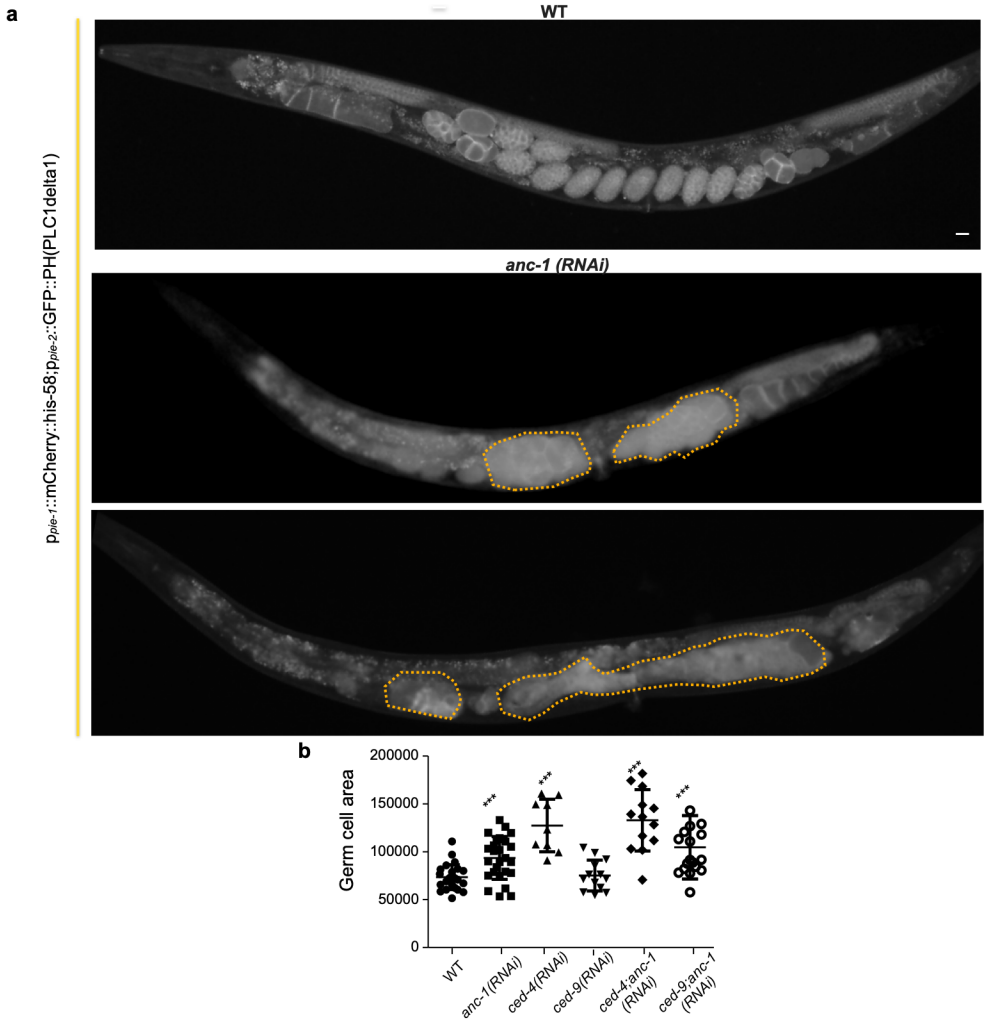

Figure 32. ANC-1 regulates germline anatomy. a) Epifluorescent microscopy of day 2 p_{pie-1}::mCherry::his-58;p_{pie-2}::GFP::PH(PLC1delta1) worms treated with control (WT), anc-1 (RNAi) after 5 generations. Dashed yellow lines indicate accumulated germ cells/oocytes (germline tumours). b) Measured germ cell area of the gonad of control (WT), *anc-1(RNAi), ced-4(RNAi), ced-9(RNAi), anc-1(RNAi);ced-4(RNAi), anc-1(RNAi);ced-9(RNAi)* (25 degrees Celsius). (without the meiotic turn & oocytes). Scale bar represents 20µm. All statistical analyses were performed using the unpaired t-test (*p<0.05,**p<0.005, ***p<0.001).

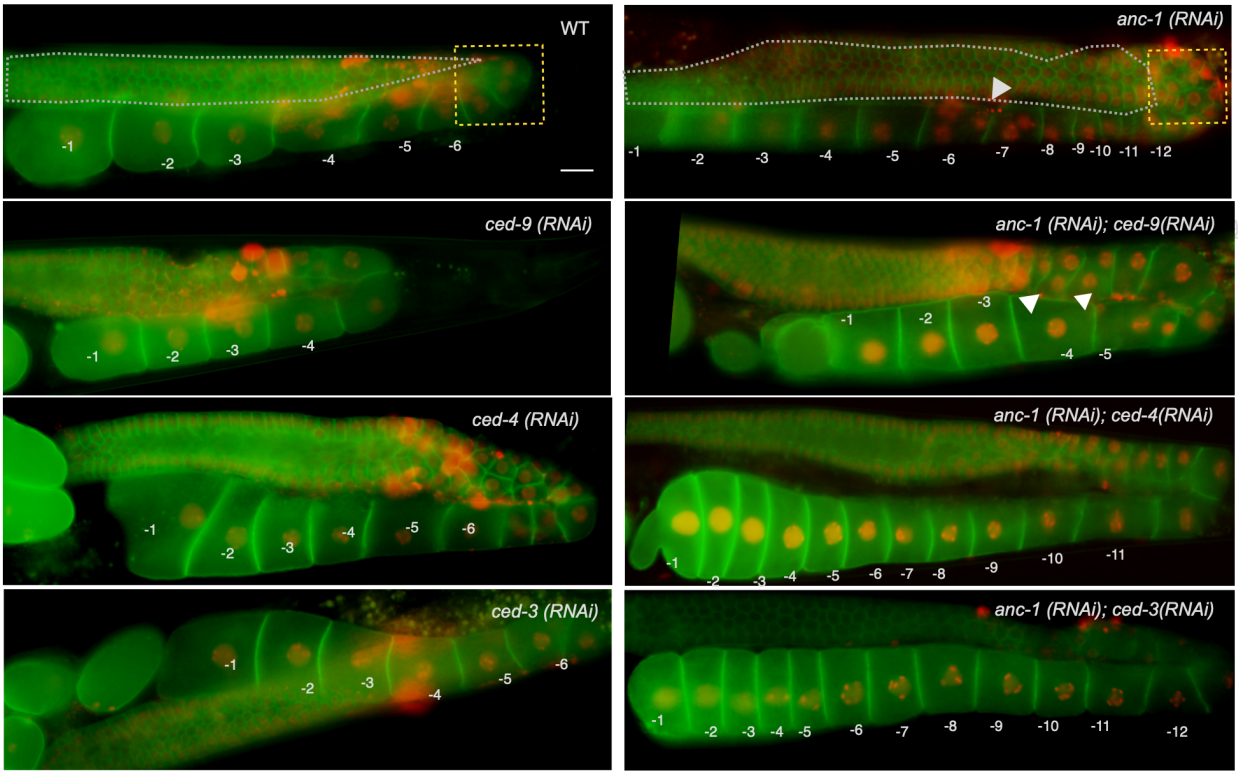

Figure 33. ANC-1 regulates germline anatomy. Epifluorescent microscopy of day 2 p_{pie-1}::mCherry::his-58;p_{pie-2}::GFP::PH(PLC1delta1) worms treated with control (WT), *anc-1(RNAi), ced-4(RNAi), ced-9(RNAi), anc-1(RNAi);ced-4(RNAi), anc-1(RNAi);ced-9(RNAi) & anc-1(RNAi);ced-3(RNAi)* (25 degrees Celsius). Arrowhead indicates multinuclearity, while numbering annotations indicate oocytes starting from the most proximal '1'. Dashed yellow

Knockdown of *anc-1* in worms grown at 25 degrees exhibited a gradual decrease in oocyte production after 7 generations, with accumulating evidence of anatomical abnormalities, irregularly sized, shaped and stacked oocytes, multinuclear germ cells and

oocytes, which are usually eliminated by apoptosis at the germ cell stage [58] (Figure 34).

Apoptotic programmed cell death clears out any aberrant or defective germ cells and selectively allows healthy cells to differentiate into oocytes. It is physiological quality control mechanism to ensure healthy offspring. However, no direct link between defective apoptosis and the mortal germline has been found [58]. Accumulation of DNA damage due to defective clearance of germ cells can stall them in meiosis, maintain them in a semi-differentiated state or instigate their uncontrollable proliferation. Nevertheless, this leads to germline senescent phenotypes, such as germline tumours and poor oocyte quality. ANC-1 ablation seems to, in part, halt apoptosis in the germline, due to the increased germline area and cell accumulation in the apoptotic loop region. However, whether ANC-1 acts through the core apoptotic machinery (CED-9/CED-4/CED-3) is unclear as double knockdown of either pro-apoptotic CED-3 and CED-4 together with ANC-1 has an additive effect in oocyte production (Figure 34).

CED-1::GFP worms were used to dissect the mechanism by which at least partially, ANC-1 regulates germline anatomy. CED-1 is a transmembrane protein expressed in engulfing somatic gonad sheath cells [59]. After one generation, there is a slight decrease in cell corpses (apoptotic bodies) being engulfed in the absence of ANC-1, as shown by both DIC and fluorescent microscopy of CED-1::GFP worms (Figure 35). Af-

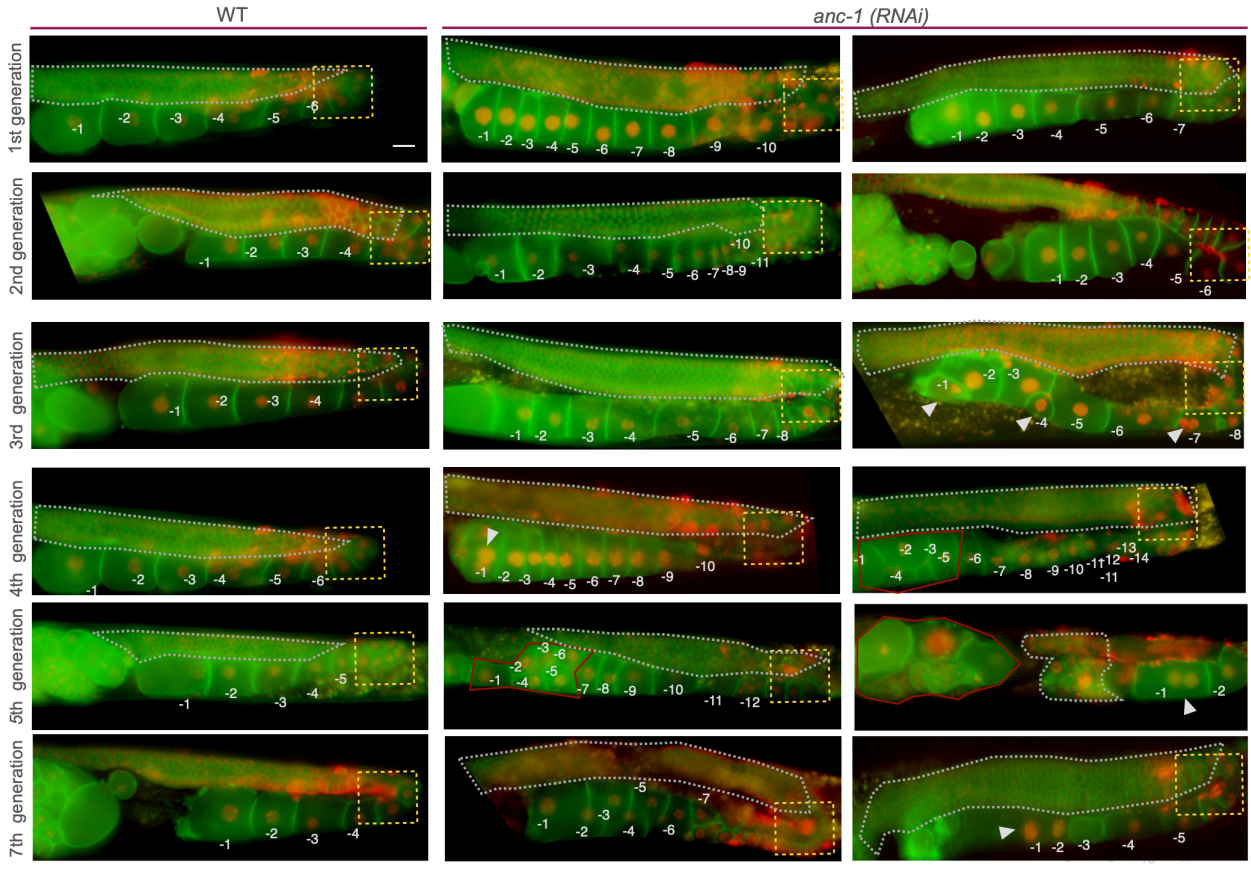

Figure 34. ANC-1 regulates germline anatomy. Epifluorescent microscopy of day 2 p_{pie-1}::mCherry::his-58;p_{pie-2}::GFP::PH(PLC1delta1) worms treated with control (WT), *anc-1 (RNAi)* for 7 generations (25 degrees Celsius). Arrowheads indicate germline defects such as multinuclearity, aberrant oocytes, while numbering annotations indicate oocytes starting from the most proximal '1'. Dashed yellow squares highlight the 'death zone' or apoptotic loop. Red shape indicates oocyte clumping (germline tumour). Scale bar represents 20µm.

ter multiple generations engulfing somatic gonad sheath cells aberrantly encircle semi-differentiated germ cells/oocytes, suggesting dysregulated cell clearance (Figure 36).

Moreover, as it was previously shown that *anc-1* mutants are more susceptible to DNA damage (Figure 29), DNA damage levels were evaluated in the absence of ANC-1. Indeed, when ANC-1 is knocked down, germ cells exhibit increased DNA damage marker RPA-1 foci formation (Figure 37). Accumulation, both in the absence of any DNA damaging agents and after exposure to UV-C irradiation is an indication that there is a defect in DNA damage clearance. This accentuates the fact that ANC-1 is integral to the germ cell nuclear quality control pathway. MEF staining of nesprin 1 and LC3 has shown that there is increased nesprin 1/LC3B colocalisation after UV-C induced DNA damage.

Thus, there is increasing evidence that ANC-1, by controlling nuclear and nucleolar homeostasis, protects the cells from malignancy as lack of the ANC-1 protein leads to accumulation of germ cells, tumor formation at the proximal gonad end, multinucleate germ cells and oocytes, increased DNA damage. Preliminary mouse data shows that multiple organs have increased size possibly implying a cancerous phenotype. Indeed mutations in *nesprin 1 & nesprin 2* have been identified in intestinal, ovarian and breast cancer [60, 61]**.** These findings require forth investigation to confirm cell transformation. The most prominent organ enlargement is that of the spleen, that could be attributed either to spleen cancer or splenomegaly. *Nesprin 2 (SYNE 2)* polymorphisms have been identified in type 2 diabetes patients with concomitant

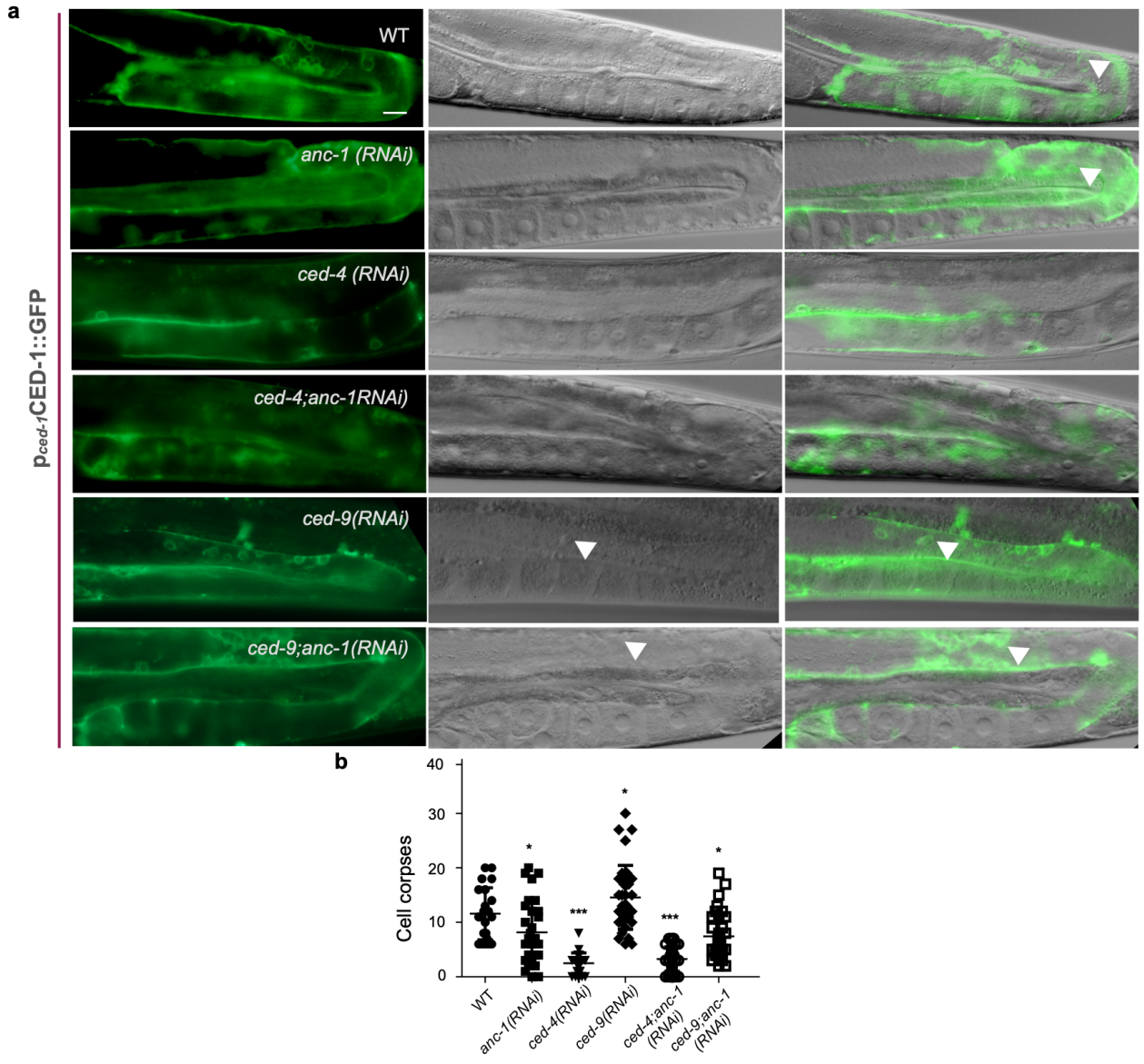

Figure 35. ANC-1 affects apoptosis. a) Epifluorescent & DIC microscopy of day 2 p_{ced-1}CED-1::GFP worms treated with control (WT), *anc-1, ced-4, ced-9, ced-3, ced-4;anc-1,ced-9;anc-1; ced-3;anc-1 (RNAi).* Arrows indicated apoptotic bodies (cell corpses). b) Number of cell corpses (CED-1-encircled bodies) per gonad in control (WT), *anc-1(RNAi), ced-4(RNAi), ced-9(RNAi), anc-1(RNAi);ced-4(RNAi), anc-1(RNAi);ced-9(RNAi).* Scale bar represents 20µm. All statistical analyses were performed using the unpaired t-test (*p<0.05,**p<0.005, ***p<0.001).

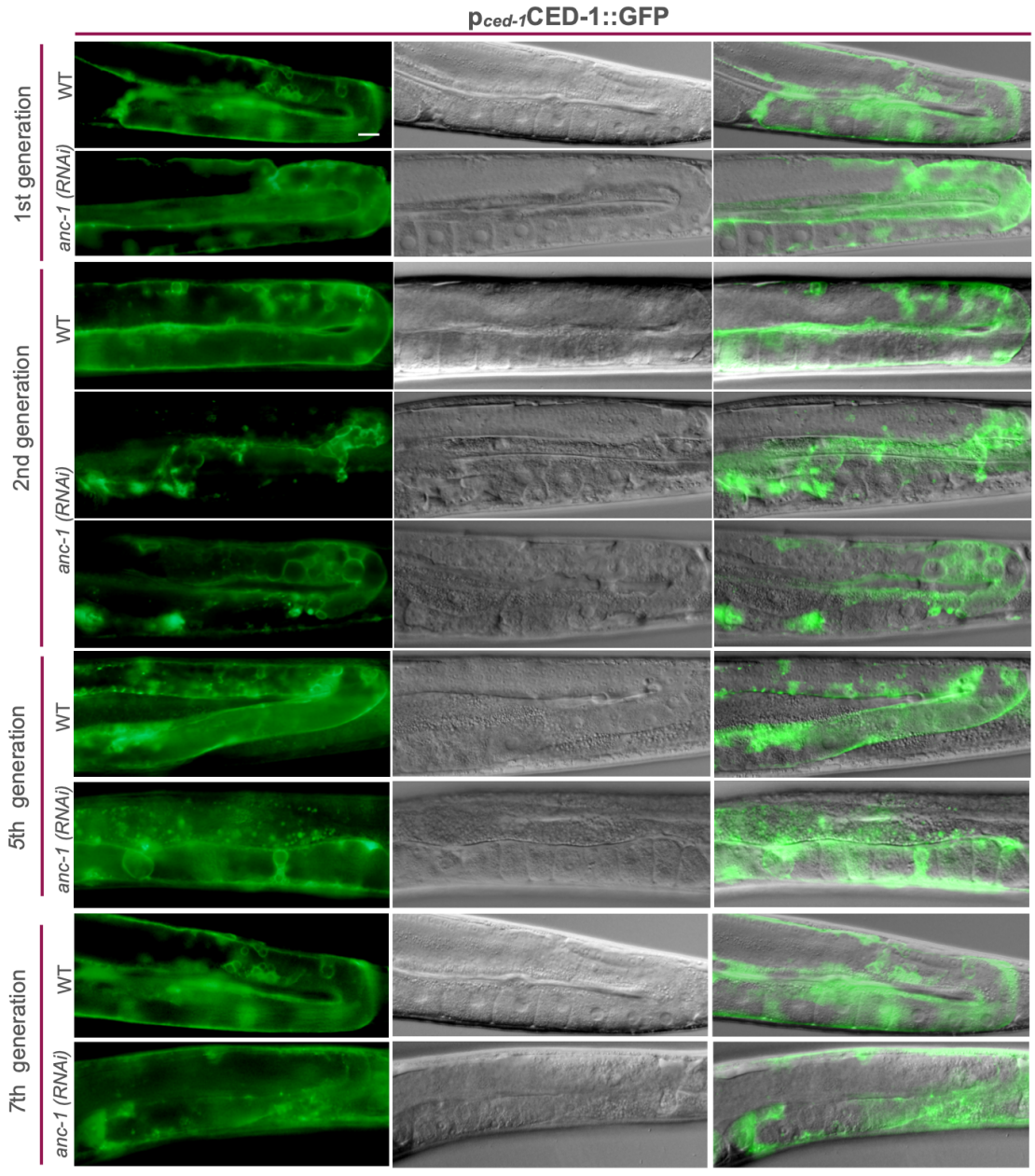

Figure 36. ANC-1 regulates apoptosis across generations. a) Epifluorescent & DIC microscopy of day 2 p_{ced-1}CED-1::GFP worms treated with control (WT), *anc-1 (RNAi)*. Arrows indicated apoptotic bodies (cell corpses). b) Number of cell corpses (CED-1-encircled bodies) per gonad in (WT), *anc-1, ced-4, ced-9, ced-3, ced-4;anc-1,ced-9;anc-1; ced-3;anc-1 (RNAi)* (25 degrees Celsius). (without the meiotic turn & oocytes). Scale bar represents 20µm.

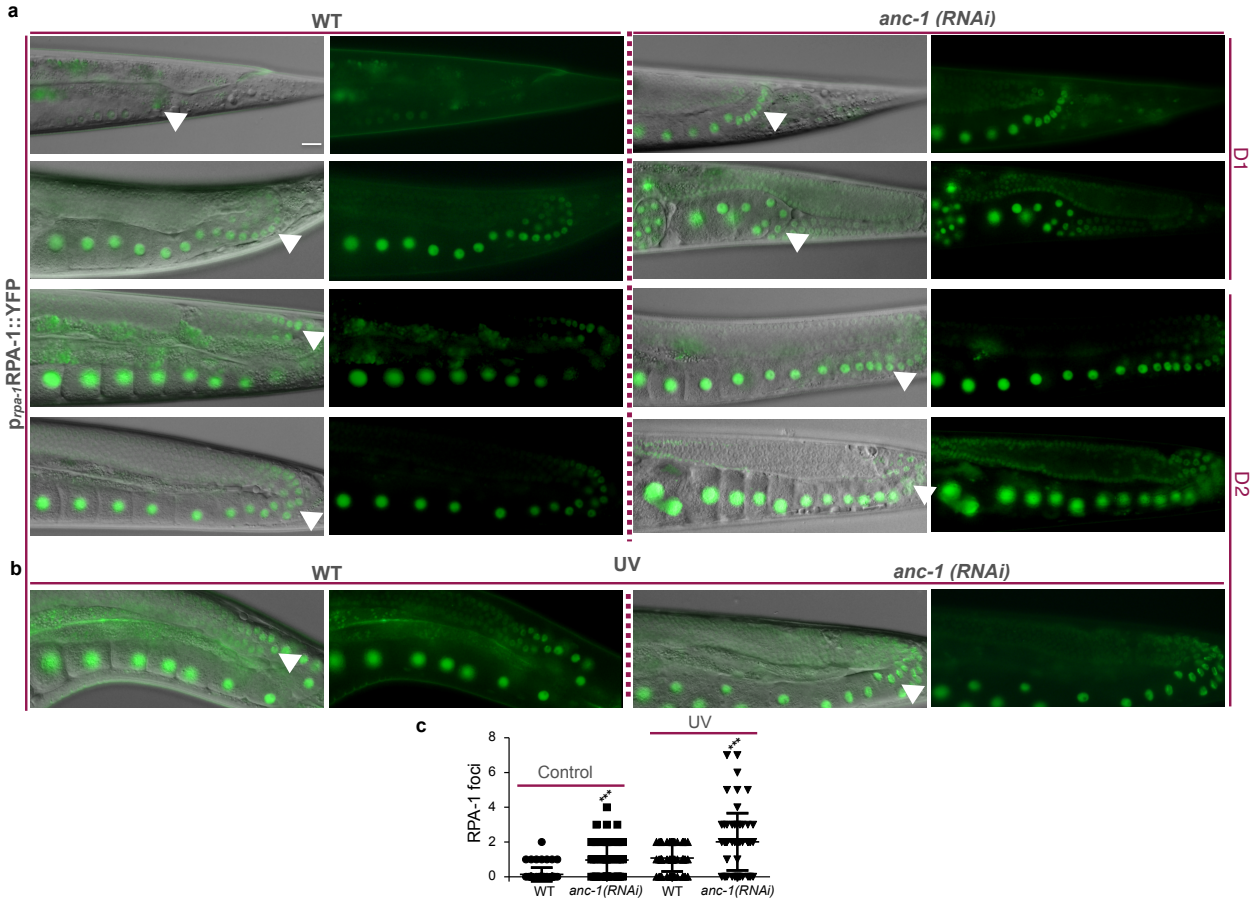

Figure 37. ANC-1 safeguards the germline genome. a) Epifluorescent & DIC microscopy of day 1 & day 2 p_{rpa-1}RPA-1::YFP worms treated with control (WT), *anc-1 (RNAi)*. Arrowheads indicate RPA-1 foci. b) UV-C induced DNA damage was performed in WT & *anc-1(RNAi)* p_{rpa-1}RPA-1::YFP (25^{o}C) c) Count of RPA-1 foci per gonad of WT & *anc-1(RNAi)*-treated of control & UV-C induced p_{rpa-1}RPA-1::YFP. All statistical analyses were performed using the unpaired t-test (*p<0.05,**p<0.005, ***p<0.001). Scale bar represents 20μm.

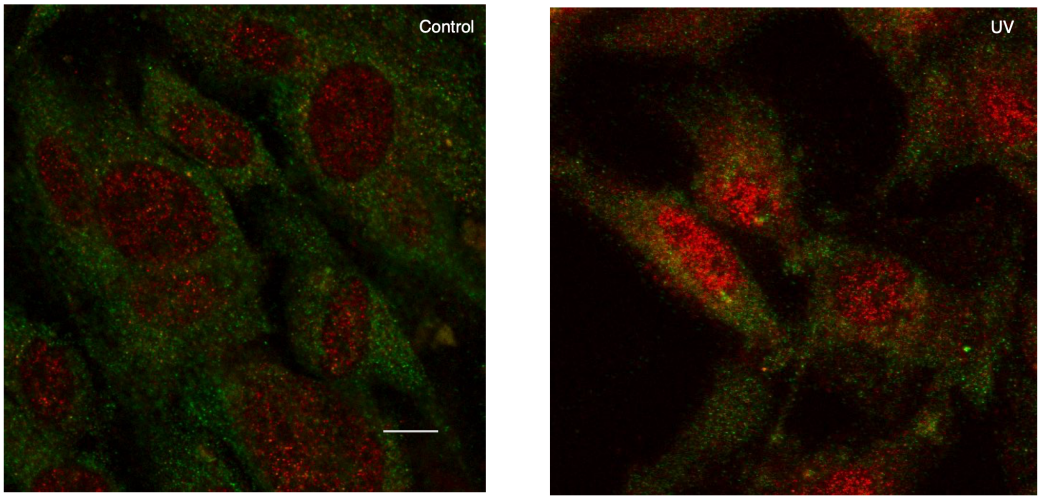

Figure 38. Nesprin 1 patten after UV-C induced DNA damage. Confocal imaging of control & UV-C irradiated primary MEFs with nesprin 1 in & LC3 double staining. Scale bar

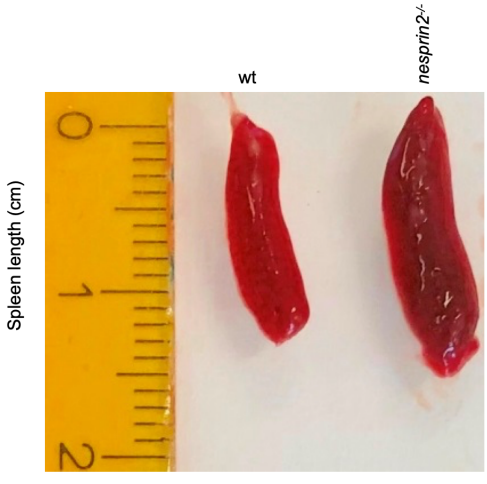

Figure 39. Splenomegaly in the absence of *nesprin 2*. Wt (left) and *nesprin2*$^{-/-}$ (right) spleens of 5 month old male mice. Ruler numbering is in centimeters.

increased sphingomyelin levels. Complementing this evidence, anatomical studies of *nesprin2*$^{-/-}$ 5-month old mice demonstrated splenomegaly (Figure 20), a pathological condition related to lysosomal storage diseases and sphingolipid accumulation (68).

4. Discussion & Conclusions

Selective autophagy of nuclear components occurs in organisms ranging from simple single cell eukaryotes to humans. Substrates can include RNA, diffuse proteins or components of the nuclear envelope, nuclear bodies and the nucleolus. In yeast, different types of micronucleophagy exist under both basal and nutrient deprivation conditions. In mammals, although there are indications of nucleophagic events under physiological conditions, nucleophagy has mainly been associated with pathology. For example, oncogenic and neurodegenerative events induce two different pathological models of nucleophagy which are different and seemingly cell-specific. In both scenarios, lamin degradation is prominent, resulting in cellular senescence and neuronal death, respectively. Hence, it could be a matter of hyperactivation of nucleophagy leading to an aging/degenerative phenotype while physiological levels of nucleophagy could preserve cellular homeostasis. Identification of potential instigators of macronucleophagy in physiology would spur new research directions in the field. Apart from neurodegeneration caused by extreme nucleophagy, an unanswered question relates to the consequences of nucleophagy deficiency. Nevertheless, fine-tuning nucleophagic degradation is potentially essential to prevent age-related disease and cancer.

Molecular pathways selectively inducing this autophagic process could also be therapeutic targets for a multitude of diseases linked to the formation of nuclear aggregates. For instance, nuclear LC3 deacetylation triggers its cytoplasmic shuttling. This

molecular pathway could be pharmacologically exploited to trigger nuclear autophagy. Identifying inducers of nucleophagy could potentially allow clearance of excess pathological aggregates, particularly because nuclear pores further restrict large protein transport causing nuclear protein accumulation.

Our study reveals that autophagic recycling of the nuclear envelope and nucleoli is key to nuclear architecture preservation which ultimately modulates nucleolar size and promotes longevity. Nesprins are outer nuclear envelope proteins which function as specific nucleophagy receptors as well as substrates to recycle themselves as well as other nucleophagic substrates. Nesprins regulate the autophagic process, while their genetic perturbation causes autophagic nuclear protein and polyglutamine protein aggregation as well as enlarged immature autophagosomal structures in the cytoplasm. They themselves are also targeted by autophagy and interact with core autophagosomal components, under both basal and nutrient stress conditions. Remarkably, nesprins are required to maintain small size nucleoli, a distinctive feature of long-lived genetic nematode backgrounds and young versus old mammalian cells.

Thus, nesprin-mediated nucleophagy is an important longevity assurance mechanism that participates downstream of life-span prolonging interventions, to maintain nuclear homeostasis and halt nucleolar expansion. Importantly, there is strong evidence that ANC-1 is rehired for efficient fertility or germline immortality, an example of repro-

ductive youthfulness. Moreover, future work should be directed to understand whether germline immortality is directly connected to nesprin, lamin or nucleolar autophagy degradation. Moreover, other nucleophagic substrates should not be excluded in nesprin-mediated autophagy. In addition, nucleophagy seems to affect other cellular processes that have been implicated in lifespan regulation, including protein synthesis and proteostasis, by regulating the abundance of nucleolar components such as fibrillarin and ribosomal RNAs. This is mediated through nesprin 2-dependent autophagic degradation of fibrillarin, which is conserved from nematodes to mammals. (Figure 40). Combined, these findings suggest a novel, evolutionarily conserved role for nuclear nesprin protein family members in nuclear autophagy and nuclear size regulation. The tight evolutionary conservation and ubiquitous expression of nodal nucleophagy regulators suggests that similar pathways promote youthfulness and delay aging across distant taxa.

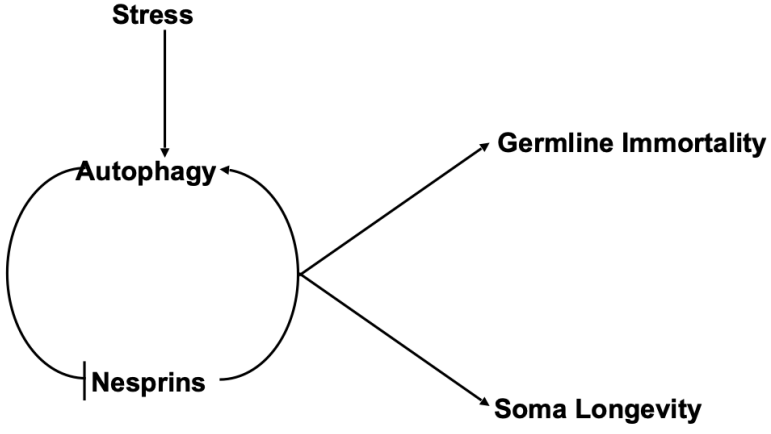

Figure 40. Schematic diagram of nucleophagic pathway. Autophagic recycling of nuclear membrane and nucleolar components, under conditions of stress, preserves nuclear architecture, restricts nucleolar size and delays aging.

Concerning its role as a nucleophagy receptor, in yeast, the Nem1/Spo7-Pah1 axis properly localizes micronucleophagy component Nvj1 (nucleus-vacuole junction 1) and nucleophagy receptor Atg39. Importantly, Nesprin 2 interacts with CTNEP1 [62][63]**.** Future experiments should be directed to further pinpoint how nesprin 2 contributes to autophagic progression and whether it contributes to autophagy of other nuclear components. Moreover, its interaction with inner nuclear components has been previously described such as with RNASE2B [64] which aids in the clearance of DNA damage marker gH2AX [65]. Its effects on the nucleolus are further substantiated as nesprin 2 interacts with nucleophosmin, a nucleolar protein which directly interacts with fibrillarin, while it also interacts with SIRT7 an rDNA transcriptional regulator [66].

Nesprin mutations have been associated with SCA1 cerebellar ataxia. Moreover, it has been shown that nesprin 2 interacts with Ataxin 1 which might explain our results of accumulated polyglutamine repeats in the *C. elegans* Q40 disease model, when the nesprin 2 orthologue, ANC-1, is absent [67, 68]. Importantly, polyglutamine diseases are not merely cytoplasmic aggregation diseases but also nuclear aggregates are formed, such as in the case of ataxin-1 with polyglutamine repeats which include protein/RNA nuclear droplets [69].

Concerning cell death and nesprins, there is conflicting data showing both their pro-apoptotic and pro-survival effects. Firstly, ANC-1 has been shown to interact with CHC-1, clathrin heavy chain orthologue and DHC-1, the dynein heavy chain homologue, which executes the engulfment of apoptotic bodies through the CED-4 pathway[70-72]. Moreover, very recently, its interaction with Bax pro-apoptotic protein was proven, which increases upon apoptotic stimuli, without clearly indicating the regulatory role of Bax on nesprin 1 and 2 [73]. Nevertheless, as CED-4 requires SUN-1/Matefin as its nuclear receptor for executing apoptosis in the germline of nematodes, a known interaction of of ANC-1, ANC-1 might also contribute to this interaction [74]. Indeed, during cisplatin-induced apoptosis, both nesprin 1 and nesprin 2 protein levels are reduced in MEFs, while in the absence of Bax, their levels remain steady [73]. Complementarily, ANC-1 & nesprin 2 both interact with amphiphysin/BIN1 [75]. An interesting scenario would be that nesprins comprise of the autophagic (nucleophagic) cell death pathway. This cellular pathway has not been fully chaaccterised, in terms of when it is physiologically activated and what occurs when it is dysfunctional. Recently, it has been shown that autophagic cell death restricts genome instability and telomere dysfunction during 'replicative crisis', a process activated before cell transformation [76]. Thus in this case autophagy acts a tumor suppressor, where telomeric DNA damage produces cytosolic DNA, fragile nuclear membranes, and macroautophagy is activated to clear out the damage and avoid malignancy. Both

nesprin 1 and nesprin 2 interact with TERF2, which maintains nuclei and protects against end-to-end fusion [77]. Moreover, nuclear membrane proteins such as SUN1 are required for inner nuclear anchoring of telomeres [78]. Germline mortal *mrt-2* mutants have defects in telomere replication. Thus, further investigation of whether telomere dysfunction is apparent in ANC-1-depleted oocytes might reveal the connection between autophagic cell death in germ cells regulated by ANC-1 to preserve genome integrity and germline immortality.

ΠΕΡΙΛΗΨΗ (ΙΙ)

Η διαλεύκανση των βασικών μοριακών μηχανισμών που διέπουν την προοδευτική μείωση της κυτταρικής λειτουργίας που συνοδεύει τη γήρανση και τελικά οδηγεί στην βιολογική φθορά, έχει άμεση επίδραση στο σχεδιασμό καινοτόμων παρεμβάσεων που θα μπορούσαν να μειώσουν ή να καθυστερήσουν την σχετιζόμενη με την ηλικία ανθρώπινη φθορά. Η γήρανση είναι μία διαδικασία που διέπεται από πολύπλοκους μηχανισμούς, οι οποίοι δεν έχουν διαλευκανθεί πλήρως ακόμα. Μία βασική αιτία είναι η βλάβη του DNA και η ρύθμιση της επιδιόρθωσής του. Αν και φυσιολογική κυτταρική διαδικασία, η σταδιακή συσσώρευση γενετικών βλαβών επηρεάζει αρνητικά βασικές λειτουργίες του κυττάρου και συντελεί σε εμφάνιση παθογενών καταστάσεων όπως ο νευροεκφυλισμός, ο διαβήτης, η καρκινογένεση και άλλες κατά την πάροδο του χρόνου. Η ανάλυση και κατανόηση των μηχανισμών απόκρισης για να αντιμετωπιστεί η συσσώρευση αυτών των βλαβών είναι καίριο ερώτημα.

Ως αποτέλεσμα στρεσσογόνων για το κύτταρο καταστάσεων μπορεί να προκληθεί κυτταρικός θάνατος νεκρωτικού τύπου και στα νευρικά κύτταρα συγκεκριμένα νευροεκφυλισμός. Χρησιμοποιήσαμε το νηματώδη *Caenorhabditis elegans* (*C. elegans*) για να μοντελοποιήσουμε τον νευροεκφυλισμό ως αποτέλεσμα συσσώρευσης γενετικών βλαβών. Με αυτόν τον τρόπο θα μπορέσουμε να κατανοήσουμε γιατί προκαλείται αυτός ο παθολογικός

νευρωνικός θάνατος και ποια μοριακά σηματοδοτικά μονοπάτια δρουν προστατευτικά. Τα ευρήματα της μελέτης αυτής κατ'επέκταση θα συμβάλλουν στο χαρακτηρισμό των μηχανισμών που διέπουν σοβαρές παθολογικές καταστάσεις στον άνθρωπο.

Υπάρχουν πολλά είδη βλαβών του DNA και οι μηχανισμοί επιδιόρθωσης του DNA που επιστρατεύονται από το κύτταρο εξαρτώνται από το είδος της βλάβης του DNA. Τα διμερή πυριμιδινών και η προσθήκη ογκωδών χημικών μορίων επιδιορθώνονται με την 'Επιδιόρθωση με εκτομή νουκλεοτιδίων' (Nucleotide excision repair pathway). Η συσσώρευση βλαβών στο DNA είναι γνωστό ότι μπορεί να προκαλέσει απόπτωση, δηλαδή ελεγχόμενο προγραμματισμένο κυτταρικό θάνατο, που συμβαίνει φυσιολογικά κατά τη διάρκεια της ανάπτυξης ενός οργανισμού. Αντιθέτως, ο νεκρωτικός κυτταρικός θάνατος είναι επιβλαβής για τον οργανισμό. Στα πλαίσια της βλάβης του DNA, η μόνη ένδειξη αυτού του τύπου θανάτου έχει καταγραφεί σε ινοβλάστες και καρκινικές κυτταρικές σειρές, αλλά όχι στο νευρικό ιστό. Μελέτες για παθήσεις που σχετίζονται με συσσώρευση βλαβών του DNA και την επιδιόρθωσή τους γίνονται κυρίως με οργανισμούς-μοντέλα που φέρουν μεταλλάξεις σε γονίδια που ρυθμίζουν τους επιδιορθωτικούς αυτούς μηχανισμούς. Για παράδειγμα, μεταλλάξεις στο γονίδιο *ERCC1* ή *ercc-1* στο *C. elegans* προκαλούν το σύνδρομο 'Cockayne' με συμπτώματα μεταξύ άλλων την πρόωρη γήρανση, την προβληματική ανάπτυξη

του νευρικού συστήματος και την υπερευαισθησία στον ήλιο. Παρά την πληθώρα των βιβλιογραφικών αναφορών σχετικά με το πώς οι μεταλλάξεις σε αυτά τα γονίδια μπορούν να συντελέσουν στην πρόωρη γήρανση και τον καρκίνο, παραμένει αδιευκρίνιστο το πώς επηρεάζουν το νευρικό σύστημα σε κυτταρικό και υποκυτταρικό επίπεδο και πως προκαλούν παθογένειες νευρολογικής φύσης *(Schumacher et al., 2010)*. Στα πλαίσια αυτής της μελέτης, ως μοντέλο χρησιμοποιήθηκε ο νηματώδης *C. elegans* και συγκεκριμένα ένα στέλεχος που φέρει μετάλλαξη στο γονίδιο *ercc-1* που ρυθμίζει την επιδιόρθωση του DNA. Στη συνέχεια, βλάβη του DNA προκλήθηκε με υπεριώδη ακτινοβολία (UV). Ο νεκρωτικός κυτταρικός θάνατος διαγνώστηκε με μεθόδους μικροσκοπίας συνδυαστικά με χρωστικές ουσίες.

Εδώ αποδείξαμε ότι η νέκρωση εμφανίζεται αυθόρμητα κατά τη διάρκεια της ενηλικίωσης και της γήρανσης του νηματώδη και σε μεταλλαγμένα *ercc-1* στελέχη. Η μικροσκοπία DIC είναι μια έγκυρη, αν και ευαίσθητη μέθοδος, για την ανίχνευση νεκρωτικών κυττάρων. Το ιωδιούχο προπίδιο, από την άλλη πλευρά, το οποίο χρησιμοποιείται σε καλλιέργειες θηλαστικών κυττάρων, μας έδωσε ποιοτικά και όχι ποσοτικά αποτελέσματα και έτσι μπορεί να χρησιμοποιηθεί μόνο συμπληρωματικά. Η μικροσκοπία φθορισμού των νευρωνικών δημοσιογράφων σε συνδυασμό με τη μικροσκοπία DIC μας επέτρεψε να απεικονίσουμε τον νεκρωτικό νευροεκφυλισμό. Επιλέξαμε να εργαστούμε με ένα διαγονιδιακό ντοπαμινερ-

γικό στέλεχος αναφοράς GFP καθώς ο νηματώδης έχει 4 ζεύγη ντοπαμινεργικών νευρώνων που ανιχνεύονται εύκολα. Τα αρχικά δεδομένα έδειξαν ότι η (ημι)πλήρης απώλεια φθορισμού, εκφυλισμένων αξόνων και νεκρωτικών κυττάρων αυξάνεται. φυσιολογικά κατά τη γήρανση ή όταν το μοριακό μονοπάτι NER είναι ελαττωματικό. Ομοίως, η ακτινοβολία UVC και το οξύ οξειδωτικό στρες φαίνεται να αυξάνουν τον νεκρωτικό ντοπαμινεργικό νευροεκφυλισμό.

Θα πρέπει να γίνει μια πιο στοχευμένη μελέτη για την επιβίωση διαφορετικών τύπων νευρώνων μετά από βλάβη του DNA με τη χρήση διαφορετικών στελεχών αναφοράς. Με αυτόν τον τρόπο, η ευαισθησία διαφορετικών τύπων νευρώνων στη βλάβη του DNA θα ανιχνευθεί αποκαλύπτοντας πιθανές συνδέσεις μεταξύ σχετικών νευρολογικών ασθενειών. Επιπλέον, η μελέτη μπορεί να επεκταθεί και σε άλλα γονίδια του NER μονοπατιού. Αυτός ο νεκρωτικός τύπος νευροεκφυλισμού μπορεί να είναι η πηγή ή ένας παράγοντας που συμβάλλει σε πολλές νευροεκφυλιστικές ασθένειες που σχετίζονται με την ηλικία καθώς προκαλεί ένα ανεξέλεγκτο φλεγμονώδες κύμα.

DNA Damage & Neurodegeneration

5. Introduction

5.1 Nucleotide excision repair pathway

DNA damage accumulation generated due to genetic or environmental stress during an individual's lifespan instigates apoptosis and senescence at the cellular level and a multitude of pathologies including age-related disorders at the organismal level. From malignancy to progeroid syndromes, increasing evidence highlights the intricacy of the DNA damage repair pathways activated to fix the damage caused.

The nucleotide excision repair pathway (NER) is triggered either by ultraviolet radiation (UV) or chemical compounds to remove helix distorting DNA lesions (69). Mutations in genes regulating this pathway cause autosomal recessive disorders such as Xeroderma pigmentosum, Cockayne syndrome, trichothiodystrophy, and UV-sensitive syndrome. The NER pathway is divided into two subpathways, the global genome NER (GG-NER) where the whole genome is checked for helix distortions, and the transcription-coupled NER (TC-NER) which is activated when there is a stall of RNA polymerase II during elongation on the template strand (70).

The GG-NER initiates with DNA damage recognition, when XPC binds to a single-stranded DNA gap. For UV-induced DNA lesions, the UV-DDB protein complex and the CRL (cullin 4A (CUL4A)– regulator of cullins 1 (ROC1) E3 ubiquitin ligase) complex are recruited to aid XPC binding. Mutliple reversible DNA verification lesion proteins are recruited TFIIH (transcription initiation factor IIH). When strand incision is performed, the step is irreversible. The endonucleases XPF–ERCC1 and XPG incise the DNA strand. This excision causes a 30 nucleotide gap. In this process, XPA is a master regulator of the GG-NER pathway as it interacts with most NER proteins while inducing the TFIIH complex to verify the DNA lesion (71). The replication protein A (RPA) prevents the non-damaged DNA strand from endonuclease cuts. Finally, gap filling and ligation is performed by replication proteins and DNA polymerases.

The TC-NER repairs DNA damage-induced lesions which stall transcription in order to restart transcription. Identification of lesions is done through detection of transcription elongation blockade of RNA polymerase II. Cockayne syndrome WD repeat proteins A and B (CSA & CSB) are then recruited to bring together the UV-DDB and XPC complexes, which are shared with the GG-NER, with UV-stimulated scaffold protein A (UVSSA), ubiquitin-specific processing protease 7 (USP7) XPA-binding protein 2 (XAB2) and high mobility group nucleosome binding domain containing protein 1 (HMGN1).

Perturbation in the GG-NER machinery can cause a skin condition, Xeroderma pigmentosum which makes the individual more prone to malignancy. XPC and XPE mutations induce only mild skin pigmentation symptoms while increasing the probability of sun triggered skin cancer by 1000 times (72). Defects in the XPA protein, which is involved in the TC-NER, induce neuronal loss and neurodegeneration in early adulthood (73). Mutations in the transcription coupled repair causes neurodevelopment disorders as well as premature aging. Cockayne syndrome symptoms, caused by Cockayne syndrome A and B (CSA & CSB), range from cachectic dwarfism, microcephaly, severe neurological problems affecting eyesight and cognition, walking and feeding following premature death at 12 years of age (74). A more severe form of Cockayne syndrome is Cerebro-oculo-facio-skeletal syndrome (COFS). Both syndromes cause premature aging coupled with pathologies found in elderly people such as atherosclerosis. XPB, XPD, XPG mutations cause a combination of photosensitivity, increased skin cancer probability and Cockayne syndrome mutations. All in all, neurodegeneration and progeria are among the most prominent features which arise from NER protein defects.

5.2 *C. elegans* as a DNA damage repair model organism

C. elegans' natural habitat is exposed to solar irradiation. However, there are other DNA damaging agents in the food and environment of the worm which form DNA lesions repaired by the NER (75).

UVB (320-290nm) and UVC irradiation (290-100nm) form bulky DNA lesions repaired by NER. UV-hypersensitive mutant worms for orthologue mammalian genes have been identified. GG-NER is mainly active in dividing cells in the germline thus UV irradiation of *xpc-1* mutant worms causes reduced embryo survival. TC-NER on the other hand is induced in the rest of soma in post-mitotic cells and *csb-1* mutants display a developmental delay after UV exposure. Worms with a deficit in proteins involved in the core NER pathway are UV-hypersensitive both in the germline and the somatic tissue such as ERCC-1 (76). UV irradiation can simultaneously and rapidly cause DNA damage to the whole or part of the worm.

5.3 Necrotic cell death in *C. elegans*

Necrosis is a mode of unprogrammed inflammatory cell death shared by both invertebrates and vertebrates. It can be triggered by exogenous environmental insults or intrinsic factors. Multiple features of the mechanism by which necrosis is triggered and the downstream effectors are shared between nematodes and mammals, thus *C. elegans* can be used as a platform to dissect necrosis in physiological and human pathologies.

Apoptosis, which is a form of programmed cell death, occurs in dividing cells, both in physiology during development and due to pathological insults. It differs mechanistically and morphologically from necrosis. Specifically, apoptosis entails cell rounding,

chromatin condensation and nuclear fragmentation while necrosis is illustrated by osmotic swelling of organelles, increased cell volume and rupture of the plasma membrane (Figure 41)(77).

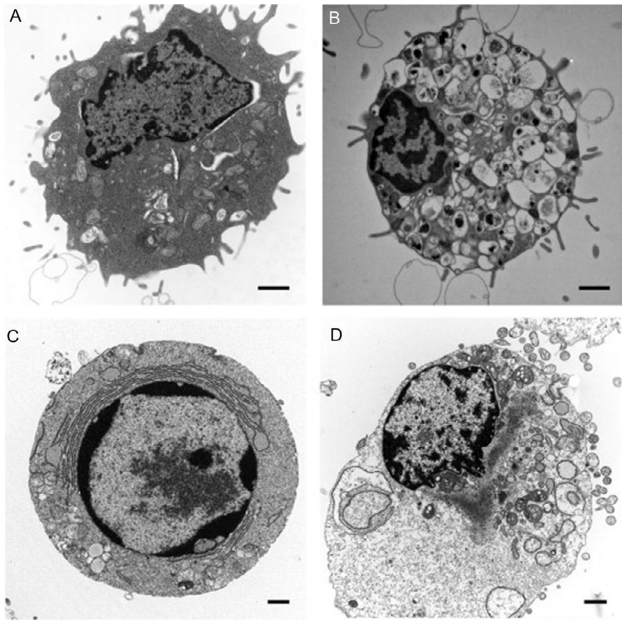

Figure 41. (A) Normal (B) Autophagic (C) Apoptotic (D) Necrotic cells. Reprinted from Edinger and Thompson (2004), copyright (2004)

Moreover, at the organismal level, a blue intense fluorescence is detected in the intestinal cells by necrosis, in a wave from the anterior to the posterior part causing cytosolic acidosis (78). The fluorescence is derived from lysosome related gut granules as anthralic acid glucose esters. This is reminiscent of mammalian necrotic propagation in excitotoxicity and neurodegeneration after ischemia. Necrosis can be visualised, due to

the nematode's transparency, with differential interference contrast (DIC) or Nomarski optics, by detecting individual nuclei.

While apoptosis occurs only during development, necrotic cell death mainly occurs during adulthood. Triggers of necrosis include ionic imbalance as modeled by ion channel mutations, heat, infection and hypo-osmotic shock. (79, 80). Next, there is a rapid increase in cytoplasmic calcium ions (Ca^{2+}) originating from the extracellular space or intracellular stores such as the endoplasmic reticulum (ER). Calpain proteases are then induced to target lysosomal proteins and break down lysosomes. Following, cathepsin proteases are released into the cytoplasm and autophagy is activated contributing to the cellular catastrophe. The conservation of function of proteins involved in the necrotic cell death pathway allow us to use it as model organism for neurodegeneration triggered by hypoxia, heat, neurotoxicity or DNA damage.

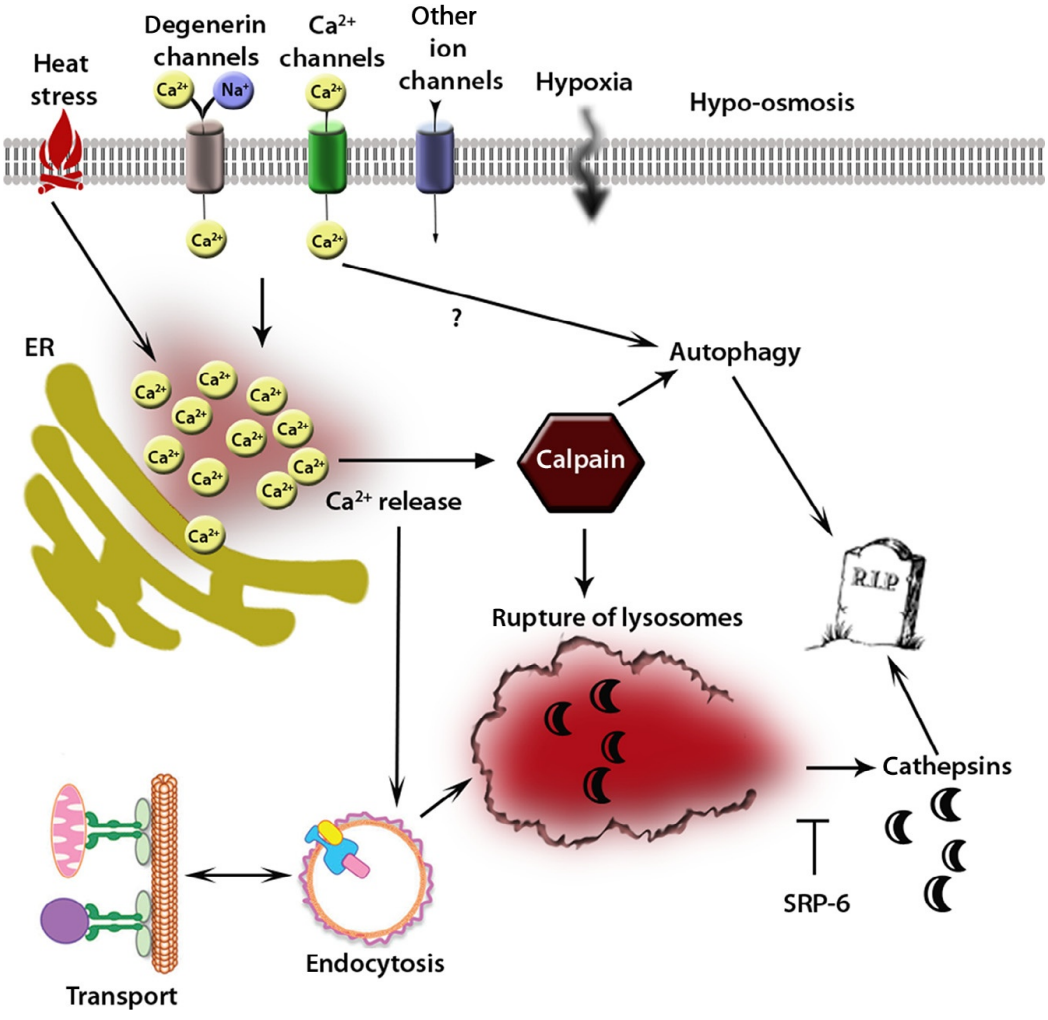

Figure 42. Necrotic cell death in *C. elegans*

5.4 DNA damage-induced neurodegeneration

DNA damage repair mechanisms are essential for organismal homeostasis and proper neuronal functions. Defects in the repair of DNA breaks caused from aging related neurodegeneration and severe neurological syndromes as described above leading to premature death. Specifically, in Alzheimer's disease (AD), there are increased DNA strand lesions and simultaneous protein reduction in repair proteins. Similarly, in Parkinson's disease (PD) and amyotrophic lateral sclerosis (ALS), single strand breaks and oxidative lesions have been detected (81). Neuron-specific conditional knockouts of the the NER pathway, particularly *Ercc1,* display reduced synaptic plasticity and memory deficits. More recently. *Ercc1* mRNA has been detected at lower levels in the blood of AD patients compared to control individuals (82).

5.5 Aim

DNA damage is a major contributing factor in aging and has been implicated in neurodegeneration. A critical question that emerges is whether intrinsic neuronal stress response pathways are induced to protect against DNA damage-triggered neurodegeneration. Moreover, although it is well established that DNA damage induces apoptosis, the contribution of inflammatory necrotic cell death to DNA damage-related pathology remains largely elusive.

6. Materias & Methods

6.1 Strains

Strains were maintained at 20^{o}C unless otherwise noted. The following strains were used in this study: N2: wild-type Bristol isolate, For intracellular Ca^{2+} monitoring experiments, transgenic animals expressing the Ca^{2+} reporter GCaMP2.0, N2; [$p_{let\text{-}858}$GCaMP2.0; rol-6], were used, for DNA damage repair mutants *ercc-1 (tm1981)*, and for dopaminergic neuron GFP expression egIs1[$p_{dat\text{-}1}$::GFP] and *ercc-1(tm1981)*;$p_{dat\text{-}1}$GFP.

6.2 UVC irradiation & microscopy (DIC & fluorescence)

Synchronized wild type N2 and animals were obtained by collecting embryos from gravid day 1 adults after treatment with bleaching solution (H_2O:Bleach:5N NaOH 7:2:1). The worms were grown on UV-killed OP50 bacteria by UVC exposure for 15 minutes, For DNA damage at the L4 developmental stage, worms were treated with 100J m^{-2} UVC irradiation using an ultraviolet crosslinker (BIO-LINK-BLX-E365, Vilber Lourmat) (83). 18 hours later, on day 1 of adulthood, worms were gently washed once from bacteria using M9. Worms were then immobilized using 15µl 20mM levamisole and mounted on slides. Microscopic examination of cell or neuron corpses were detected at 40X magnification using DIC with a Zeiss AxioImager Z2 epifluorescence microscope. For egIs1[$p_{dat\text{-}1}$::GFP], which express GFP in dopaminergic neurons only under the *dat*-

1 promoter, loss of fluorescence captured by fluorescence microscopy with simultaneous detection of neuronal corpses by DIC was performed. 100 animals were counted in 3 independent experiments.

For acute oxidative stress, paraquat was added on NGM plates, at a final concentration of 10 mM per plate on top of UV-treated OP50 bacteria, and 100 day 4 adults were plated. One day later, worms were scored for survival. Three biological repeats were performed.

To detect spontaneous necrosis or neurodegeneration during aging, day 4 and day 8 adults N2 or day 6 and day 8 adults egIs1[$p_{dat\text{-}1}$::GFP] respectively, were used. Worms were washed 3x with M9 buffer immobilized using 15µl 20mM levamisole and mounted on slides. Microscopic examination of cell or neuron corpses were detected at 40X magnification using DIC with a Zeiss AxioImager Z2 epifluorescence microscope. Loss of fluorescence captured by fluorescence microscopy with simultaneous detection of neuronal corpses by DIC was performed.

6.3 Propridium iodide staining

For propidium iodide staining, a fluorescent dye staining necrotic cells and excluded from live cells and apoptotic bodies, young adult worms were incubated for 3 h in 10 µM propidium iodide (Sigma) in M9 buffer, 18 hours after UVC irradiation 100J m^{-2} UVC irradiation using an ultraviolet crosslinker (BIO-LINK-BLX-E365, Vilber Lourmat),

and visualized using a compound epifluorescence microscope for both fluorescence and necrotic corpses using DIC.

6.4 Ca^{2+} monitoring

For intracellular Ca^{2+} monitoring experiments, transgenic animals expressing the Ca2+ reporter GCaMP2.0 were examined under a Zeiss AxioImager Z2 epifluorescence microscope. For UV induced DNA damage, L4 worms were treated with 100L/m2 as described above. Whole body images were taken at 10X as fluorescence is evident mainly in the intestine. The emission intensity of GCaMP2.0 was calculated by using the ImageJ software (http://rsb.info.nih.gov/ij/).

6.5 Statistics

Mean values were compared using unpaired t-tests was performed. Error bars indicate standard deviation. Each assay was repeated at least three times. We used the Prism software package (GraphPad Software, San Diego, USA) for statistical analyses.

7. Main results

7.1 Necrotic cell death in aged NER-deficient worms

Initially, our first question raised was whether neurodegeneration due to deficiency in the NER DNA damage repair mechanism is due to necrotic cell death. To detect spontaneous necrotic cell death during aging, UV-hypersensitive mutants, *ercc-1* mutants were used which are defective in the NER pathway. DIC microscopy of D4 adults and D7 adults illustrates that necrotic corspes increase during physiological aging in nematodes (arrowheads) (Figure 43a). Quantification of corpses shows that there is a significant increase of necrotic insults during aging in DNA damage hypersensitive mutants (Figure 43b). Therefore, the NER pathway modulated homeostasis and prevents inflammatory necrotic catastrophe.

Next, we used different UV irradiation intensities to induce DNA damage triggered necrotic mechanisms in L4 worms. In particular, the GCaMP2.0 was used to monitor the increase in intracellular Ca^{2+} levels, the initial step for the induction of the necrotic pathway (Figure 44). We simultaneously checked the health status of the UV-irradiated worms in terms of overall survival and movement. $100J/m^2$ was the ideal UVC intensity chosen for further experiments. We further checked whether propidium iodide (PI) staining is effective in complementing DIC microscopy in detecting necrotic corpses (Figure 45). Although there were some cells which were both stained with necrotic

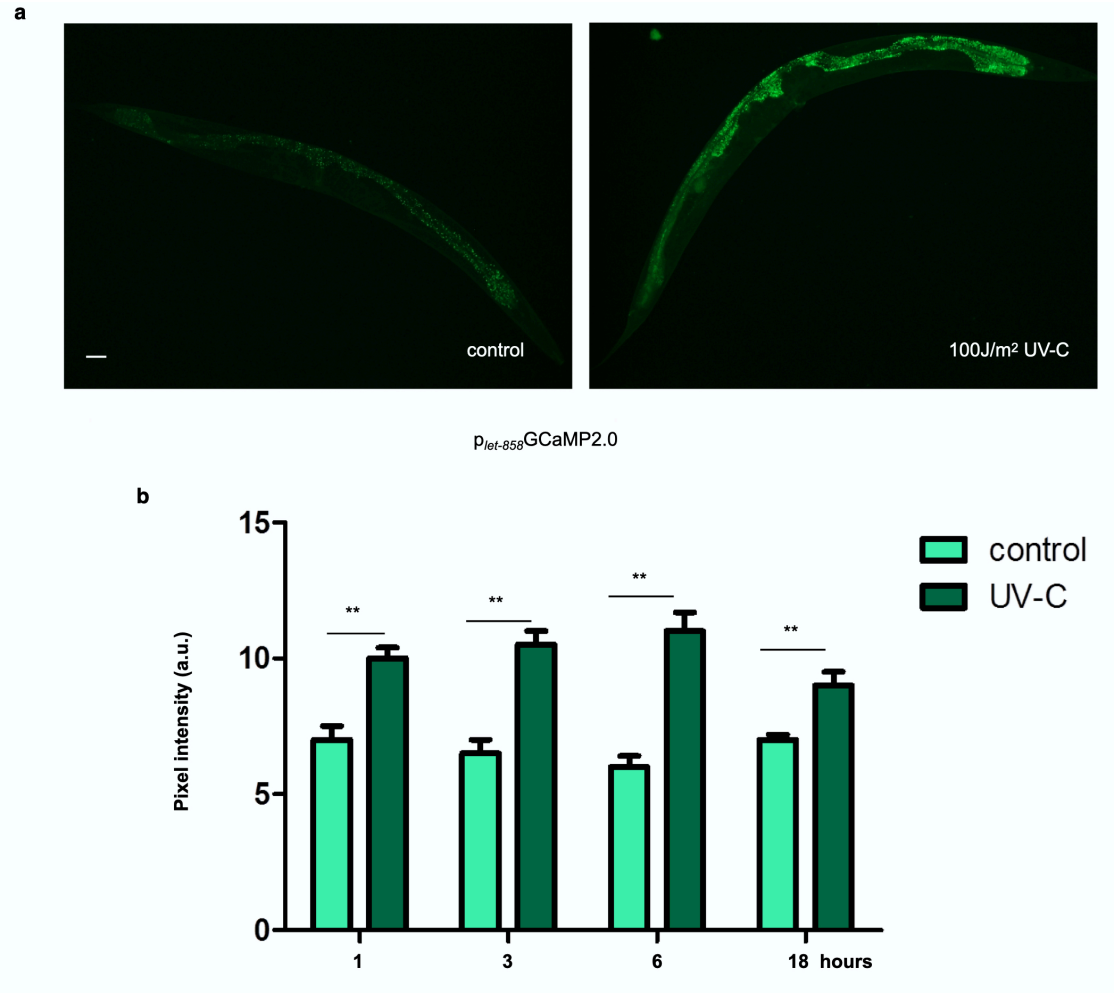

Figure 44. Cytoplasmic Ca^{2+} increases upon UV-C irradiation. Relative cytoplasmic calcium levels at the indicated time points after UV-C irradiation.

corpses and red fluorescence, the diffuse and intense fluorescence was not appropriate for our experimental question.

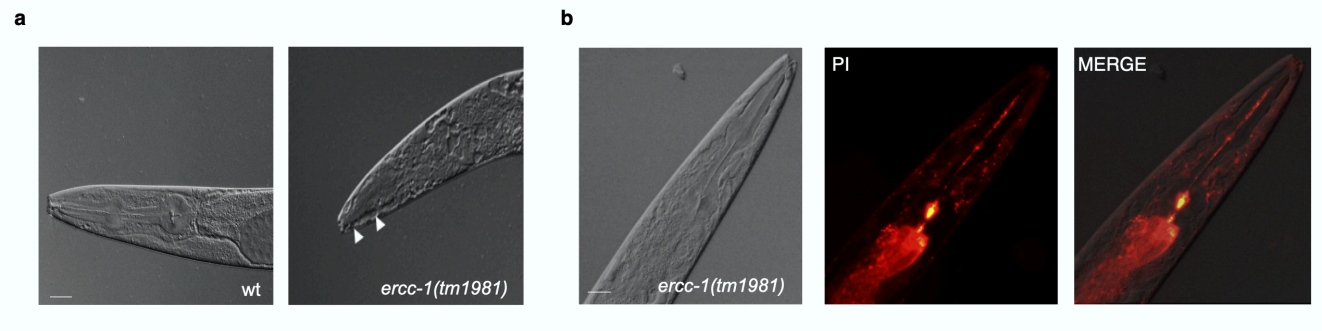

Figure 45. Increased necrotic corpses in NER deficient worms. DIC & fluorescent microscopy with and without propidium iodide staining (PI) of day 1 adults. Scale bar represents 20μm.

7.2 Neurodegeneration in NER-deficient worms

We next investigated whether necrosis, which is observed both in UV-hypersensitive mutants and after UVC irradiation, occurs in neurons ultimately causing neurodegeneration. We used a transgenic strain which is a transcriptional reporter expressing GFP under the control of *dat-1* promoter, $p_{dat\text{-}1}$::GFP, thus in dopaminergic neurons. *C. elegans* has four pairs of dopaminergic neurons which spontaneously degenerate with age. We generated a double transgenic worm *ercc-1(tm1981);* egIs1[$p_{dat\text{-}1}$::GFP] to detect whether DNA damage hypersensitive mutants exhibit increased neurodegeneration in their dopaminergic neurons. Thus, we compared wild type and *ercc-1* mutants during adulthood and aging for number of dopaminergic neurons and signs of neurodegeneration in the soma and/or their axons. Both GFP fluorescence and DIC were assessed from day 3 to day 8 of adulthood (Figure 46).

We further examined whether neurodegeneration is more prominent in NER-deficient animals after environmental or intrinsic stresses such as DNA damage and oxidative stress. Indeed, there is a noteworthy increase in dopaminergic neuronal loss

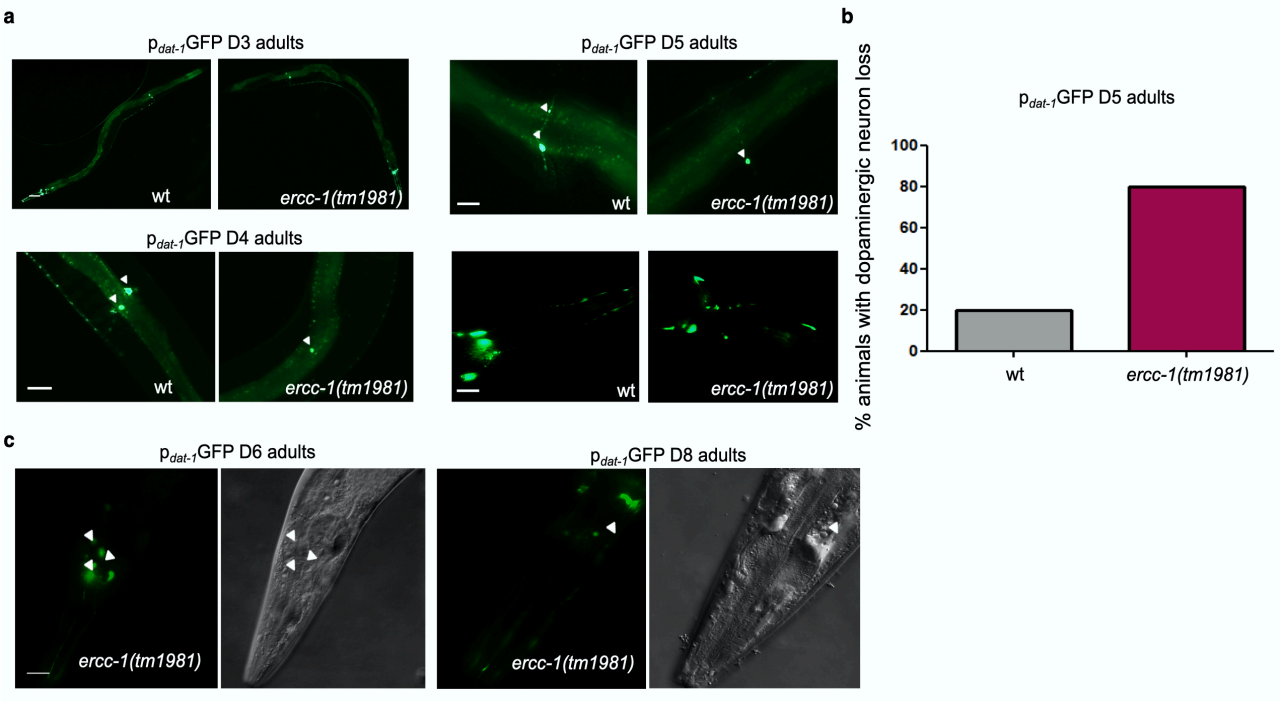

Figure 46. Increased spontaneous neurodegeneration in NER-deficient worms. a) Fluorescent microscopy of $p_{dat\text{-}1}$GFP and *ercc-1(tm1981)*;$p_{dat\text{-}1}$GFP at day 3 and day 5 b) Calculation of proportion of animals with dopaminergic neuron loss at day 5 of adulthood. Scale bar represents 20μm.

in *ercc-1* mutants after UV-C irradiation. Moreover, there were signs of initial stages of axonal neurodegeneration after acute oxidative stress in *ercc-1* mutants (Figure 47).

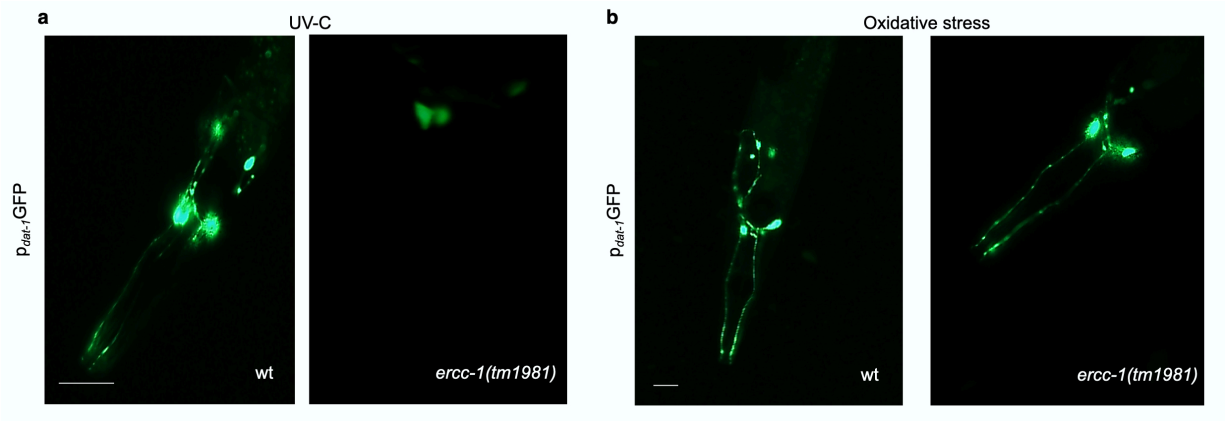

Figure 47. Increased neurodegeneration after DNA damage and oxidative stress. Fluorescent microscopy of D1 (a) or D5 $p_{dat\text{-}1}$GFP worms (b) after UV-C and paraquat treatment, respectively. Scale bar represents 20μm.

8. Discussion & Conclusion

DNA damage repair mechanisms are critical for cell survival and organismal homeostasis. Pathologies caused by defects in the DNA damage repair pathways have severe neurological phenotypes. The NER pathway is responsible for fixing a multitude of DNA lesions such as cyclobutane-pyrimidine dimers (CPDs) and 6–4 pyrimidine–pyrimidone photoproducts (6–4PPs), which are the major lesions induced by UV radiation, intrinsic or environmental bulky chemical adducts, and cyclopurines triggered by reactive oxygen species. Neurodegeneration is evident in syndromes caused by mutation in genes regulating the NER pathway, such as Cockayne syndrome, xeroderma pigmentosum, and trichothiodystrophy (81).

Neurons are post-mitotic cells and after DNA damage in age-related pathologies such as Alzheimers disease and aging, there is experimental evidence suggesting reentry in the cell cycle and subsequent apoptosis (84). In *C. elegans,* somatic cells are post-mitotic thus cell death occurs independently of the cell cycle. Necrosis is an inflammatory catastrophic type of spontaneous cell death.

Here we demonstrated that necrosis occurs spontaneously during adulthood and aging in NER *ercc-1* mutants. DIC microscopy is a valid albeit delicate method to detect necrotic corspes. Propidium iodide on the other hand, which is used in mammalian cell cultures, provided us with qualitative rather than quantitative results and thus can be

used complementarily. Imaging of neuronal reporters with fluorescence microscopy in combination with DIC microscopy allowed us to visualize necrotic neurodegeneration. We chose to work with a transgenic dopaminergic GFP reporter strain as the nematode has four pairs of dopaminergic neurons which are easily detected. Initial data showed that (in)complete loss of fluorescence, degenerating (blebbing) axons and necrotic corpses increased either physiologically during aging or when the NER pathway is defective. Similarly, UV-C irradiation and acute oxidative stress seem to increase necrotic dopaminergic neurodegeneration.

A more deliberate study on the survival of different types of neurons against DNA damage should be performed by using different reporter strains. In that way, the sensitivity of different types of neurons in DNA damage will be detected revealing possible connections between associated neurological diseases Moreover, the study can be expanded to other genes of the NER pathway by using either mutant strains available or by performing *RNAi*. This necrotic type of neurodegeneration can be the source or a contributing factor of many age-related neurodegenerative diseases as it causes an uncontrollable inflammatory wave. Neurons are mostly post-mitotic and thus can accumulate DNA lesions over time which contribute to age-related neuropathology.

9. References

1. Mizushima N, Levine B. Autophagy in mammalian development and differentiation. Nature cell biology. 2010 Sep;12(9):823-30. PubMed PMID: 20811354. Pubmed Central PMCID: 3127249.

2. Kirkin V, Rogov VV. A Diversity of Selective Autophagy Receptors Determines the Specificity of the Autophagy Pathway. Molecular cell. 2019 Oct 17;76(2):268-85. PubMed PMID: 31585693.

3. Kraft C, Martens S. Mechanisms and regulation of autophagosome formation. Current opinion in cell biology. 2012 Aug;24(4):496-501. PubMed PMID: 22664348.

4. Birgisdottir AB, Lamark T, Johansen T. The LIR motif - crucial for selective autophagy. Journal of cell science. 2013 Aug 1;126(Pt 15):3237-47. PubMed PMID: 23908376.

5. Shaid S, Brandts CH, Serve H, Dikic I. Ubiquitination and selective autophagy. Cell death and differentiation. 2013 Jan;20(1):21-30. PubMed PMID: 22722335. Pubmed Central PMCID: 3524631.

6. Ryan TA, Tumbarello DA. Optineurin: A Coordinator of Membrane-Associated Cargo Trafficking and Autophagy. Frontiers in immunology. 2018;9:1024. PubMed PMID: 29867991. Pubmed Central PMCID: 5962687.

7. von Muhlinen N, Thurston T, Ryzhakov G, Bloor S, Randow F. NDP52, a novel autophagy receptor for ubiquitin-decorated cytosolic bacteria. Autophagy. 2010 Feb;6(2):288-9. PubMed PMID: 20104023.

8. Lamark T, Johansen T. Aggrephagy: selective disposal of protein aggregates by macroautophagy. International journal of cell biology. 2012;2012:736905. PubMed PMID: 22518139. Pubmed Central PMCID: 3320095.

9. Palikaras K, Lionaki E, Tavernarakis N. Coordination of mitophagy and mitochondrial biogenesis during ageing in C. elegans. Nature. 2015 May 28;521(7553):525-8. PubMed PMID: 25896323. Epub 2015/04/22.

10. Wang Y, Liu N, Lu B. Mechanisms and roles of mitophagy in neurodegenerative diseases. CNS neuroscience & therapeutics. 2019 Jul;25(7):859-75. PubMed PMID: 31050206. Pubmed Central PMCID: 6566062.

11. Zhang J, Ney PA. Role of BNIP3 and NIX in cell death, autophagy, and mitophagy. Cell death and differentiation. 2009 Jul;16(7):939-46. PubMed PMID: 19229244. Pubmed Central PMCID: 2768230.

12. Chen M, Chen Z, Wang Y, Tan Z, Zhu C, Li Y, et al. Mitophagy receptor FUNDC1 regulates mitochondrial dynamics and mitophagy. Autophagy. 2016;12(4):689-702. PubMed PMID: 27050458. Pubmed Central PMCID: 4836026.

13. Papandreou ME, Tavernarakis N. Monitoring Autophagic Responses in Caenorhabditis elegans. Methods in enzymology. 2017;588:429-44. PubMed PMID: 28237114.

14. Klionsky DJ, Abdelmohsen K, Abe A, Abedin MJ, Abeliovich H, Acevedo Arozena A, et al. Guidelines for the use and interpretation of assays for monitoring autophagy (3rd edition). Autophagy. 2016;12(1):1-222. PubMed PMID: 26799652. Pubmed Central PMCID: 4835977.

15. Zhang H, Chang JT, Guo B, Hansen M, Jia K, Kovacs AL, et al. Guidelines for monitoring autophagy in Caenorhabditis elegans. Autophagy. 2015;11(1):9-27. PubMed PMID: 25569839. Pubmed Central PMCID: 4502811.

16. Hansen M, Chandra A, Mitic LL, Onken B, Driscoll M, Kenyon C. A role for autophagy in the extension of lifespan by dietary restriction in C. elegans. PLoS Genet. 2008 Feb;4(2):e24. PubMed PMID: 18282106. Pubmed Central PMCID: PMC2242811. Epub 2008/02/20.

17. Rubinsztein DC, Marino G, Kroemer G. Autophagy and aging. Cell. 2011 Sep 2;146(5):682-95. PubMed PMID: 21884931.

18. Matecic M, Smith DL, Pan X, Maqani N, Bekiranov S, Boeke JD, et al. A microarray-based genetic screen for yeast chronological aging factors. PLoS Genet. 2010 Apr 22;6(4):e1000921. PubMed PMID: 20421943. Pubmed Central PMCID: PMC2858703. Epub 2010/04/28.

19. Toth ML, Sigmond T, Borsos E, Barna J, Erdelyi P, Takacs-Vellai K, et al. Longevity pathways converge on autophagy genes to regulate life span in Caenorhabditis elegans. Autophagy. 2008 Apr;4(3):330-8. PubMed PMID: 18219227.

20. Simonsen A, Cumming RC, Brech A, Isakson P, Schubert DR, Finley KD. Promoting basal levels of autophagy in the nervous system enhances longevity and oxidant resistance in adult Drosophila. Autophagy. 2008 Feb;4(2):176-84. PubMed PMID: 18059160. Epub 2007/12/07.

21. Lapierre LR, De Magalhaes Filho CD, McQuary PR, Chu CC, Visvikis O, Chang JT, et al. The TFEB orthologue HLH-30 regulates autophagy and modulates longevity in Caenorhabditis elegans. Nature communications. 2013;4:2267. PubMed PMID: 23925298. Pubmed Central PMCID: PMC3866206. Epub 2013/08/09.

22. Pyo JO, Yoo SM, Ahn HH, Nah J, Hong SH, Kam TI, et al. Overexpression of Atg5 in mice activates autophagy and extends lifespan. Nature communications. 2013;4:2300. PubMed PMID: 23939249. Pubmed Central PMCID: 3753544.

23. Lipinski MM, Zheng B, Lu T, Yan Z, Py BF, Ng A, et al. Genome-wide analysis reveals mechanisms modulating autophagy in normal brain aging and in Alzheimer's disease. Proceedings of the National Academy of Sciences of the United States of America. 2010 Aug 10;107(32):14164-9. PubMed PMID: 20660724. Pubmed Central PMCID: 2922576.

24. Melendez A, Talloczy Z, Seaman M, Eskelinen EL, Hall DH, Levine B. Autophagy genes are essential for dauer development and life-span extension in C. elegans. Science. 2003 Sep 5;301(5638):1387-91. PubMed PMID: 12958363.

25. Suh Y, Atzmon G, Cho MO, Hwang D, Liu B, Leahy DJ, et al. Functionally significant insulin-like growth factor I receptor mutations in centenarians. Proceedings of the National Academy of Sciences of the United States of America. 2008 Mar 4;105(9):3438-42. PubMed PMID: 18316725. Pubmed Central PMCID: 2265137.

26. Harrison DE, Strong R, Sharp ZD, Nelson JF, Astle CM, Flurkey K, et al. Rapamycin fed late in life extends lifespan in genetically heterogeneous mice. Nature. 2009 Jul 16;460(7253):392-5. PubMed PMID: 19587680. Pubmed Central PMCID: PMC2786175. Epub 2009/07/10.

27. Johnson SC, Rabinovitch PS, Kaeberlein M. mTOR is a key modulator of ageing and age-related disease. Nature. 2013 Jan 17;493(7432):338-45. PubMed PMID: 23325216. Pubmed Central PMCID: 3687363.

28. Park D, Jeong H, Lee MN, Koh A, Kwon O, Yang YR, et al. Resveratrol induces autophagy by directly inhibiting mTOR through ATP competition. Scientific reports. 2016 Feb 23;6:21772. PubMed PMID: 26902888. Pubmed Central PMCID: 4763238.

29. Eisenberg T, Knauer H, Schauer A, Buttner S, Ruckenstuhl C, Carmona-Gutierrez D, et al. Induction of autophagy by spermidine promotes longevity. Nature cell biology. 2009 Nov;11(11):1305-14. PubMed PMID: 19801973.

30. Komatsu M, Waguri S, Chiba T, Murata S, Iwata J, Tanida I, et al. Loss of autophagy in the central nervous system causes neurodegeneration in mice. Nature. 2006 Jun 15;441(7095):880-4. PubMed PMID: 16625205. Epub 2006/04/21.

31. Martin DD, Ladha S, Ehrnhoefer DE, Hayden MR. Autophagy in Huntington disease and huntingtin in autophagy. Trends in neurosciences. 2015 Jan;38(1):26-35. PubMed PMID: 25282404.

32. Kaushik S, Cuervo AM. Degradation of lipid droplet-associated proteins by chaperone-mediated autophagy facilitates lipolysis. Nature cell biology. 2015 Jun;17(6):759-70. PubMed PMID: 25961502. Pubmed Central PMCID: 4449813.

33. Rodriguez A, Duran A, Selloum M, Champy MF, Diez-Guerra FJ, Flores JM, et al. Mature-onset obesity and insulin resistance in mice deficient in the signaling adapter p62. Cell Metab. 2006 Mar;3(3):211-22. PubMed PMID: 16517408. Epub 2006/03/07.

34. Hetzer MW. The nuclear envelope. Cold Spring Harbor perspectives in biology. 2010 Mar;2(3):a000539. PubMed PMID: 20300205. Pubmed Central PMCID: 2829960.

35. Mijaljica D, Devenish RJ. Nucleophagy at a glance. Journal of cell science. 2013 Oct 1;126(Pt 19):4325-30. PubMed PMID: 24013549.

36. Rahman MA, Mostofa MG, Ushimaru T. The Nem1/Spo7-Pah1/lipin axis is required for autophagy induction after TORC1 inactivation. FEBS J. 2018 May;285(10):1840-60. PubMed PMID: 29604183. Epub 2018/04/01.

37. Krick R, Muehe Y, Prick T, Bremer S, Schlotterhose P, Eskelinen EL, et al. Piecemeal microautophagy of the nucleus requires the core macroautophagy genes. Mol Biol Cell. 2008 Oct;19(10):4492-505. PubMed PMID: 18701704. Pubmed Central PMCID: PMC2555948. Epub 2008/08/15.

38. Scott SV, Nice DC, 3rd, Nau JJ, Weisman LS, Kamada Y, Keizer-Gunnink I, et al. Apg13p and Vac8p are part of a complex of phosphoproteins that are required for cytoplasm to vacuole targeting. The Journal of biological chemistry. 2000 Aug 18;275(33):25840-9. PubMed PMID: 10837477.

39. Oku M, Maeda Y, Kagohashi Y, Kondo T, Yamada M, Fujimoto T, et al. Evidence for ESCRT- and clathrin-dependent microautophagy. The Journal of cell biology. 2017 Oct 2;216(10):3263-74. PubMed PMID: 28838958. Pubmed Central PMCID: 5626533.

40. Huang H, Kawamata T, Horie T, Tsugawa H, Nakayama Y, Ohsumi Y, et al. Bulk RNA degradation by nitrogen starvation-induced autophagy in yeast. The EMBO journal. 2015 Jan 13;34(2):154-68. PubMed PMID: 25468960. Pubmed Central PMCID: 4337068.

41. Papandreou ME, Tavernarakis N. Nucleophagy: from homeostasis to disease. Cell death and differentiation. 2019 Mar;26(4):630-9. PubMed PMID: 30647432. Pubmed Central PMCID: 6460388.

42. Millen JI, Krick R, Prick T, Thumm M, Goldfarb DS. Measuring piecemeal microautophagy of the nucleus in Saccharomyces cerevisiae. Autophagy. 2009 Jan;5(1):75-81. PubMed PMID: 18989095. Epub 2008/11/08.

43. Sargsyan A, Cai J, Fandino LB, Labasky ME, Forostyan T, Colosimo LK, et al. Rapid parallel measurements of macroautophagy and mitophagy in mammalian cells using a single fluorescent biosensor. Scientific reports. 2015 Jul 28;5:12397. PubMed PMID: 26215030. Pubmed Central PMCID: 4517063.

44. Mochida K, Oikawa Y, Kimura Y, Kirisako H, Hirano H, Ohsumi Y, et al. Receptor-mediated selective autophagy degrades the endoplasmic reticulum and the nucleus. Nature. 2015 Jun 18;522(7556):359-62. PubMed PMID: 26040717. Epub 2015/06/05.

45. Huang R, Xu Y, Wan W, Shou X, Qian J, You Z, et al. Deacetylation of nuclear LC3 drives autophagy initiation under starvation. Molecular cell. 2015 Feb 5;57(3):456-66. PubMed PMID: 25601754. Epub 2015/01/21.

46. Isakson P, Holland P, Simonsen A. The role of ALFY in selective autophagy. Cell death and differentiation. 2013 Jan;20(1):12-20. PubMed PMID: 22653340. Pubmed Central PMCID: PMC3524637. Epub 2012/06/02.

47. Simon HU, Yousefi S, Schmid I, Friis R. ATG5 can regulate p53 expression and activation. Cell Death Dis. 2014 Jul 17;5:e1339. PubMed PMID: 25032862. Pubmed Central PMCID: PMC4123099. Epub 2014/07/18.

48. Lee IH, Kawai Y, Fergusson MM, Rovira, II, Bishop AJ, Motoyama N, et al. Atg7 modulates p53 activity to regulate cell cycle and survival during metabolic stress. Science. 2012 Apr 13;336(6078):225-8. PubMed PMID: 22499945. Pubmed Central PMCID: 4721513.

49. Shoji JY, Kikuma T, Arioka M, Kitamoto K. Macroautophagy-mediated degradation of whole nuclei in the filamentous fungus Aspergillus oryzae. PloS one. 2010 Dec 20;5(12):e15650. PubMed PMID: 21187926. Pubmed Central PMCID: 3004950.

50. Papandreou ME, Tavernarakis N. Nucleophagy mediators and mechanisms. Progress in molecular biology and translational science. 2020;172:1-14. PubMed PMID: 32620238.

51. Akinduro O, Sully K, Patel A, Robinson DJ, Chikh A, McPhail G, et al. Constitutive Autophagy and Nucleophagy during Epidermal Differentiation. The Journal of investigative dermatology. 2016 Jul;136(7):1460-70. PubMed PMID: 27021405. Epub 2016/03/30.

52. Uhler C, Shivashankar GV. Nuclear Mechanopathology and Cancer Diagnosis. Trends in cancer. 2018 Apr;4(4):320-31. PubMed PMID: 29606315.

53. Dou Z, Xu C, Donahue G, Shimi T, Pan JA, Zhu J, et al. Autophagy mediates degradation of nuclear lamina. Nature. 2015 Nov 5;527(7576):105-9. PubMed PMID: 26524528. Pubmed Central PMCID: PMC4824414. Epub 2015/11/03.

54. Wang AS, Ong PF, Chojnowski A, Clavel C, Dreesen O. Loss of lamin B1 is a biomarker to quantify cellular senescence in photoaged skin. Scientific reports. 2017 Nov 15;7(1):15678. PubMed PMID: 29142250. Pubmed Central PMCID: 5688158.

55. Lan YY, Londono D, Bouley R, Rooney MS, Hacohen N. Dnase2a deficiency uncovers lysosomal clearance of damaged nuclear DNA via autophagy. Cell reports. 2014 Oct 9;9(1):180-92. PubMed PMID: 25284779. Pubmed Central PMCID: PMC4555847. Epub 2014/10/07.

56. Baron O, Boudi A, Dias C, Schilling M, Nolle A, Vizcay-Barrena G, et al. Stall in Canonical Autophagy-Lysosome Pathways Prompts Nucleophagy-Based Nuclear Breakdown in Neurodegeneration. Curr Biol. 2017 Dec 4;27(23):3626-42 e6. PubMed PMID: 29174892. Pubmed Central PMCID: PMC5723708. Epub 2017/11/28.

57. Golden TR, Beckman KB, Lee AH, Dudek N, Hubbard A, Samper E, et al. Dramatic age-related changes in nuclear and genome copy number in the nematode Caenorhabditis elegans. Aging cell. 2007 Apr;6(2):179-88. PubMed PMID: 17286610. Pubmed Central PMCID: 2049047.

58. McGee MD, Weber D, Day N, Vitelli C, Crippen D, Herndon LA, et al. Loss of intestinal nuclei and intestinal integrity in aging C. elegans. Aging cell. 2011 Aug;10(4):699-710. PubMed PMID: 21501374. Pubmed Central PMCID: 3135675.

59. Bonne G, Di Barletta MR, Varnous S, Becane HM, Hammouda EH, Merlini L, et al. Mutations in the gene encoding lamin A/C cause autosomal dominant Emery-Drei-

fuss muscular dystrophy. Nature genetics. 1999 Mar;21(3):285-8. PubMed PMID: 10080180.

60. Schreiber KH, Kennedy BK. When lamins go bad: nuclear structure and disease. Cell. 2013 Mar 14;152(6):1365-75. PubMed PMID: 23498943. Pubmed Central PMCID: 3706202.

61. Banerjee I, Zhang J, Moore-Morris T, Pfeiffer E, Buchholz KS, Liu A, et al. Targeted ablation of nesprin 1 and nesprin 2 from murine myocardium results in cardiomyopathy, altered nuclear morphology and inhibition of the biomechanical gene response. PLoS Genet. 2014 Feb;10(2):e1004114. PubMed PMID: 24586179. Pubmed Central PMCID: 3930490.

62. Warren DT, Tajsic T, Porter LJ, Minaisah RM, Cobb A, Jacob A, et al. Nesprin-2-dependent ERK1/2 compartmentalisation regulates the DNA damage response in vascular smooth muscle cell ageing. Cell death and differentiation. 2015 Sep;22(9):1540-50. PubMed PMID: 25744025. Pubmed Central PMCID: PMC4532777. Epub 2015/03/07.

63. Duncan FE, Jasti S, Paulson A, Kelsh JM, Fegley B, Gerton JL. Age-associated dysregulation of protein metabolism in the mammalian oocyte. Aging cell. 2017 Dec;16(6):1381-93. PubMed PMID: 28994181. Pubmed Central PMCID: PMC5676066. Epub 2017/10/11.

64. Buchwalter A, Hetzer MW. Nucleolar expansion and elevated protein translation in premature aging. Nat Commun. 2017 Aug 30;8. PubMed PMID: WOS:000408694500001. English.

65. Tiku V, Jain C, Raz Y, Nakamura S, Heestand B, Liu W, et al. Small nucleoli are a cellular hallmark of longevity. Nat Commun. 2017 Aug 30;8. PubMed PMID: WOS:000408695700001. English.

66. Cao K, Graziotto JJ, Blair CD, Mazzulli JR, Erdos MR, Krainc D, et al. Rapamycin reverses cellular phenotypes and enhances mutant protein clearance in Hutchinson-Gilford progeria syndrome cells. Science translational medicine. 2011 Jun 29;3(89):89-ra58. PubMed PMID: 21715679.

67. Papp MI, Lantos PL. Accumulation of tubular structures in oligodendroglial and neuronal cells as the basic alteration in multiple system atrophy. Journal of the neurological sciences. 1992 Feb;107(2):172-82. PubMed PMID: 1314292.

68. . !!! INVALID CITATION !!!

69. Kusakabe M, Onishi Y, Tada H, Kurihara F, Kusao K, Furukawa M, et al. Mechanism and regulation of DNA damage recognition in nucleotide excision repair. Genes and environment : the official journal of the Japanese Environmental Mutagen Society. 2019;41:2. PubMed PMID: 30700997. Pubmed Central PMCID: 6346561.

70. Marteijn JA, Lans H, Vermeulen W, Hoeijmakers JH. Understanding nucleotide excision repair and its roles in cancer and ageing. Nature reviews Molecular cell biology. 2014 Jul;15(7):465-81. PubMed PMID: 24954209.

71. Scharer OD. Nucleotide excision repair in eukaryotes. Cold Spring Harbor perspectives in biology. 2013 Oct 1;5(10):a012609. PubMed PMID: 24086042. Pubmed Central PMCID: 3783044.

72. DiGiovanna JJ, Kraemer KH. Shining a light on xeroderma pigmentosum. The Journal of investigative dermatology. 2012 Mar;132(3 Pt 2):785-96. PubMed PMID: 22217736. Pubmed Central PMCID: 3279615.

73. Niedernhofer LJ, Bohr VA, Sander M, Kraemer KH. Xeroderma pigmentosum and other diseases of human premature aging and DNA repair: molecules to patients. Mechanisms of ageing and development. 2011 Jun-Jul;132(6-7):340-7. PubMed PMID: 21708183. Pubmed Central PMCID: 3474983.

74. Karikkineth AC, Scheibye-Knudsen M, Fivenson E, Croteau DL, Bohr VA. Cockayne syndrome: Clinical features, model systems and pathways. Ageing research reviews. 2017 Jan;33:3-17. PubMed PMID: 27507608. Pubmed Central PMCID: 5195851.

75. Rieckher M, Bujarrabal A, Doll MA, Soltanmohammadi N, Schumacher B. A simple answer to complex questions: Caenorhabditis elegans as an experimental model for examining the DNA damage response and disease genes. Journal of cellular physiolo-

gy. 2018 Apr;233(4):2781-90. PubMed PMID: 28463453. Pubmed Central PMCID: 5562273.

76. Lans H, Vermeulen W. Nucleotide Excision Repair in Caenorhabditis elegans. Molecular biology international. 2011;2011:542795. PubMed PMID: 22091407. Pubmed Central PMCID: 3195855.

77. Nikoletopoulou V, Tavernarakis N. Necrotic cell death in Caenorhabditis elegans. Methods in enzymology. 2014;545:127-55. PubMed PMID: 25065889.

78. Coburn C, Allman E, Mahanti P, Benedetto A, Cabreiro F, Pincus Z, et al. Anthranilate fluorescence marks a calcium-propagated necrotic wave that promotes organismal death in C. elegans. PLoS biology. 2013 Jul;11(7):e1001613. PubMed PMID: 23935448. Pubmed Central PMCID: 3720247.

79. Syntichaki P, Tavernarakis N. The biochemistry of neuronal necrosis: rogue biology? Nature reviews Neuroscience. 2003 Aug;4(8):672-84. PubMed PMID: 12894242.

80. Kourtis N, Nikoletopoulou V, Tavernarakis N. Small heat-shock proteins protect from heat-stroke-associated neurodegeneration. Nature. 2012 Oct 11;490(7419):213-8. PubMed PMID: 22972192.

81. Madabhushi R, Pan L, Tsai LH. DNA damage and its links to neurodegeneration. Neuron. 2014 Jul 16;83(2):266-82. PubMed PMID: 25033177. Pubmed Central PMCID: 5564444.

82. Jensen HLB, Lillenes MS, Rabano A, Gunther CC, Riaz T, Kalayou ST, et al. Expression of nucleotide excision repair in Alzheimer's disease is higher in brain tissue than in blood. Neuroscience letters. 2018 Apr 13;672:53-8. PubMed PMID: 29474873.

83. Charmpilas N, Kounakis K, Tavernarakis N. Monitoring Mitophagy During Aging in Caenorhabditis elegans. Methods in molecular biology. 2018;1759:151-60. PubMed PMID: 28324491.

84. Fielder E, von Zglinicki T, Jurk D. The DNA Damage Response in Neurons: Die by Apoptosis or Survive in a Senescence-Like State? Journal of Alzheimer's disease : JAD. 2017;60(s1):S107-S31. PubMed PMID: 28436392.